8-2023

Impact of Renewables on Grid Strength, Transient Stability, and Grid Operation Characterization

Abigail E. Till
University of Tennessee, Knoxville, byg166@vols.utk.edu

To the Graduate Council:

I am submitting herewith a dissertation written by Abigail E. Till entitled "Impact of Renewables on Grid Strength, Transient Stability, and Grid Operation Characterization." I have examined the final electronic copy of this dissertation for form and content and recommend that it be accepted in partial fulfillment of the requirements for the degree of Doctor of Philosophy, with a major in Electrical Engineering.

Yilu Liu, Major Professor

We have read this dissertation and recommend its acceptance:

Fangxing Li, Shutang You, Wenpeng Yu

Accepted for the Council:

Dixie L. Thompson

Vice Provost and Dean of the Graduate School

(Original signatures are on file with official student records.)

Impact of Renewables on Grid Strength, Transient Stability, and Grid Operation Characterization

A Dissertation Presented for the
Doctor of Philosophy
Degree
The University of Tennessee, Knoxville

Abigail Ellice Till
August 2023

ACKNOWLEDGEMENTS

I would like to start by thanking my advisor, Dr. Yilu Liu. Her support and patient guidance were instrumental in completing my Ph. D. degree. I would also like to thank my committee members: Dr. Fangxing Li, Dr. Shutang You, and Dr. Wenpeng Yu. Thank you for your feedback and guidance for my research.

I am grateful for all of my colleagues in the Power IT Laboratory. In particular I would like to thank my mentors: Dr. Ling Wu, Dr. Shutang You, Dr. Lakshmi Sundaresh, Dr. Xianda Deng, and Dr. Zhihao Jiang. Your guidance on my projects and navigating the requirements of graduate school is deeply appreciated.

I am also grateful to Southern Company and their contribution to Chapter 3 of my work. I am thankful to all my colleagues there, and particularly would like to thank Dr. Clifton Black and Dr. Shih-Min Hsu for their guidance on my project.

Thank you to all my friends at Fellowship Church Knoxville and at The Church at Brook Hills in Birmingham, for always being willing to encourage and pray for me throughout this process. To my friends there who were also working through or had completed their own advanced degree, I appreciated all the advice and comradery provided through different but similar shared experience.

Finally I would like to thank my family. My parents, Lynn and David Till, thank you for always supporting me, including letting me know that you would always love me whether or not I completed the degree. And thank you to my brothers: Dr. Micah Till, Dr. John Till, and Jeremy Till.

ABSTRACT

Increasing amounts of inverter based resources (IBR) are being added to the grid. With environmental and climate change concerns, even more is projected to be added. Many companies and regions are setting goals for high levels of renewables.

As IBR are added to the grid, it changes how the power system responds to disturbances. With less traditional synchronous machines on the system, this decreases the inertia and can add stability concerns. Studies are required to know how power systems will respond to the change in generation resources. This dissertation contributes to studying transient stability and grid strength on the North American transmission system to help determine the future state of the system.

Monitoring of the power system is also important to provide awareness of the system state. Especially as the generation mix changes and uncertainties are added to the grid, it is vital to have an accurate understanding of whether the system is in normal operation or experiencing stress. It is important to have early awareness of system stress to be able to prevent instability. This dissertation will also explore potential methods to monitor for early awareness of system stress.

This dissertation documents the efforts to study and monitor current and future changes on the power system. Chapter 1 presents a study of the impact of high penetration of IBR on grid strength, in both the Eastern Interconnection (EI) and Western Interconnection (WI). Chapter 2 documents a study of the

impact of high photovoltaic (PV) penetration on transient stability in the Electric Reliability Council of Texas (ERCOT) System. And Chapter 3 describes an effort to study active power and voltage angle data on the Southern Company system in order to investigate voltage angle difference as an indicator of early event awareness due to stress on the system caused by power flow through an interface.

TABLE OF CONTENTS

LIST OF TABLES

LIST OF FIGURES

CHAPTER ONE
STUDY OF IMPACT OF HIGH PENETRATION OF INVERTER BASED RESOURCES ON GRID STRENGTH

1.1 Introduction

The power system generation mix is changing, currently seeing retirements of coal-fired generation and an increase in gas plants and inverter based resources (IBR) such as wind and solar generation [1]. As generation changes occur on the power system, it is important to study the effect on the system to ensure continued reliable service and determine areas on the grid that might need reinforcement to remain strong.

Grid strength is described in [2] as “a characteristic of an electrical power system that relates to the size of the change in voltage following a fault or disturbance on the power system.” Grid strength is related to the grid stiffness or the ability of the power system to keep the voltage at the desired value with external perturbations [3]. A strong bus would have little voltage change resulting from a perturbation on the grid [4].

Inverter based resources (IBR) can have an adverse impact on bulk power systems, particularly in buses or areas with weak grid strength [4]. Because IBRs have power electronic converters they differ from synchronous generators in their ability to add inertia and short-circuit current to the grid [3]. Thus it is important to know the impacts as IBRs increase in percentage of generation [5].

Short circuit apparent power (SCMVA) is the short-circuit capacity at a bus [6]. Short circuit ratio (SCR) is used to describe the ratio of the short circuit capacity with respect to connecting a source to the grid [6] [7]. SCMVA is a common metric used when evaluating grid strength, often as part of the SCR calculation in regards to adding specific sources [3]-[4][5][6][7][8] [9].

This work investigates the grid strength in the EI and WI. It determines the strength of the grid as conventional generation is replaced with renewable generation. It also studies the potential to add more IBR to increase generation capacity.

1.2 Analysis of Grid Strength on the Eastern Interconnection when Converting All Conventional Generators to IBRs

1.2.1 Model Overview

The model used for this first part of the study was the Multi-Regional Modeling Working Group (MMWG) 2025 Summer PSS®E model.

1.2.2 Method

This part of the study looked at converting all conventional synchronous generators within the EI to IBRs, using wind machines in PSS®E, and testing the grid strength. Any renewables already modeled in the system were not changed, in particular nuclear and hydroelectric plants identified in [10]. The grid strength was measured using SCMVA, calculated in PSS®E using IEC-60909 fault calculations [11], as a percentage of the base SCMVA given by equation (1)

$$\Delta SCMVA\% = \frac{SCMVA_{converted\ case} - SCMVA_{base\ case}}{SCMVA_{base\ case}} \quad (1)$$

where $SCMVA_{converted\ case}$ is the case after the conventional generators have been converted to IBRs and $SCMVA_{base\ case}$ is the original case before it was altered, and $\Delta SCMVA\%$ is the resulting change in SCMVA between the base case and the converted case as a percent value of the base case. This approach relates the new SCMVA value to the old so that it is apparent how the value has changed, and converts the difference to a percentage of the original case to make it easier to read.

The conventional generators were replaced with IBR one area at a time and the SCMVA was calculated for all buses in that area that were 345 kV and above. The results were then graphed using a colormap on a map of the EI region. Later the study was run again converting the generators for the entire EI all at once instead of by area. The results were graphed and compared to the results of converting the generators by area.

To further study the effect of IBR on the SCMVA, the hydroelectric and nuclear generators were also replaced with IBR generation. The SCMVA was then studied with all machines being IBR.

After the SCMVA results were obtained, the capacity for additional IBR generation was measured. The SCR, used to define the strength of the grid, is defined in [6] as:

$$SCR = \frac{S_{SCMVA}}{P_{RMW}} \tag{2}$$

where S_{SCMVA} is the short-circuit MVA capacity at a bus before connecting a new generation source and P_{RMW} is the rated megawatt value of the new connected source.

Since a weak grid is considered to be an SCR of 3 or lower [7] [8], equation (2) can be rewritten as:

$$P_{RMW} = \frac{S_{SCMVA}}{SCR} \quad (3)$$

and the calculated SCMVA value for each bus can be used with an SCR of 3 to determine what the maximum generation hosting capacity is for each bus.

1.2.3 Results

The impact on SCMVA that converting conventional generation to IBR had on each bus at a value 345 kV and above was graphed using MATLAB and is shown in Fig. 1. As can be seen from the figure there were many buses that had a decrease in SCMVA. All of the buses had at least a slight decrease. To help show more clearly the change in SCMVA, the colorbar in Fig. 2 was changed to have more colors and less of a range so that the few buses that had a large change would not keep the majority of the buses from showing notable change. The data is the same in Fig. 1 and Fig. 2, and it is only the colorbar that has been altered.

The data was then further broken down to try and create an easier to read display. The data was segmented into three graphs with different ranges of $\Delta SCMVA\%$. The data points were split into three approximately equal groups, approximate due to some rounding in case the total number of points was not

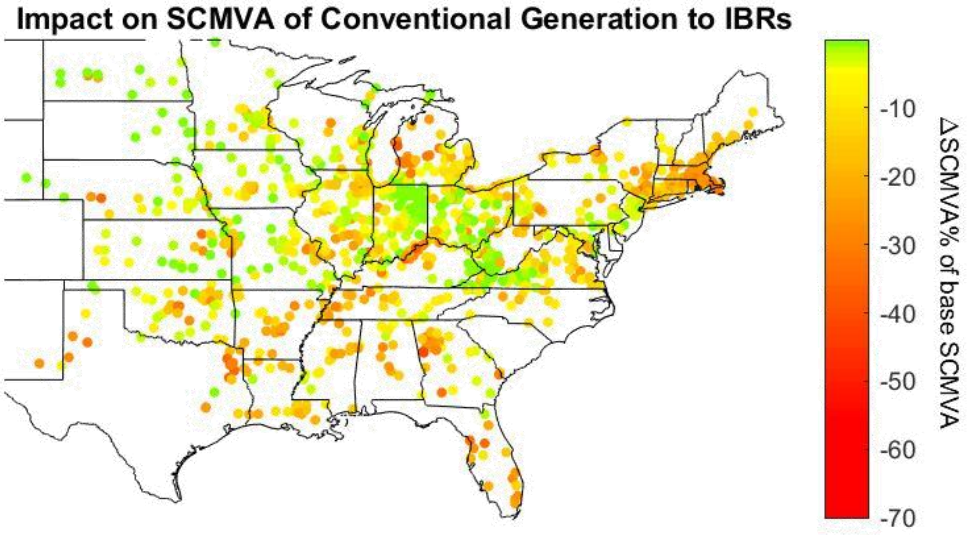

Fig. 1. Impact on SCMVA at buses in EI when conventional generation changed to IBR.

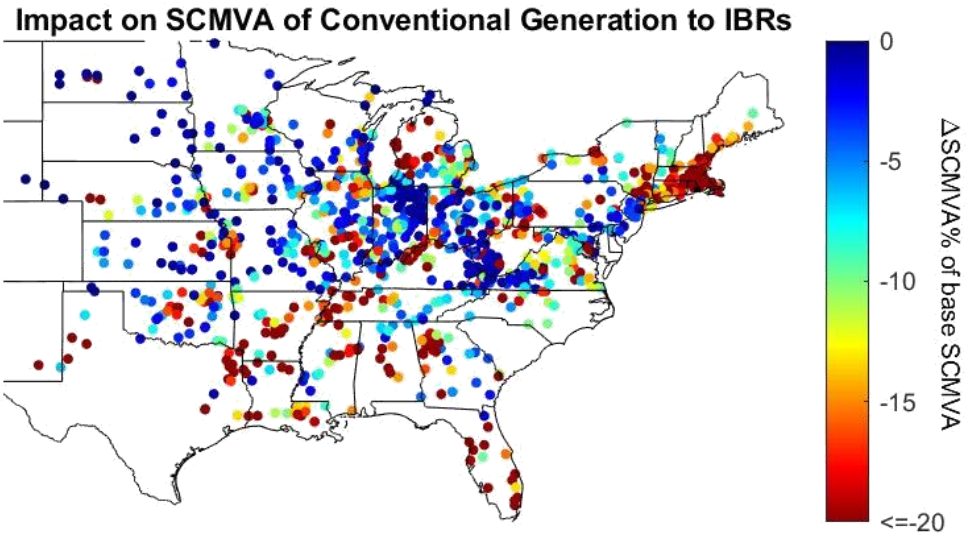

Fig. 2. Zoomed in scale of impact on SCMVA at buses in EI when conventional generation changed to IBR.

divisible by three and to make the graph titles more readable by splitting on a whole number. The three graphs are shown in Fig. 3-Fig. 5.

In Fig. 3 it can be seen that a lot of the data points have a change of 4% or lower worse than the base case SCMVA. Fig. 4 shows the middle data set with a difference of 4% to 15% less SCMVA than the base case. Fig. 5 shows the last segment as between 15% and 71% less SCMVA than the base case. From these graphs it can be seen that while there are some pretty significant changes from the base case to the SCMVA from the base case to the fully IBR case, that's true at only a small amount of the buses. A majority of the data has less than a 15% change in SCMVA.

The method was later changed to convert the generators for the whole case at once instead of for one area at a time. A graph for this is shown in Fig. 6, with Fig. 7 being a graph of the same data zoomed in for a portion of the color bar. The graph is further broken up into segments in Fig. 8-Fig. 10.

It can be seen from Fig. 8-Fig. 10 that converting all the generation at once instead of one area at a time does have some effect on the SCMVA. It is a similar change in SCMVA, but further reduced from the base case to convert the generation for the whole case all at once. To investigate this further, a graph was created to display the difference between converting all of the generation at once and just converting by area, and is shown in Fig. 11.

Along with the difference between the two conversion methods, Fig. 11 displays some statistics for the difference in the SCMVA. The maximum

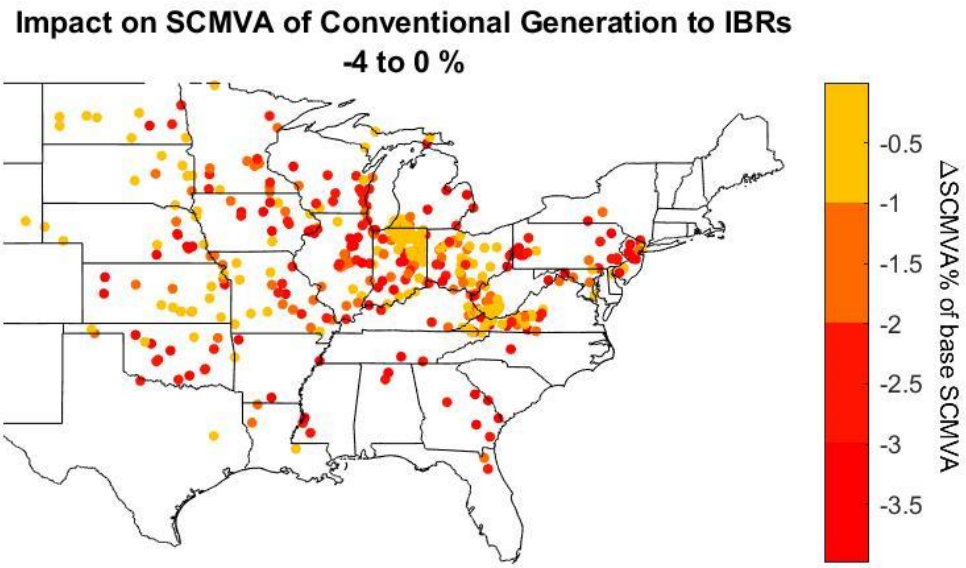

Fig. 3. Impact on SCMVA at buses in EI when conventional generation changed to IBR – Segment 1.

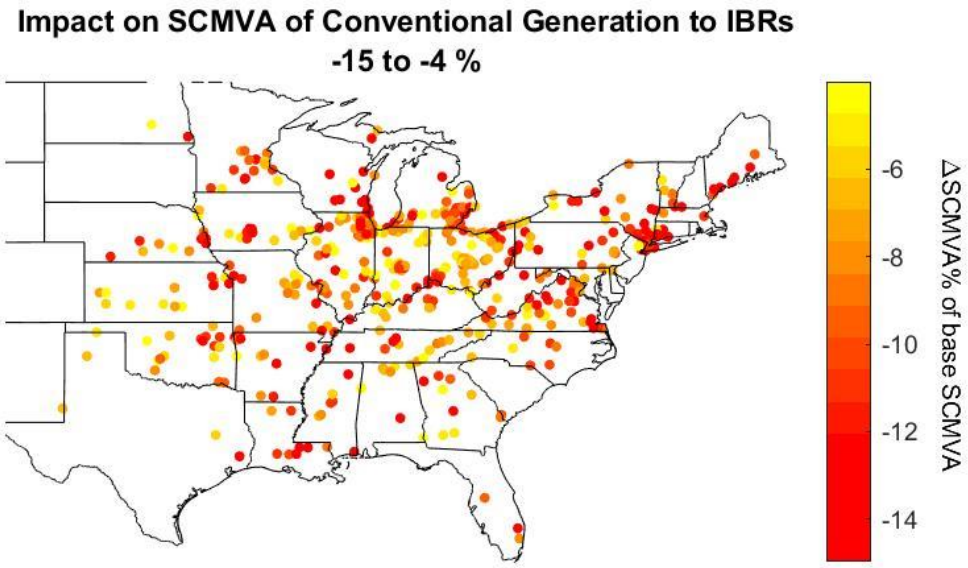

Fig. 4. Impact on SCMVA at buses in EI when conventional generation changed to IBR – Segment 2.

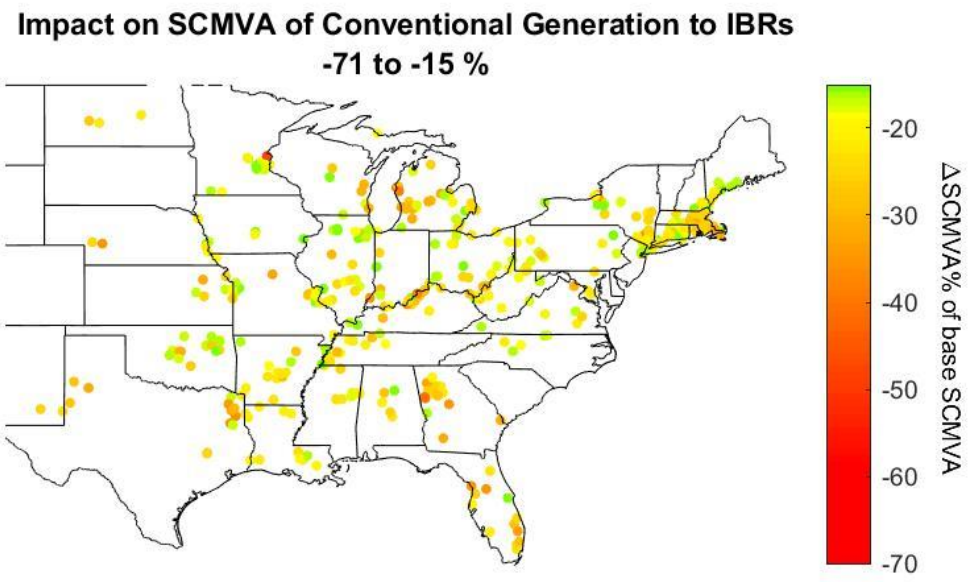

Fig. 5. Impact on SCMVA at buses in EI when conventional generation changed to IBR – Segment 3.

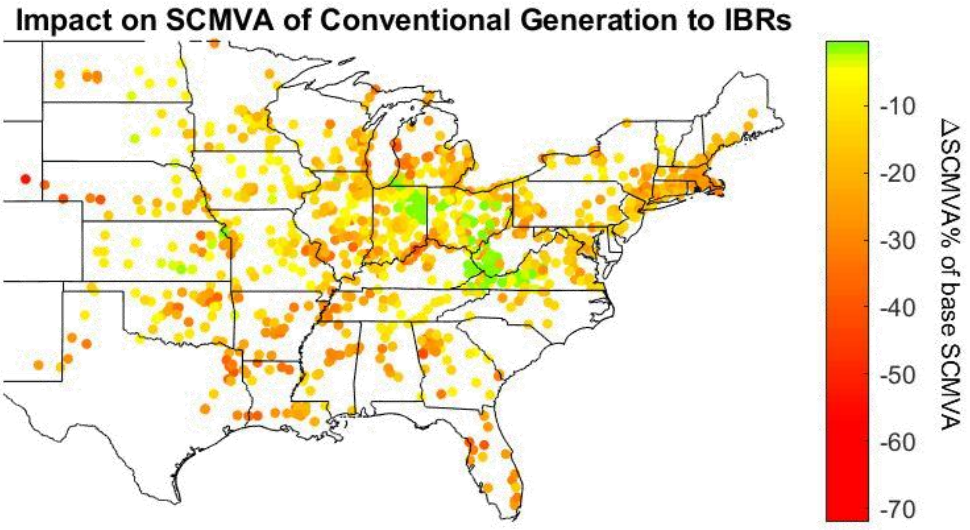

Fig. 6. Impact on SCMVA when converting generation to IBR for whole system.

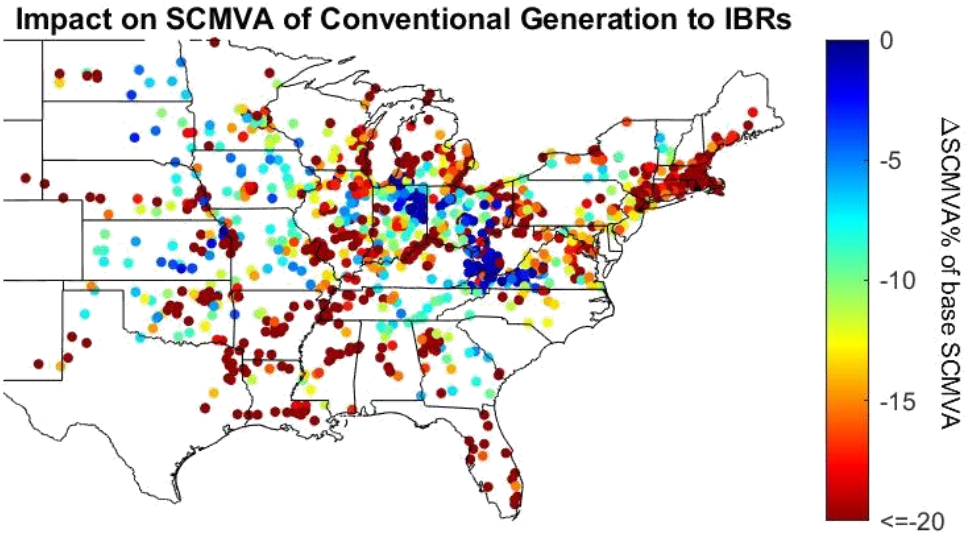

Fig. 7. Zoomed in scale of impact on SCMVA when converting generation to IBR for whole system.

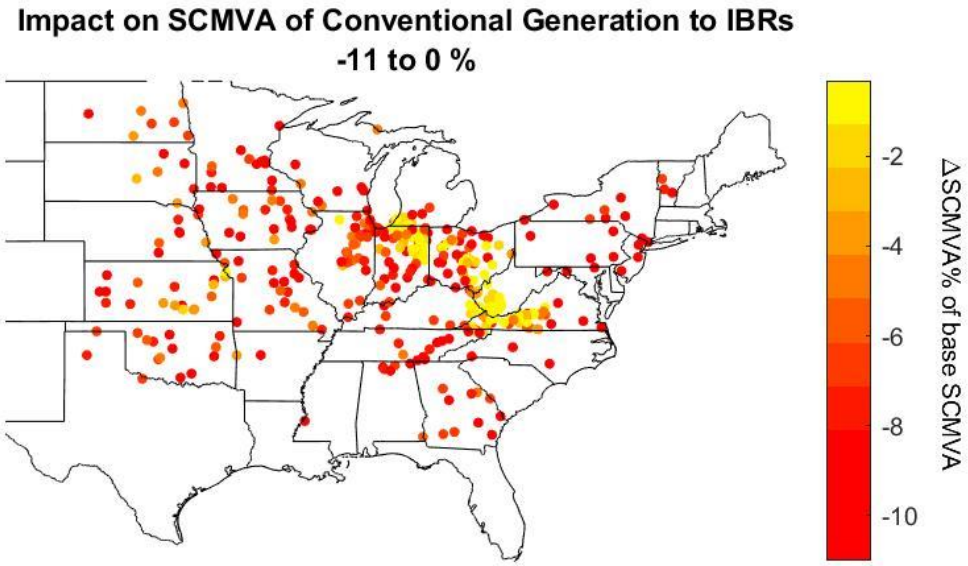

Fig. 8. Impact on SCMVA when converting generation to IBR for whole system – Segment 1.

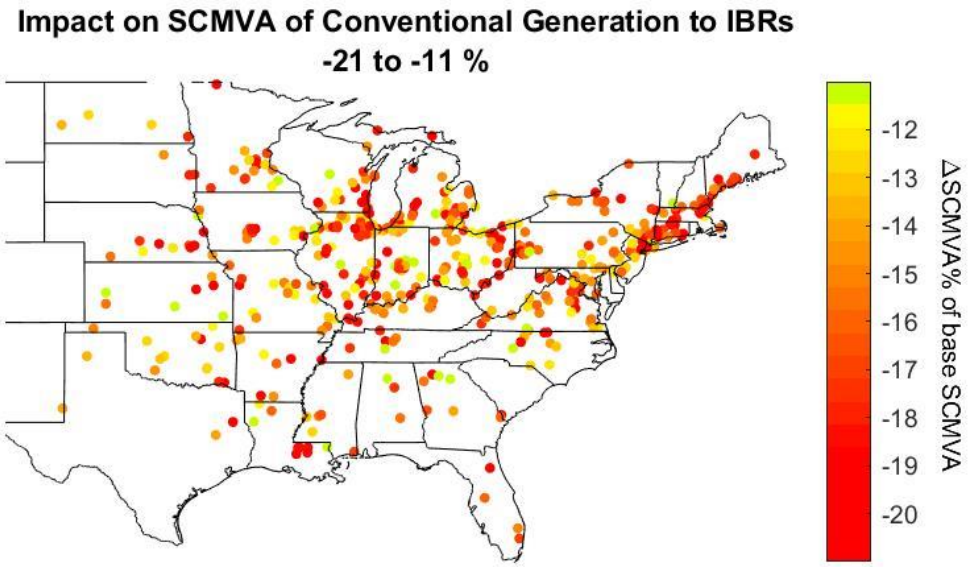

Fig. 9. Impact on SCMVA when converting generation to IBR for whole system – Segment 2.

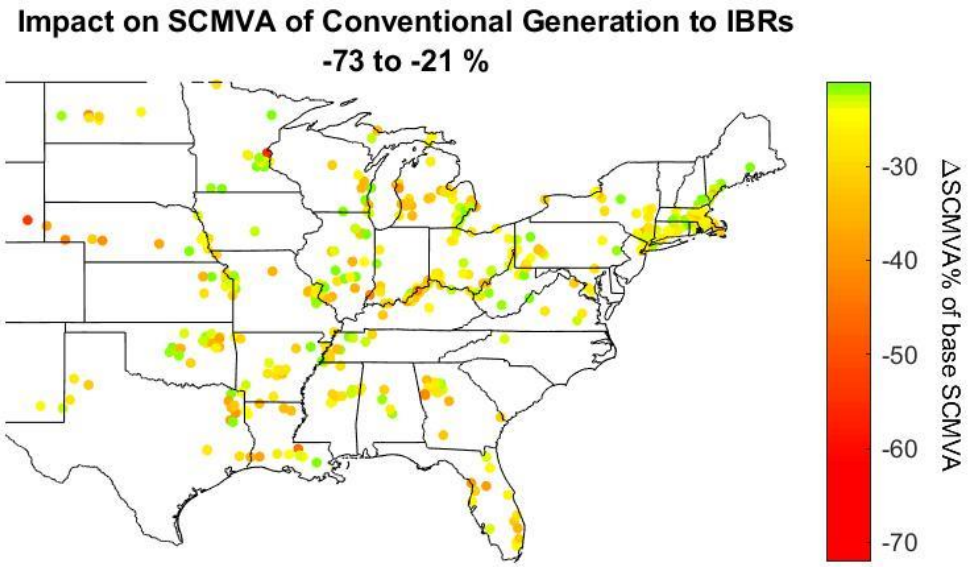

Fig. 10. Impact on SCMVA when converting generation to IBR for whole system – Segment 3.

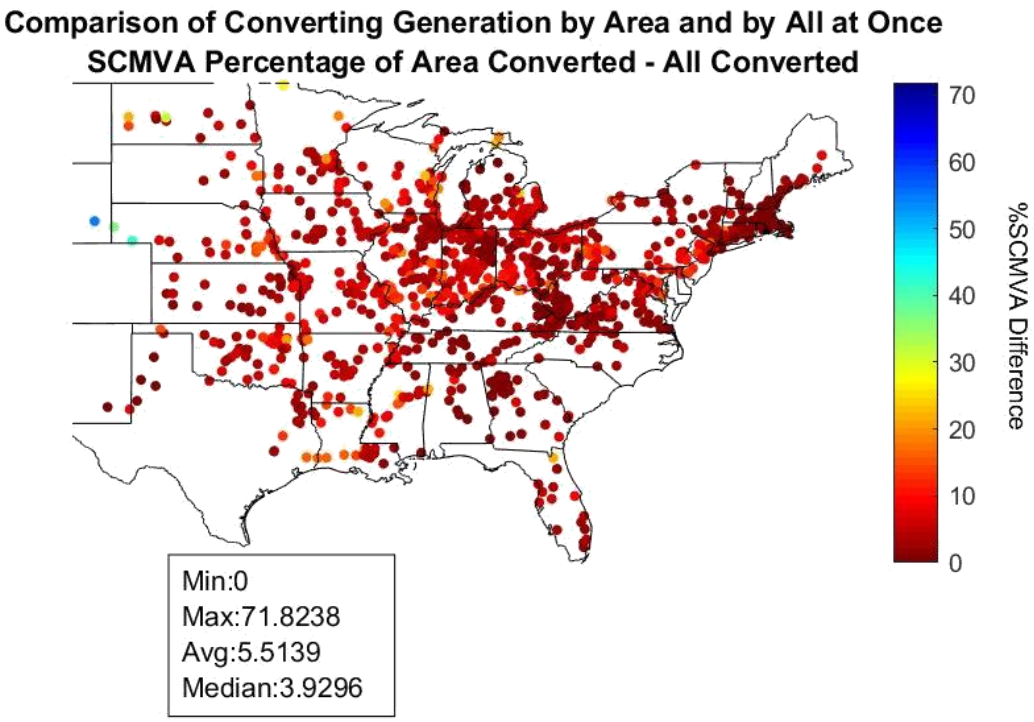

Fig. 11. Difference between converting by area and converting whole case in SCMVA percentage.

difference between the two methods was approximately 71.8%. However, the average difference between the methods was only approximately 5.5%.

To test the SCMVA if the generation becomes 100% IBR, the nuclear and hydroelectric generators were also converted to IBR machines. The measured SCMVA is shown in Fig. 12. Segmented graphs are shown in Fig. 13-Fig. 15. The SCMVA did decrease slightly with the nuclear and hydroelectric plants converted to IBR machines. To compare the different methods numerically, Table 1 was created.

Table 1 shows a comparison between the different analyses performed, comparing the minimum, maximum, average, and median percent changes for each method. It compares converting the generators and measuring the SCMVA one area at a time, converting the generators and measuring the SCMVA for the whole system all at once, and then further converting all the generators, even the renewable synchronous generators, to IBR and measuring the SCMVA for the whole system all at once. As can be seen from Table 1, the SCMVA decreases further from the base case as the generators are converted all at the same time, and then a slightly further decrease as the renewable synchronous generators are converted to IBR machines.

After the SCMVA analysis, the IBR hosting capacity could be calculated. The hosting capacity is shown in Fig. 16. This shows at each bus the maximum MW value that a newly added IBR could be rated.

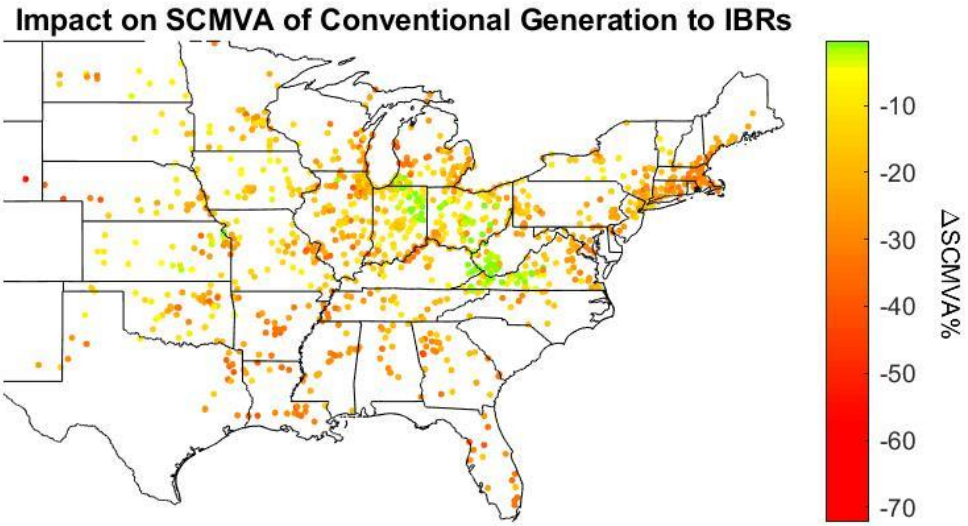

Fig. 12. SCMVA with all generation IBR.

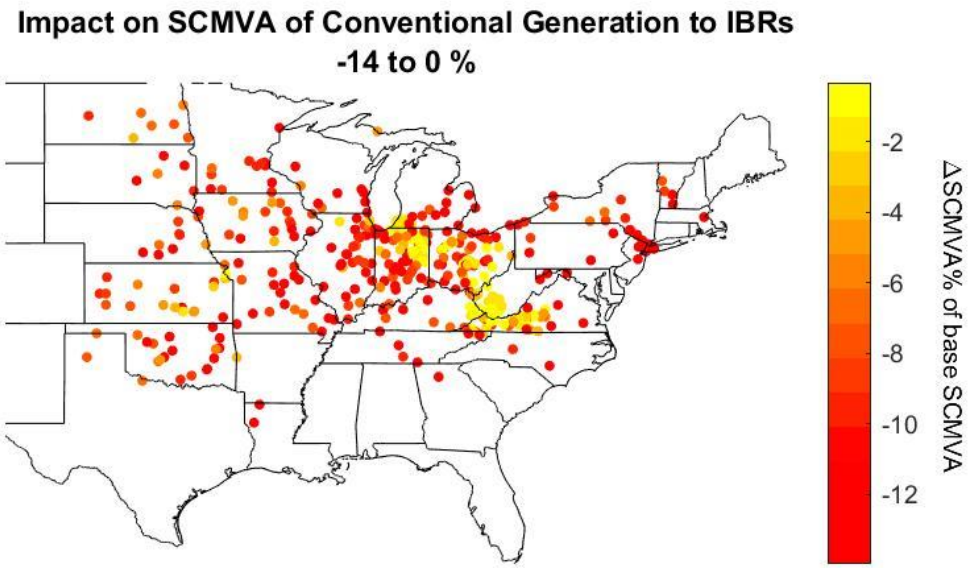

Fig. 13. SCMVA with all generation IBR – Segment 1.

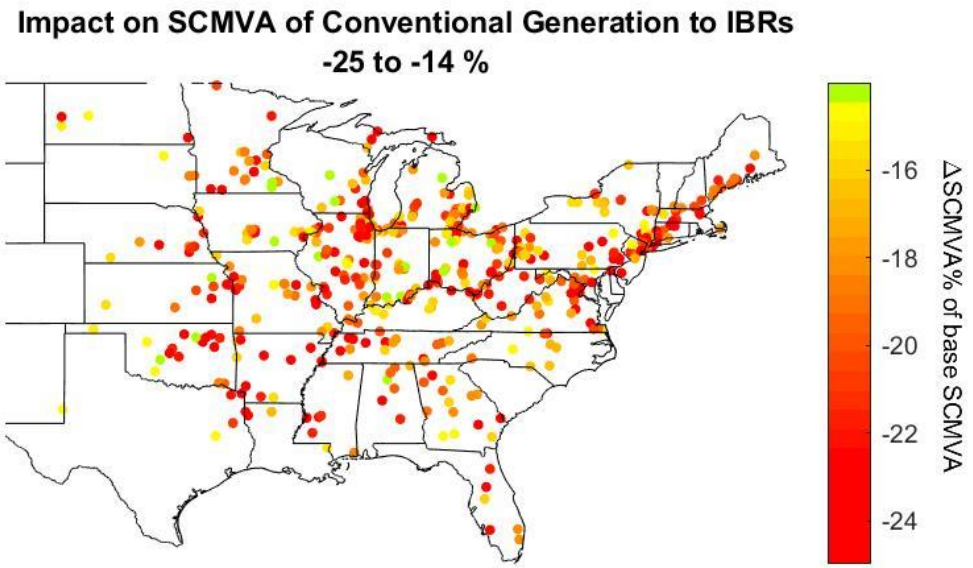

Fig. 14. SCMVA with all generation IBR – Segment 2.

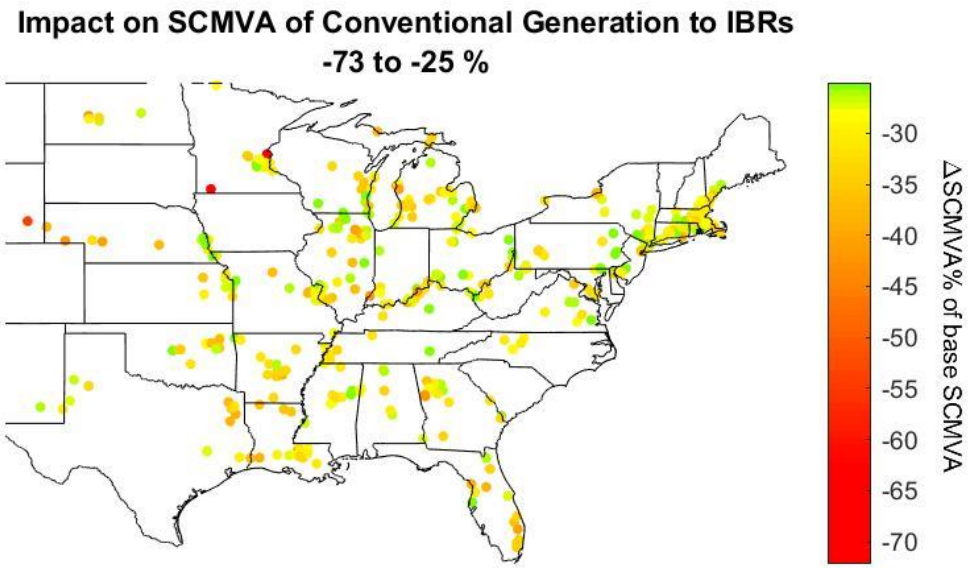

Fig. 15. SCMVA with all generation IBR – Segment 3.

Table 1. SCMVA value comparison by method in EI.

	min %	max %	avg %	med %
convert by area	-70.14	0.00	-11.92	-9.50
convert by all	-72.06	-0.32	-17.43	-16.55
100% IBR	-72.19	-0.33	-19.94	-19.97

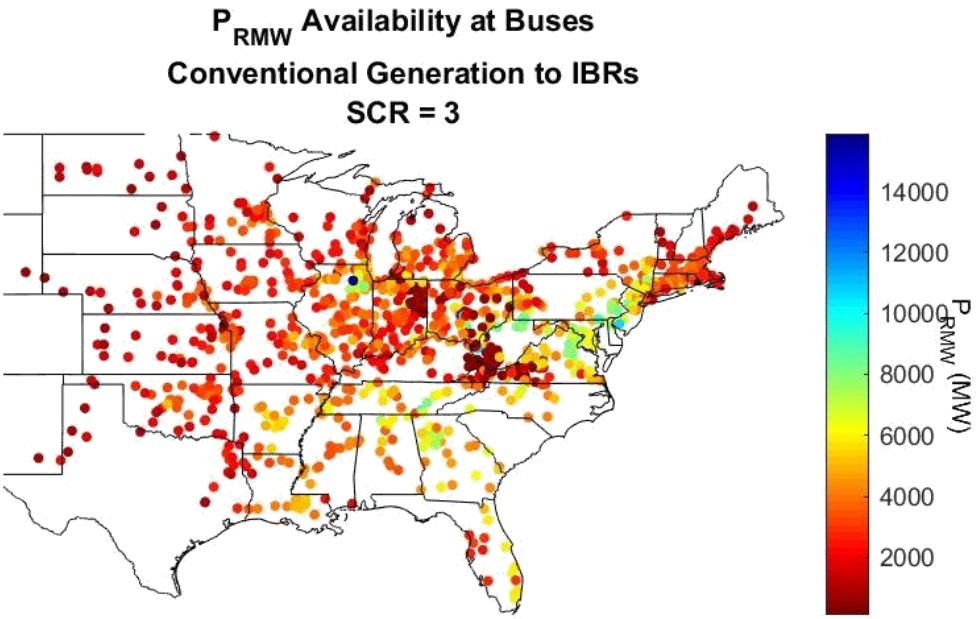

Fig. 16. IBR hosting capacity in EI with conventional generation changed to IBR.

The graphs for hosting capacity were also separate into segmented graphs. For the hosting capacity the graphs were segmented for the base case to have three approximately equal data sets. The hosting for the fully renewable case uses the same range as determined by the base case, which means that the data will not be spread equally across the three graphs, but will be easier to compare the change from the base case. The segmented graphs are shown in Fig. 17-Fig. 22.

Comparing Fig. 17 and Fig. 18, the first segment with the lowest hosting capacity, shows that there are more data points for the fully renewable case, so there is less IBR hosting capacity when the grid already contains a large amount of IBR. The middle segment is hard to identify the trend just from looking at the points in Fig. 19 and Fig. 20, but comparing Fig. 21 and Fig. 22 does show that the trend continues through the segmented graphs with less data points for the fully IBR case in the segment with the highest hosting capacity, and therefore less IBR hosting capacity for the fully IBR case than the base case.

The graph with the nuclear and hydroelectric generation converted to IBR as well for 100% IBR generation is shown in Fig. 23. The segmented graphs are shown in Fig. 24-Fig. 26.

Table 2 shows a comparison between the different analyses performed, comparing the minimum, maximum, average, and median values for the generation that can be added. Table 2 shows the base case so the cases with the generation altered can be compared. As the generation is converted to IBR

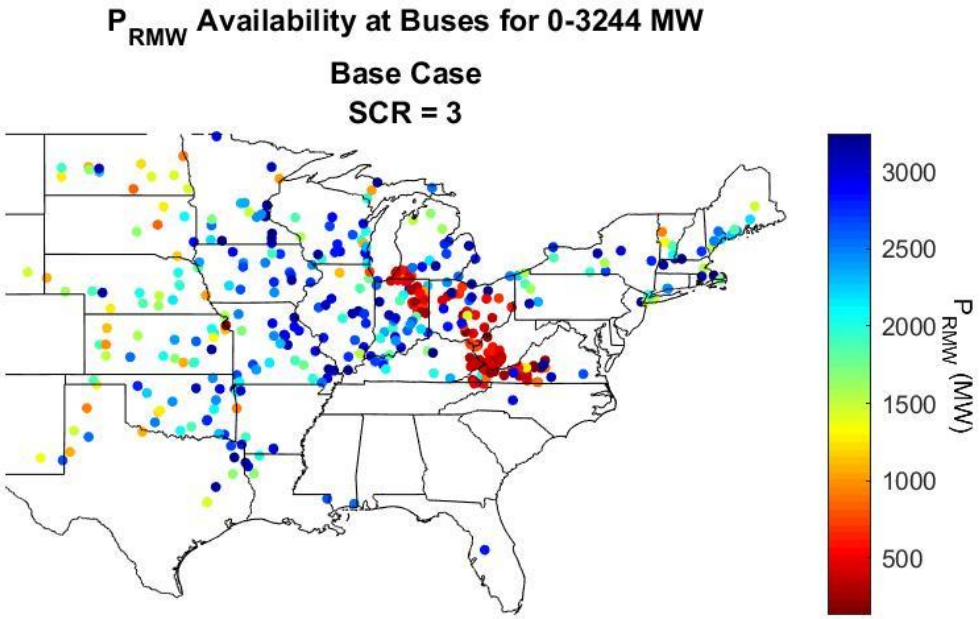

Fig. 17. IBR hosting capacity in EI with base case – Segment 1.

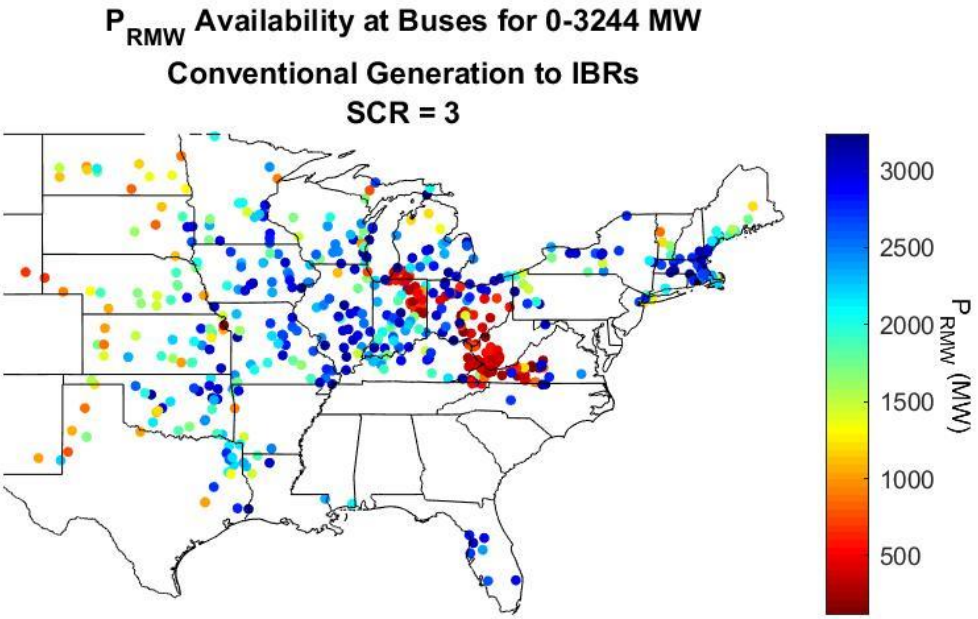

Fig. 18. IBR hosting capacity in EI with fully renewable case – Segment 1.

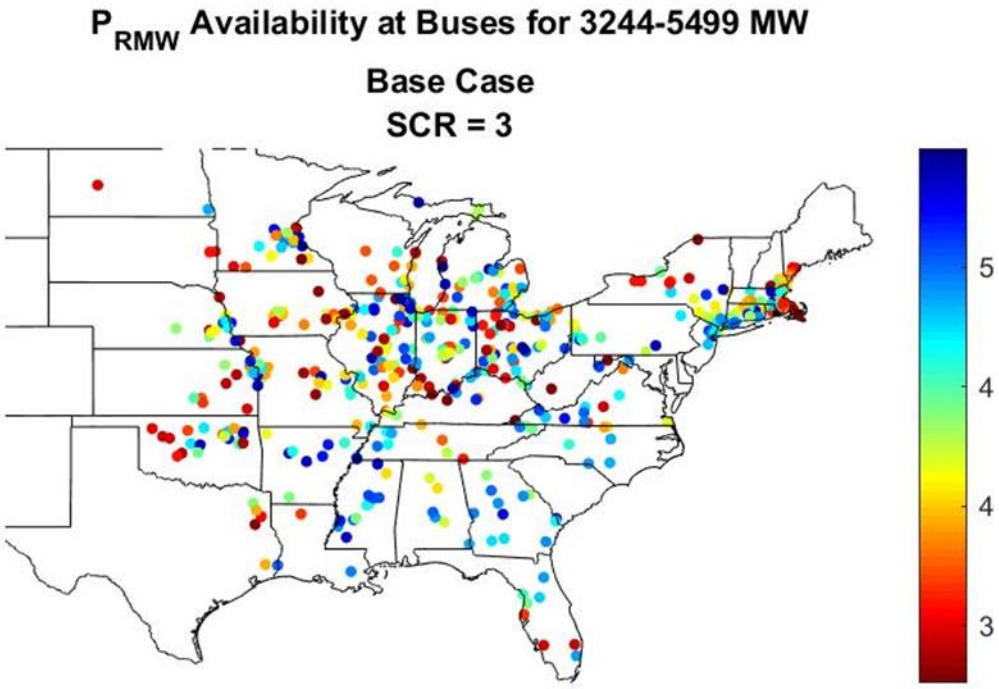

Fig. 19. IBR hosting capacity in EI with base case – Segment 2.

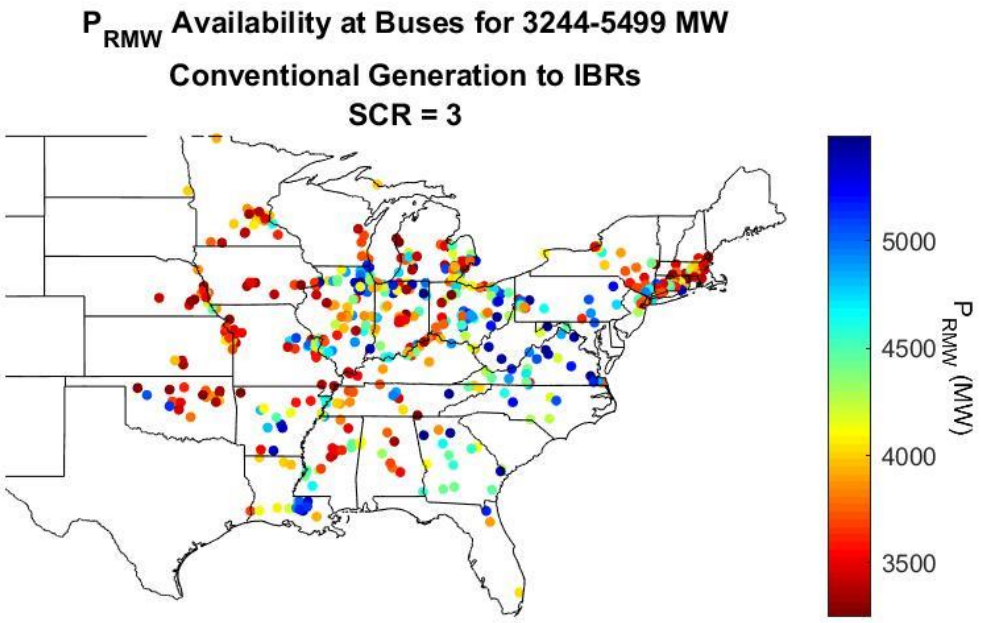

Fig. 20. IBR hosting capacity in EI with fully renewable case – Segment 2.

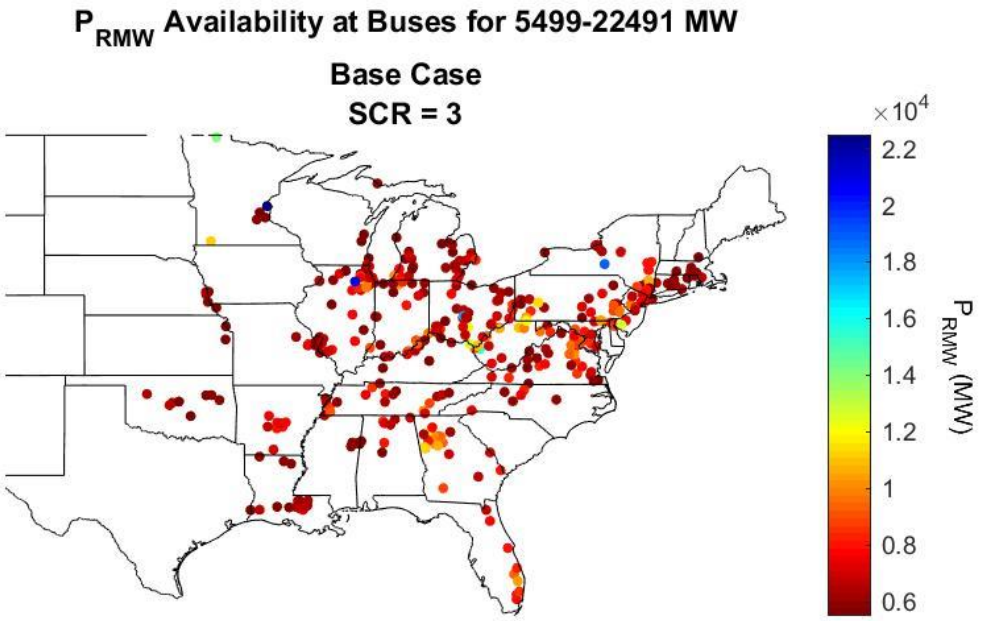

Fig. 21. IBR hosting capacity in EI with base case – Segment 3.

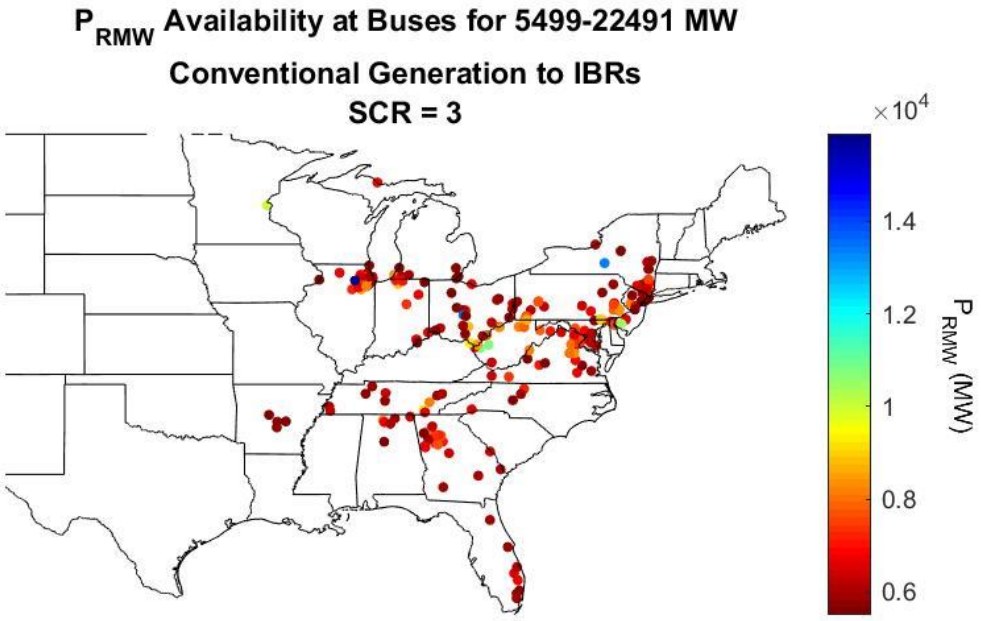

Fig. 22. IBR hosting capacity in EI with fully renewable case – Segment 3.

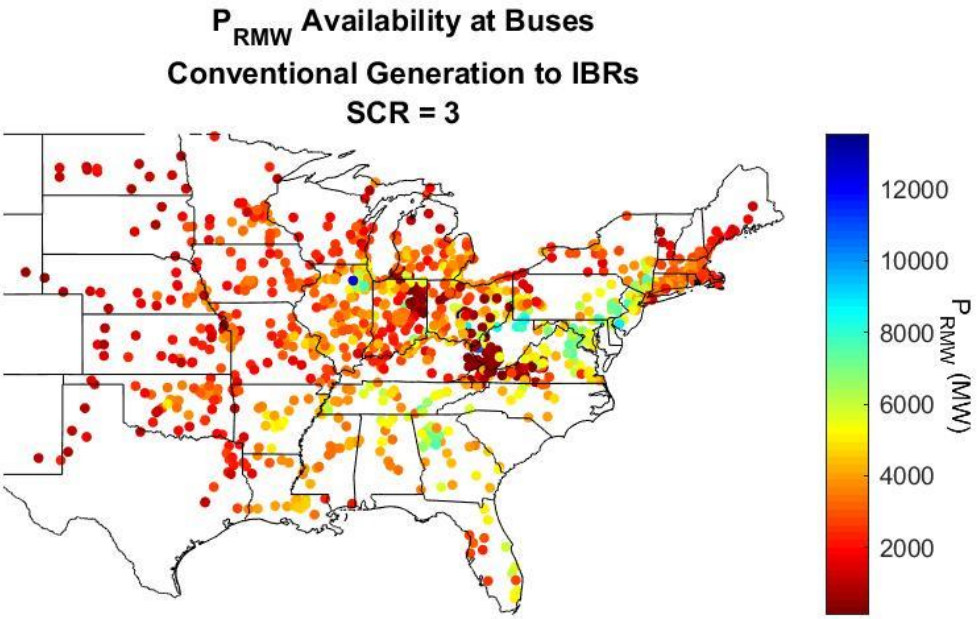

Fig. 23. IBR hosting capacity in EI with all generation IBR.

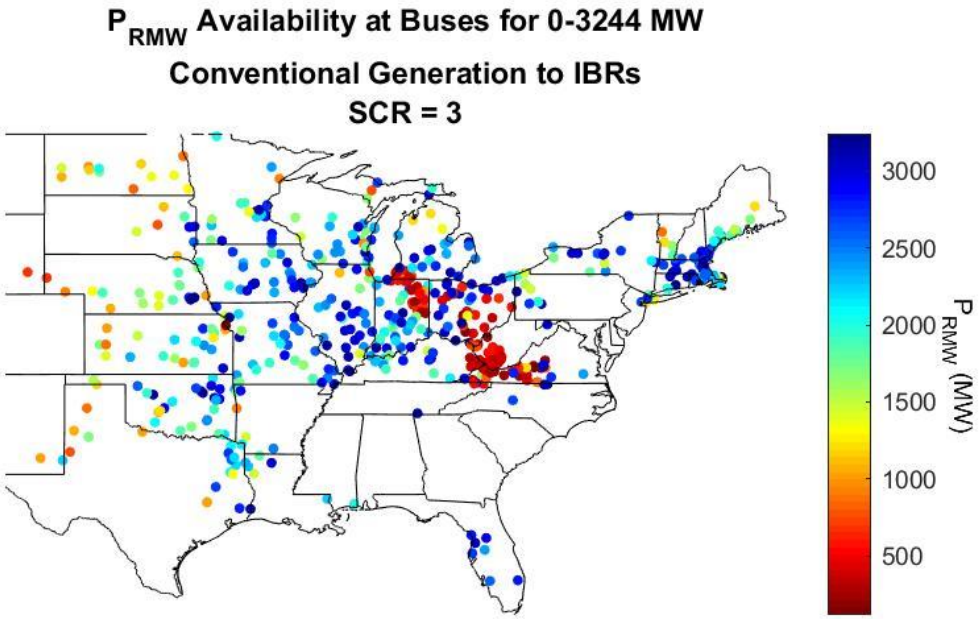

Fig. 24. IBR hosting capacity in EI with all generation IBR – segment 1.

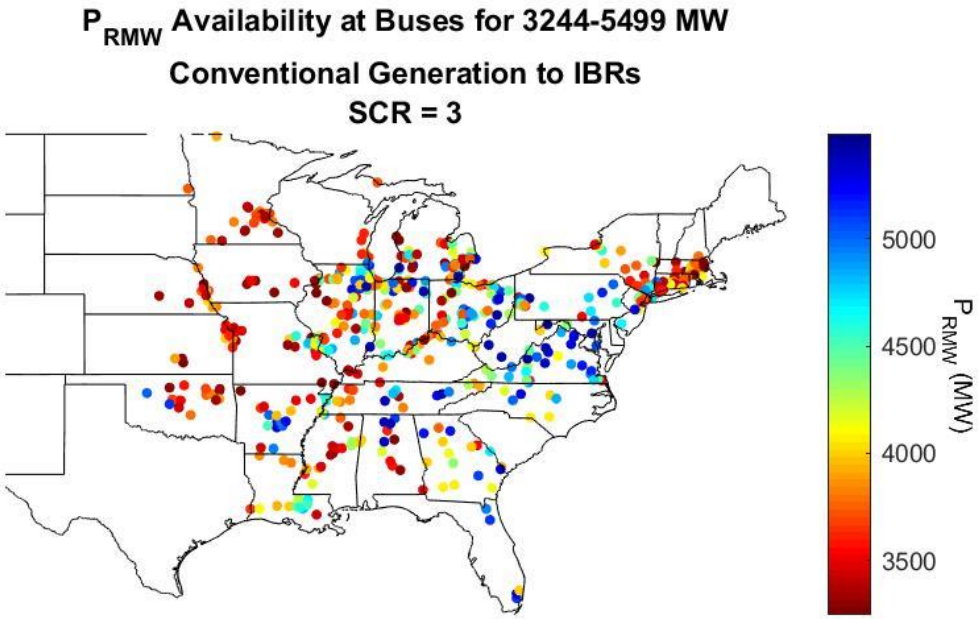

Fig. 25. IBR hosting capacity in EI with all generation IBR – segment 2.

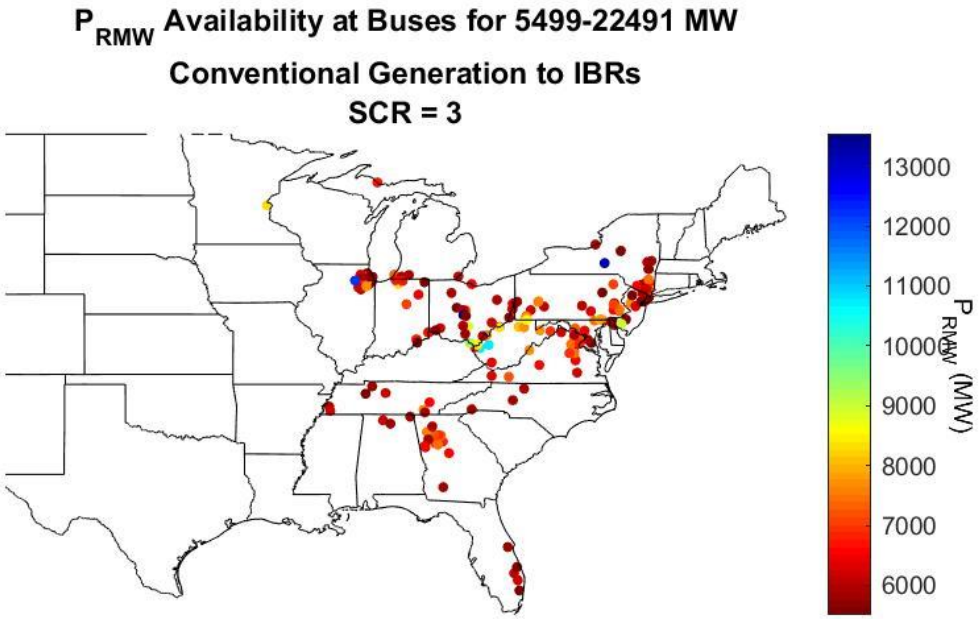

Fig. 26. IBR hosting capacity in EI with all generation IBR – segment 3.

Table 2. P_{RMW} value comparison by method in EI.

	min (MW)	max (MW)	avg (MW)	med (MW)
Base case	132.26	22490.59	4677.01	4411.60
convert by area	114.38	16671.73	3990.86	3767.96
convert by all	114.38	15883.30	3713.12	3518.21
100% IBR	114.38	13541.33	3563.80	3415.06

the hosting capacity decreases, and decreases further with increasing IBR.

1.3 Analysis of Grid Strength on the Eastern Interconnection at Different Levels of PV Penetration

1.3.1 Model Overview

For the second part of the study, EI cases at hypothetical varying photovoltaic (PV) penetrations were used. The cases consisted of no wind or PV, and 5%, 25%, 45%, and 65% PV with 15% wind each.

1.3.2 Method

This part of the study tested each level of PV penetration against the base case, using the equation given in equation (2)

$$\frac{SCMVA_{renewable} - SCMVA_{no\ renewable}}{SCMVA_{no\ renewable}} \quad (2)$$

where $SCMVA_{renewable}$ is the case at the level of PV being tested and $SCMVA_{no\ renewable}$ is the case that has no PV or wind generation. For this method, instead of testing by converting all the conventional synchronous generation to IBR at once, it was tested at different levels and compared.

The SCMVA was calculated for all buses in that area that were 345 kV and above. The simulation was run 4 times for the four different levels of PV penetration. The results were then graphed using a colormap on a map of the EI region.

The IBR hosting capacity was also analyzed, with the same method described in Section 1.2.2.

1.3.3 Results

The impact on SCMVA that each PV penetration level had on each bus was graphed using MATLAB and is shown in Fig. 27-Fig. 30. As can be seen from the figure there were many buses that had a decrease in SCMVA. For the case of 15% wind and 5% PV, there was one bus that had no change in SCMVA. Other than that all the buses had at least a slight decrease.

Table 3 shows a numerical comparison for the SCMVA for the different renewable levels. The table shows the percentage change minimum, maximum, average, and median values. From this table it can be seen that as renewables are added, the SCMVA has a trend of decreasing further as IBR are increased.

Fig. 31 shows the hosting capacity for the no renewable case, and Fig. 32 shows the hosting capacity for the maximum renewable case used, the 80% renewable case. Since it is difficult to see the difference from these graphs, the segmented graphs are shown in Fig. 33-Fig. 47 for better comparison.

From Fig. 33-Fig. 37, the first segment and lowest hosting capacity, It can be seen that there are more data points, or less hosting capacity, as the renewables increase, but also that it is a slow change for each step of the renewable cases increasing. Again, with the middle segments, Fig. 38-Fig. 42, it is harder to tell the change in overall hosting capacity from these graphs. Combined with the third segment, Fig. 43-Fig. 47, however, we can see that the overall trend is indeed less hosting capacity at higher levels of IBR, as with these graphs again there are less data points in the third segment, or high range of hosting capacity, as the renewable amount increases.

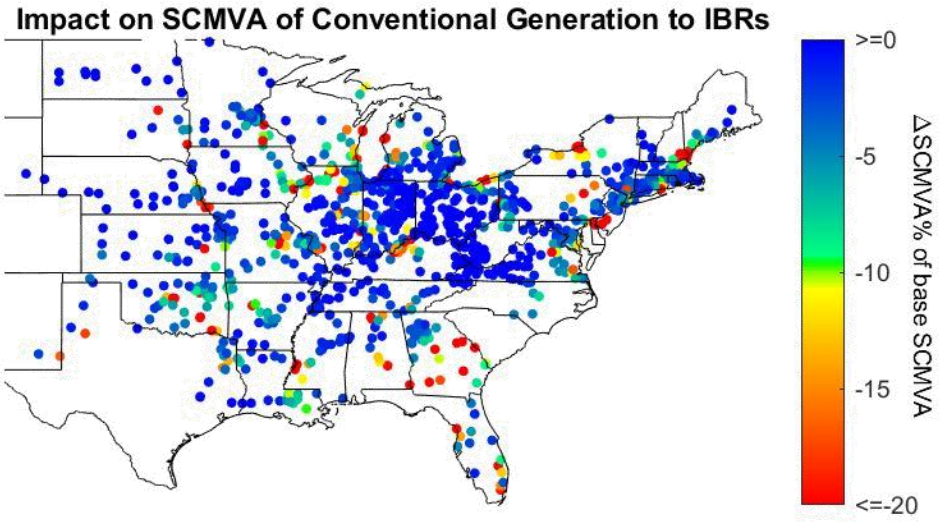

Fig. 27. Impact on SCMVA at buses due to 15% wind and 5% PV penetration.

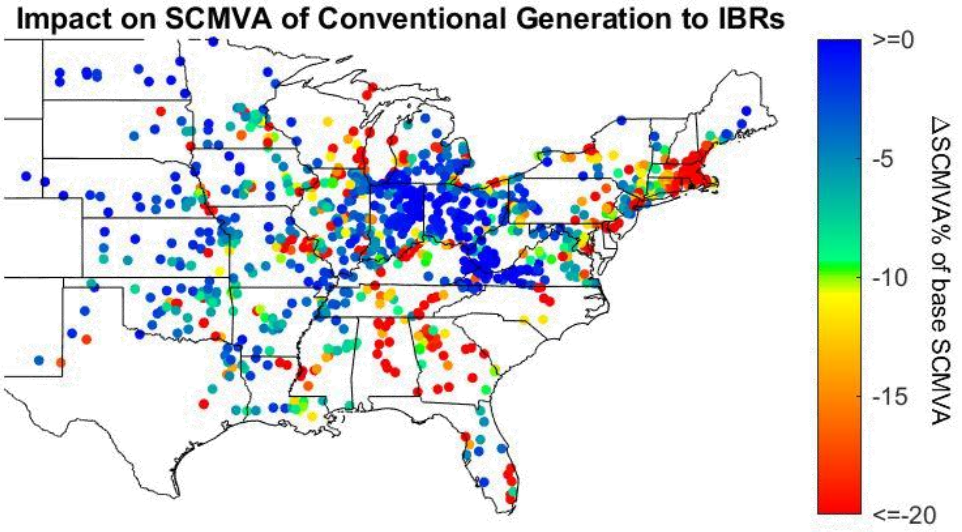

Fig. 28. Impact on SCMVA at buses due to 15% wind and 25% PV penetration.

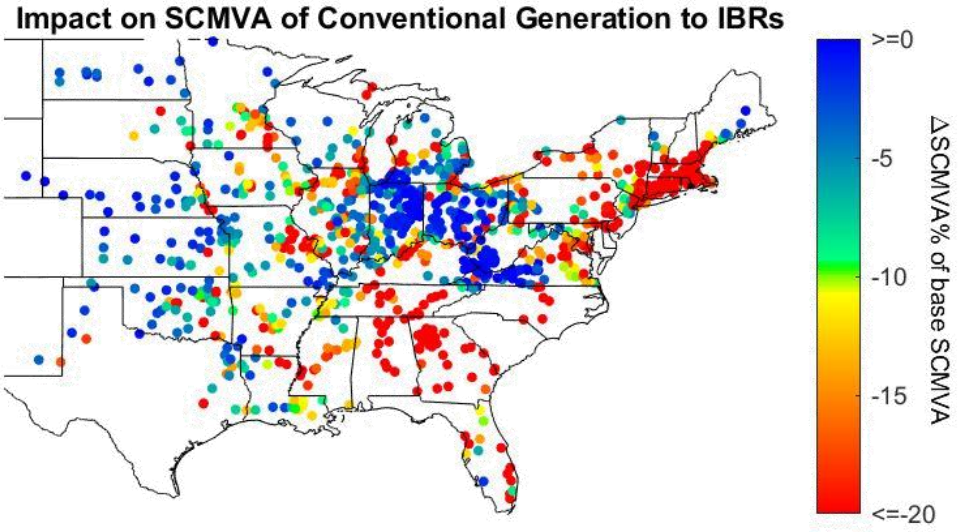

Fig. 29. Impact on SCMVA at buses due to 15% wind and 45% PV penetration.

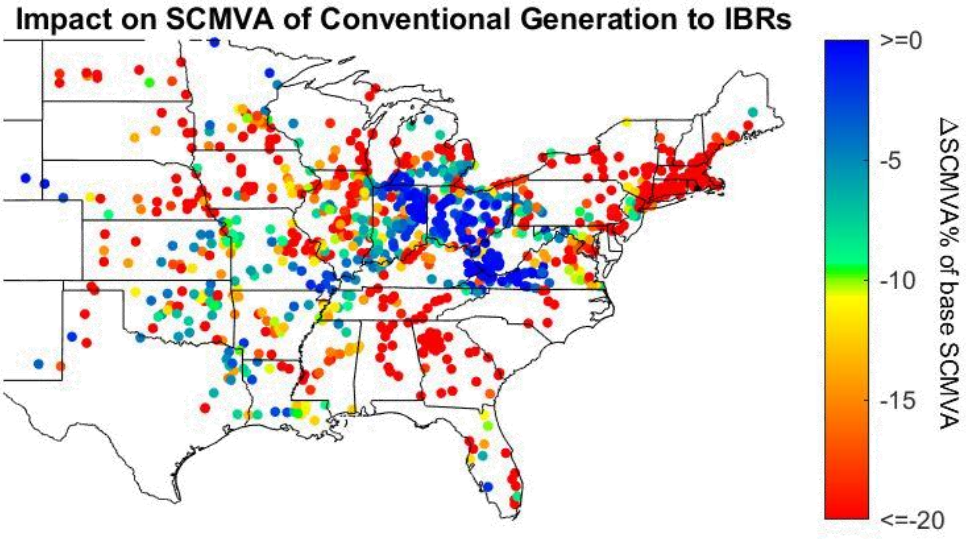

Fig. 30. Impact on SCMVA at buses due to 15% wind and 65% PV penetration.

Table 3. SCMVA value comparison for differing renewable levels.

	min %	max %	avg %	med %
15WT 5PV	-51.34	0.00	-4.71	-2.05
15WT 25PV	-53.75	-0.02	-9.32	-5.92
15WT 45PV	-55.32	-0.04	-13.80	-10.22
15WT 65PV	-67.96	-0.05	-16.71	-13.38

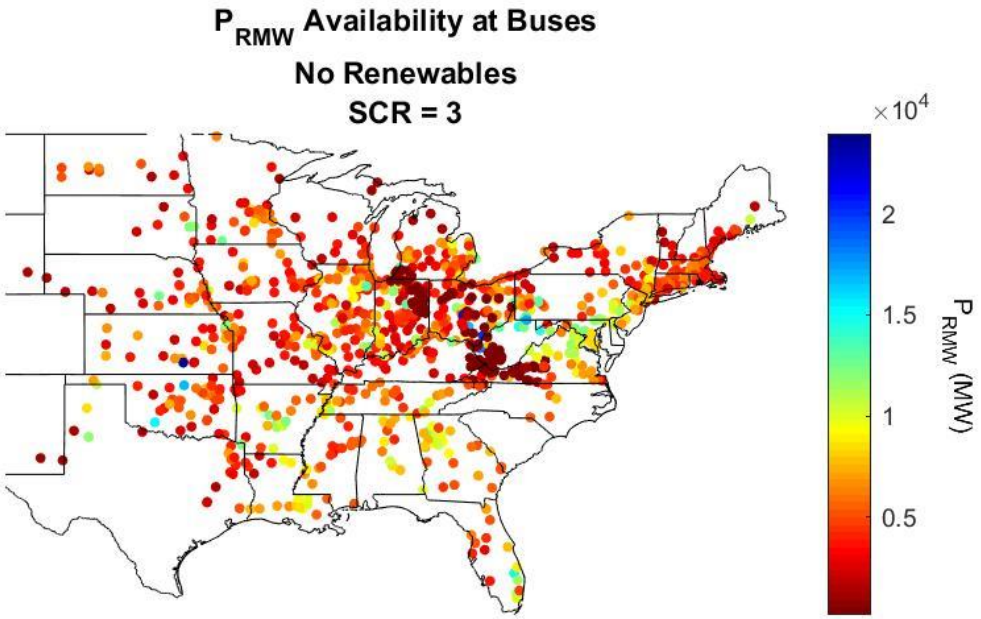

Fig. 31. IBR hosting capacity for no renewables case.

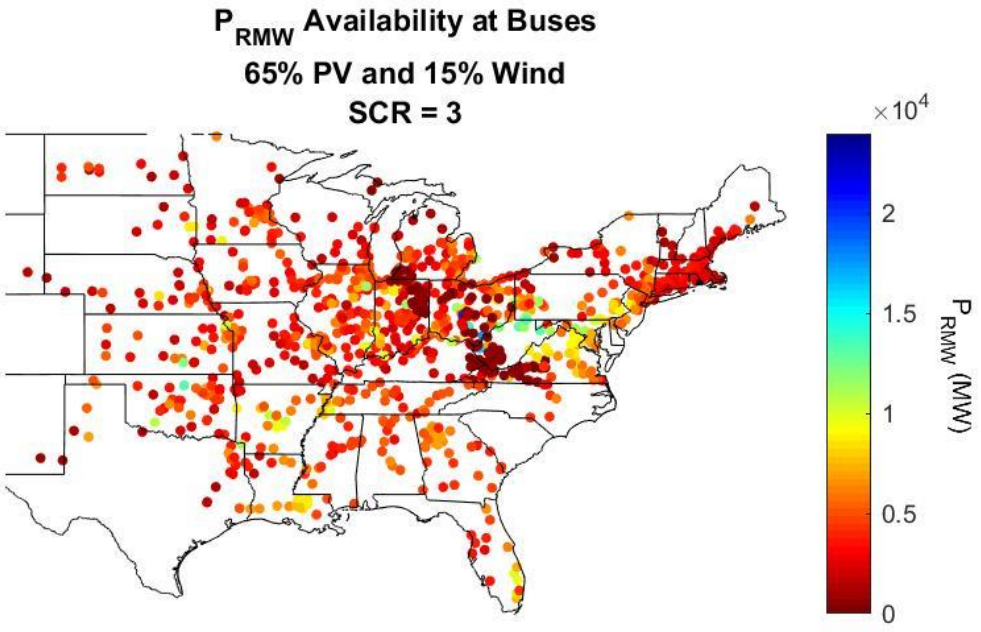

Fig. 32. IBR hosting capacity for 80% renewables case.

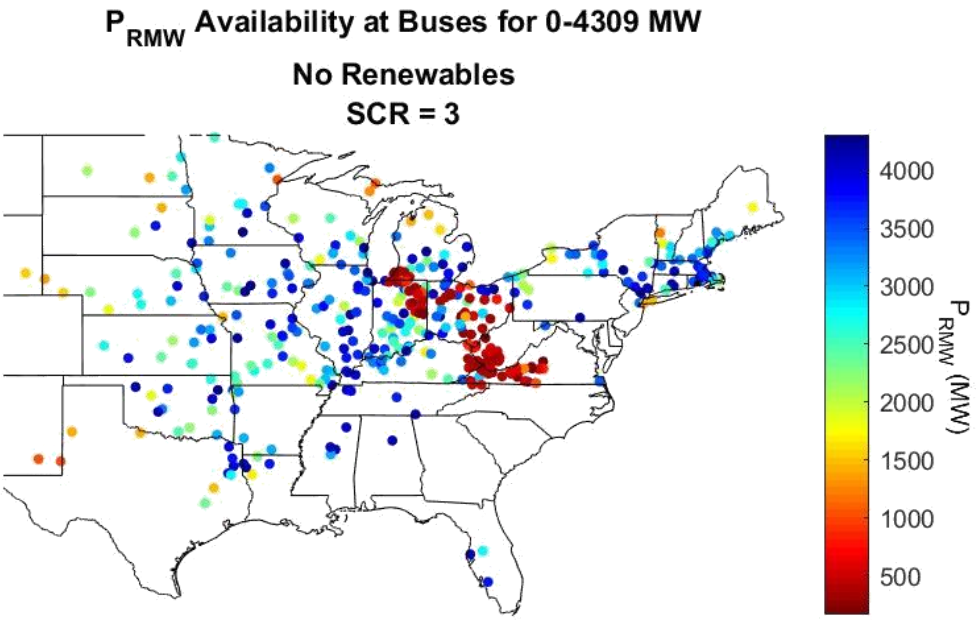

Fig. 33. IBR hosting capacity for no renewables case – segment 1.

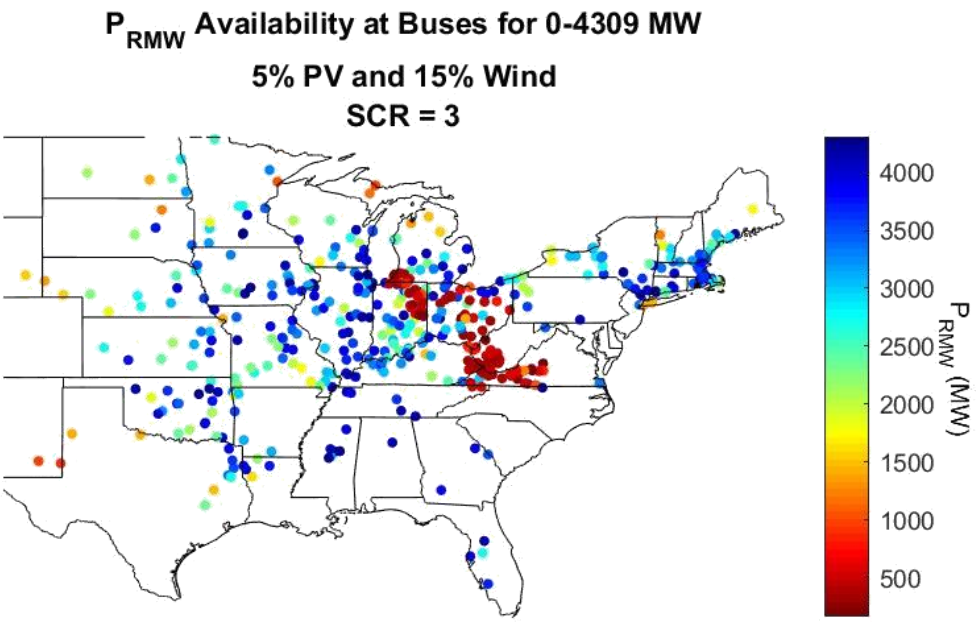

Fig. 34. IBR hosting capacity for 20% renewables case – segment 1.

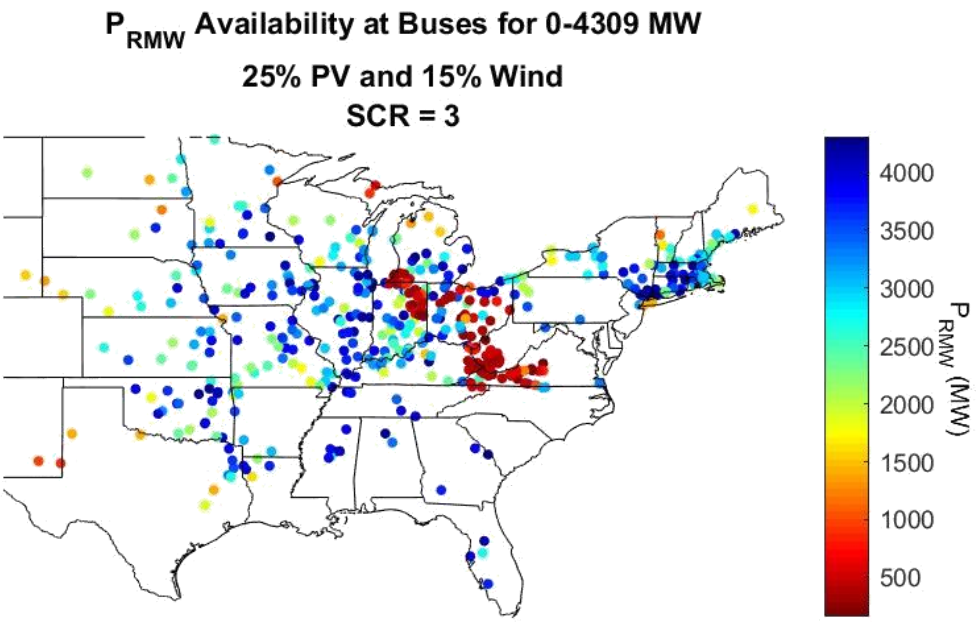

Fig. 35. IBR hosting capacity for 40% renewables case – segment 1.

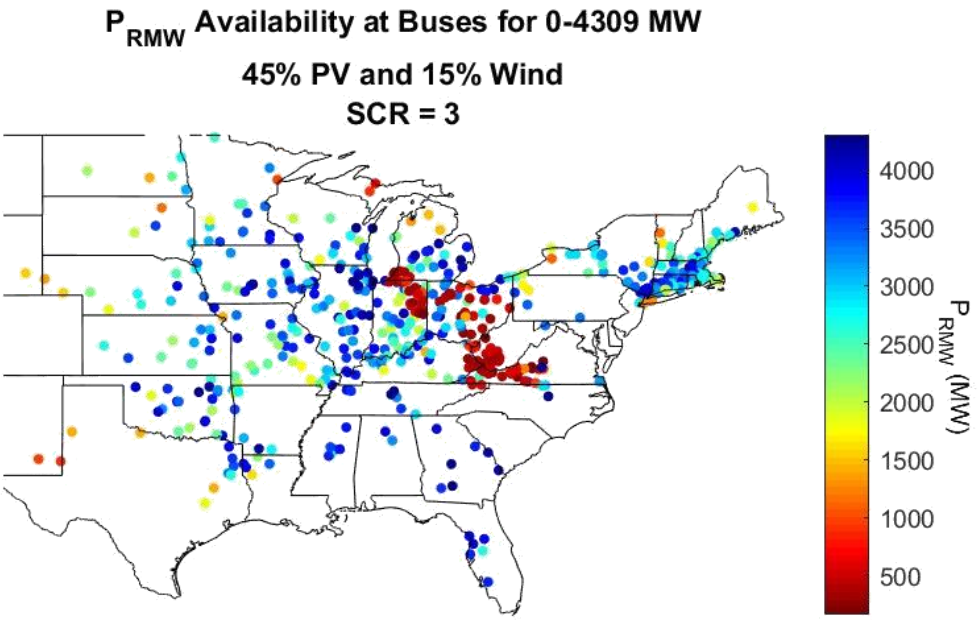

Fig. 36. IBR hosting capacity for 60% renewables case – segment 1.

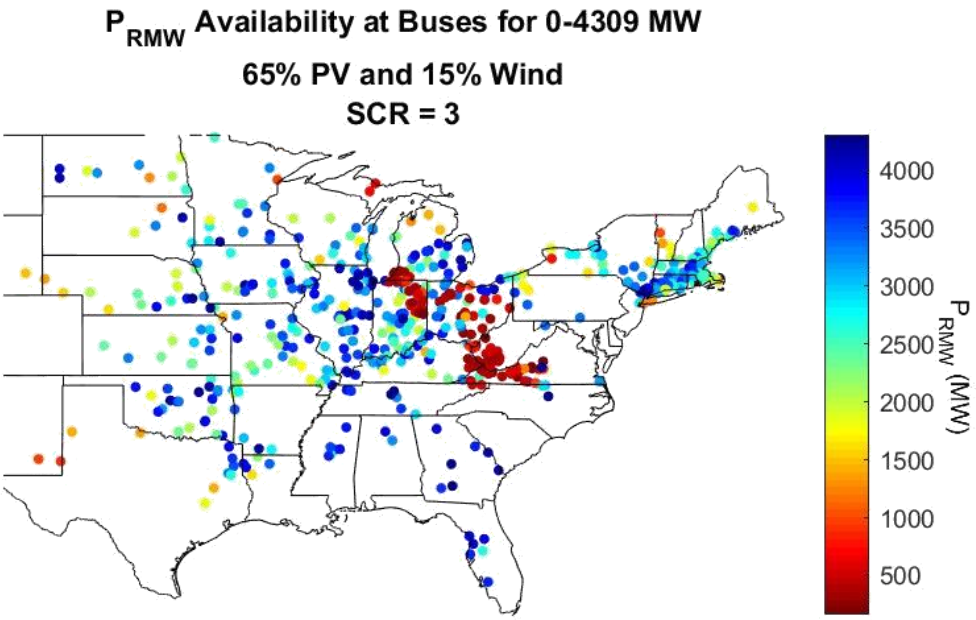

Fig. 37. IBR hosting capacity for 80% renewables case – segment 1.

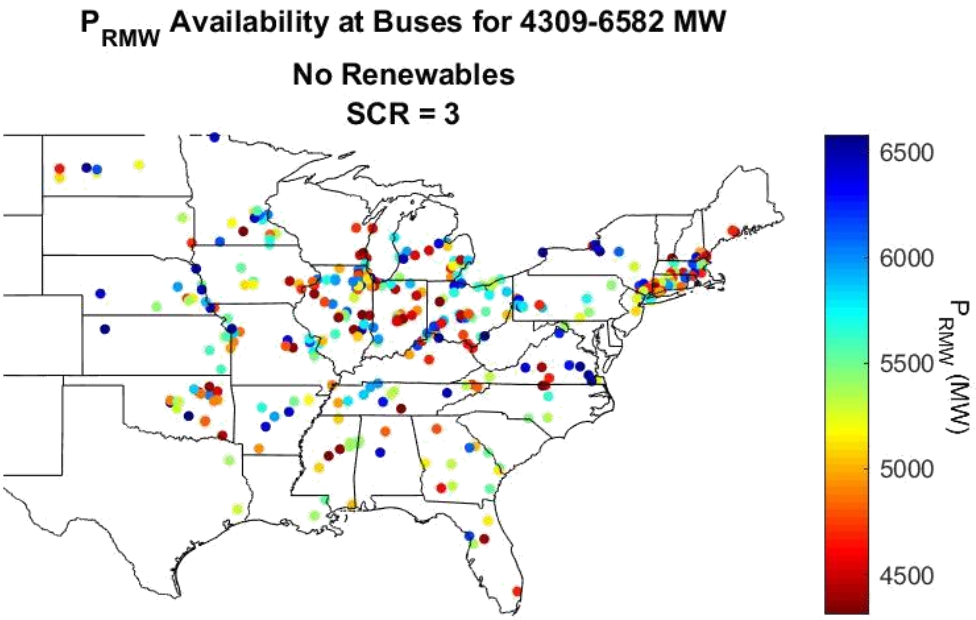

Fig. 38. IBR hosting capacity for no renewables case – segment 2.

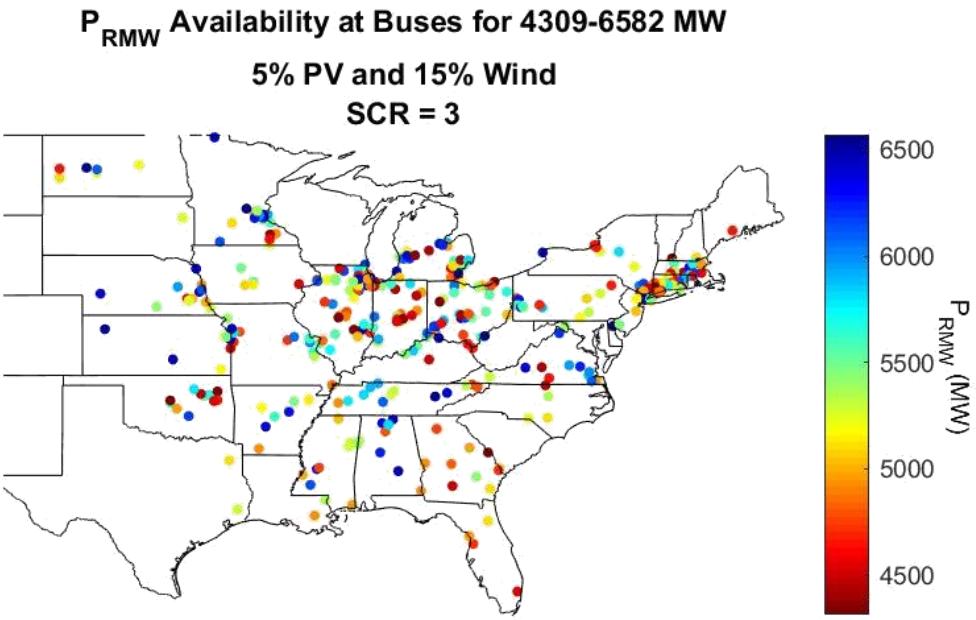

Fig. 39. IBR hosting capacity for 20% renewables case – segment 2.

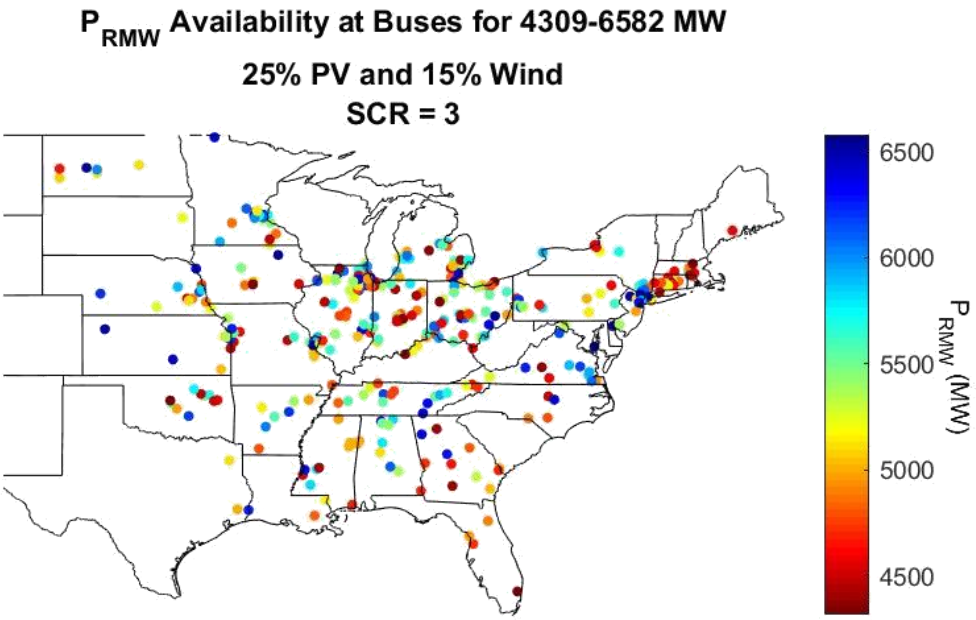

Fig. 40. IBR hosting capacity for 40% renewables case – segment 2.

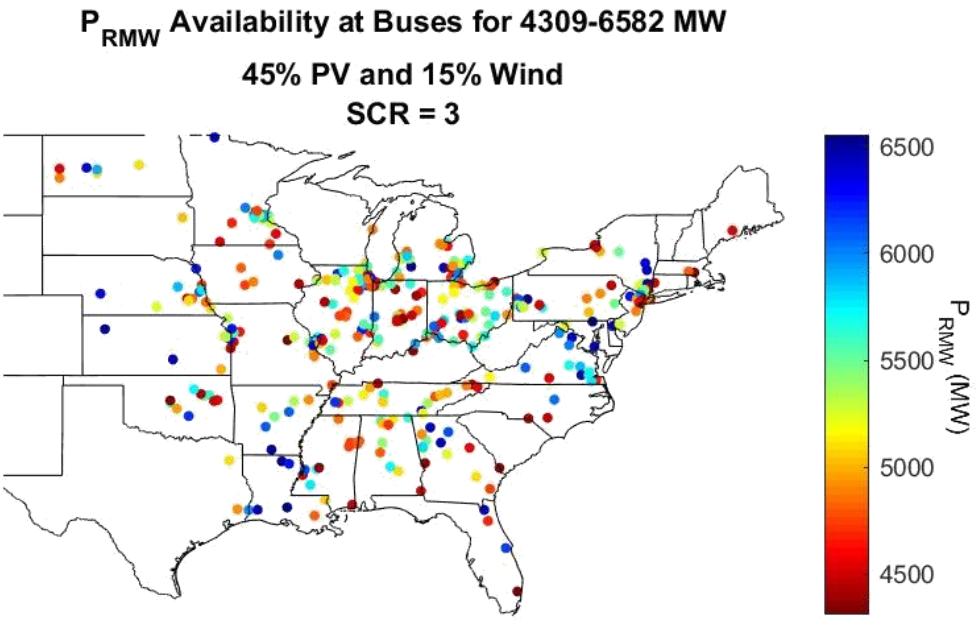

Fig. 41. IBR hosting capacity for 60% renewables case – segment 2.

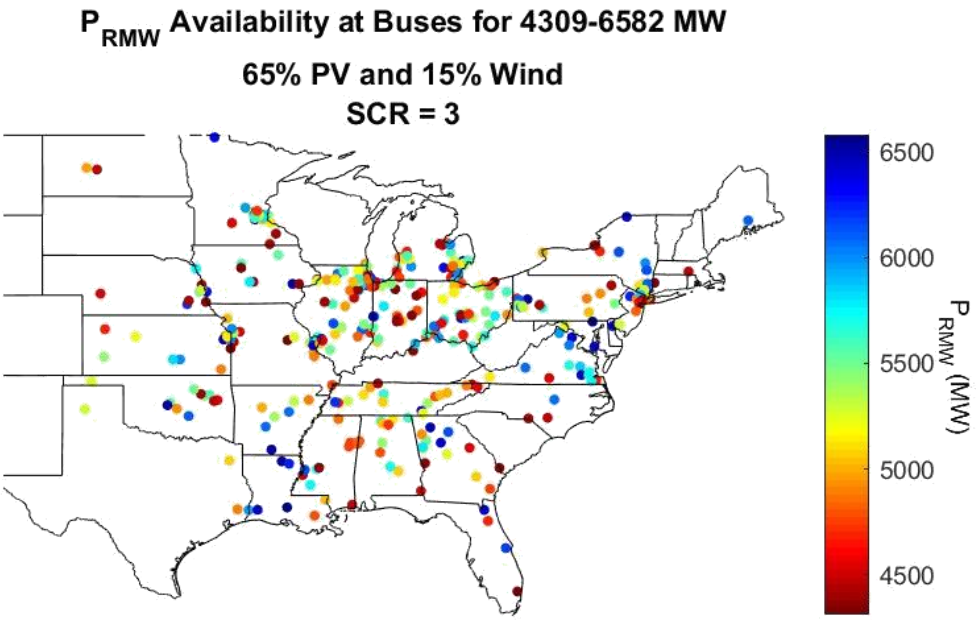

Fig. 42. IBR hosting capacity for 80% renewables case – segment 2.

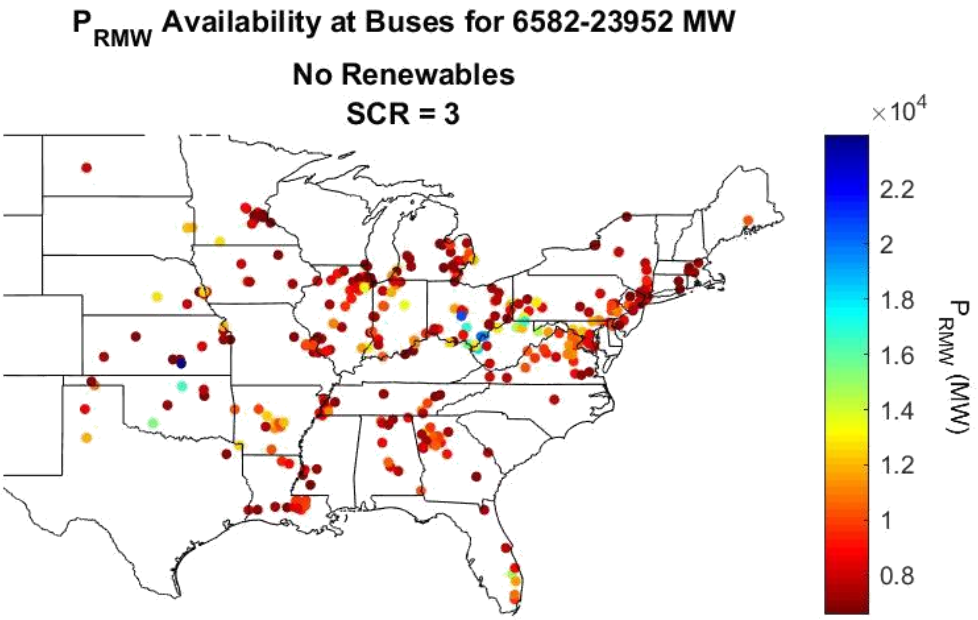

Fig. 43. IBR hosting capacity for no renewables case – segment 3.

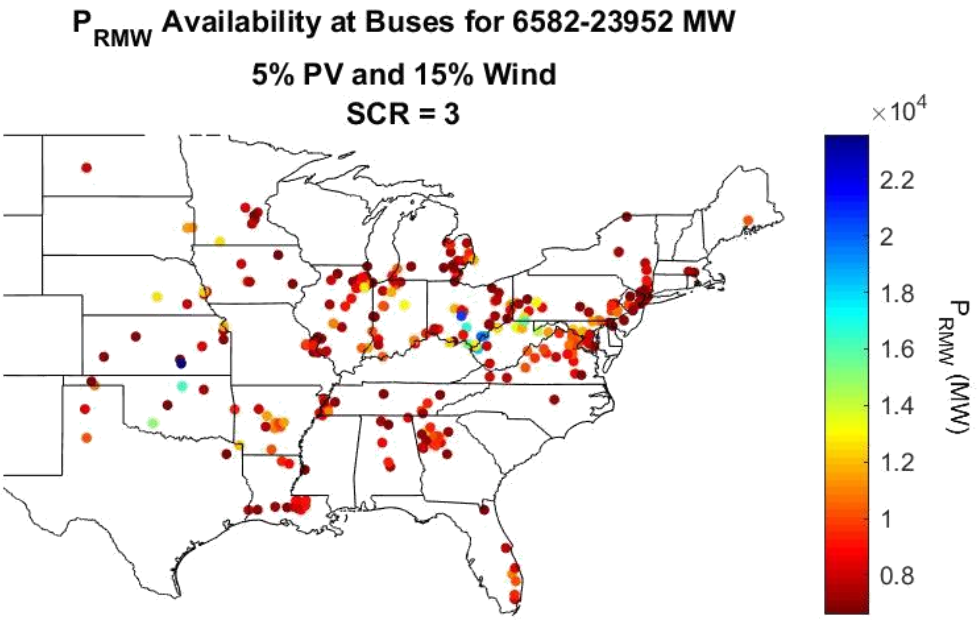

Fig. 44. IBR hosting capacity for 20% renewables case – segment 3.

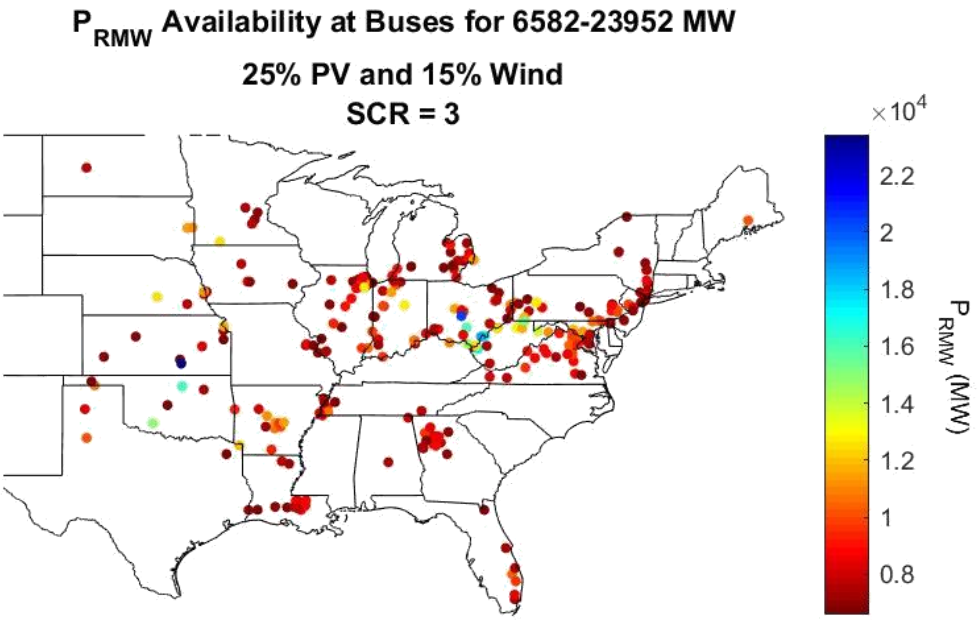

Fig. 45. IBR hosting capacity for 40% renewables case – segment 3.

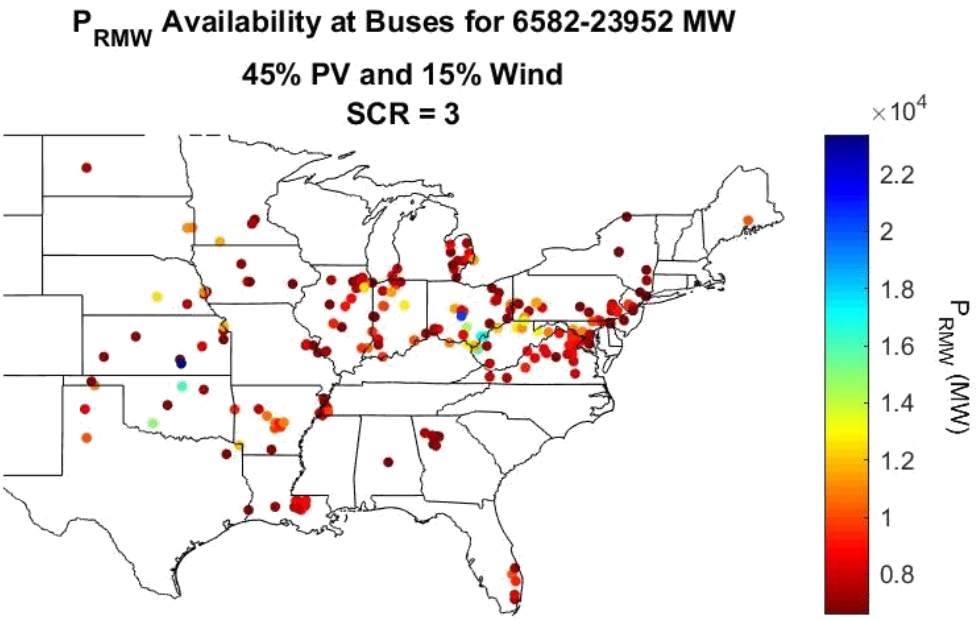

Fig. 46. IBR hosting capacity for 60% renewables case – segment 3.

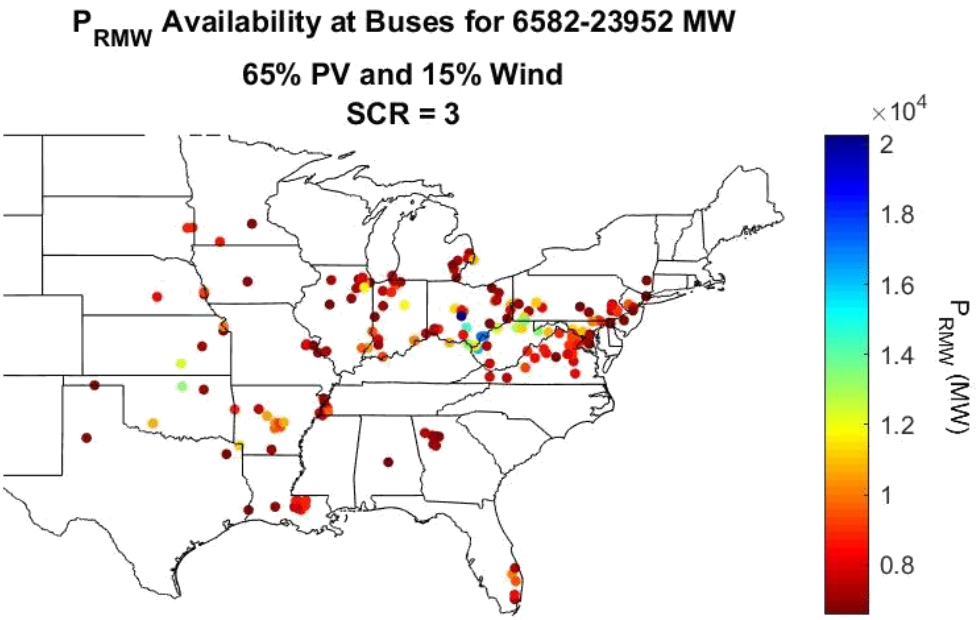

Fig. 47. IBR hosting capacity for 80% renewables case – segment 3.

Table 4 shows the comparison for the IBR hosting capacity with increasing levels of renewables on the grid. It shows the minimum, maximum, average, and median generator rating that can be added before the grid becomes weak. It can be seen that as an increasing level of renewables are already on the system, there is less capacity for adding more.

1.4 Analysis of Grid Strength on the Western Interconnection when Converting all Synchronous Generation to IBR

1.4.1 Model Overview

The analysis in this section was performed using a 2019 summer Western Electricity Coordinating Council (WECC) PSS®E case.

1.4.2 Method

The method used for this section is the same as described in Section 1.2.2, converting all the synchronous generators at the same time.

1.4.3 Results

The impact on SCMVA when converting all conventional synchronous generation to IBR is shown in Fig. 48.

The available hosting capacity for the base case is shown in Fig. 49. Fig. 50 displays the hosting capacity available after the hosting capacity has been converted to IBRs. Segmented graphs are shown in Fig. 51-Fig. 56.

Similar to the other test cases, we can see from Fig. 49-Fig. 56 that as the IBR increases the IBR hosting capacity at each bus decreases.

1.5 Conclusion

As observed in the results, the SCMVA decreases when IBR is added.

Table 4. P_{RMW} value comparison for differing renewable levels.

	min (MW)	max (MW)	avg (MW)	med (MW)
0WT 0PV	164.48	23951.99	5714.05	5367.39
15WT 5PV	164.47	23579.58	5394.18	5036.39
15WT 25PV	164.41	23414.25	5093.79	4731.34
15WT 45PV	164.24	23392.01	4787.85	4473.70
15WT 65PV	164.24	20271.85	4603.74	4332.05

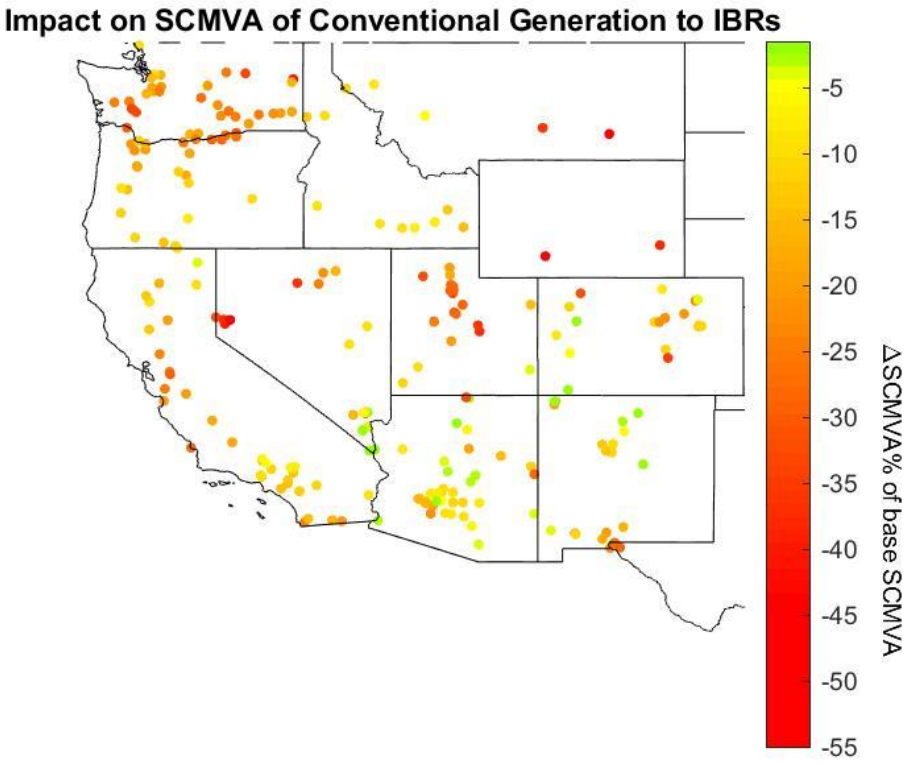

Fig. 48. Impact on SCMVA when converting conventional generation to IBR on WECC system.

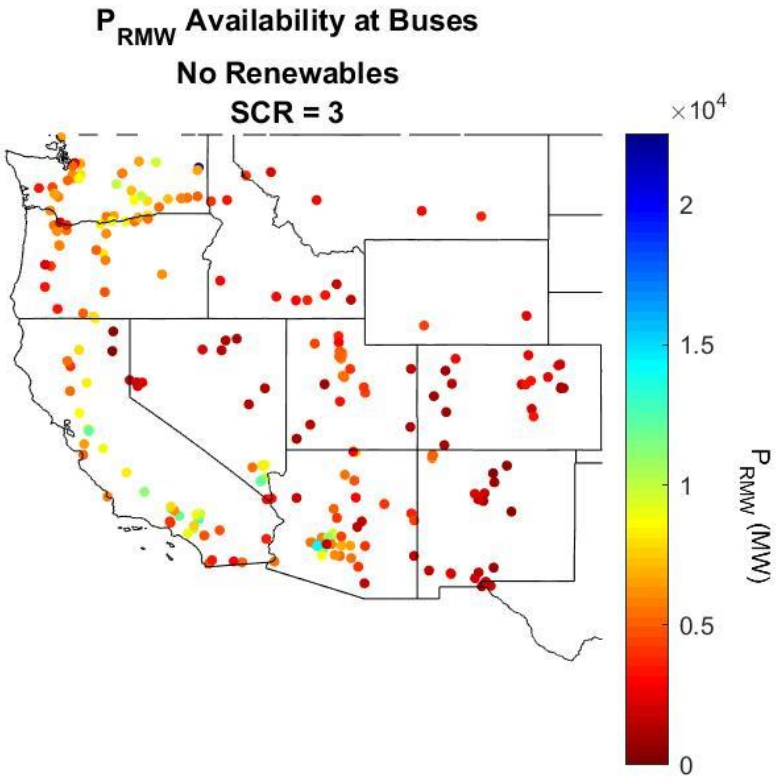

Fig. 49. IBR hosting capacity for WECC base case.

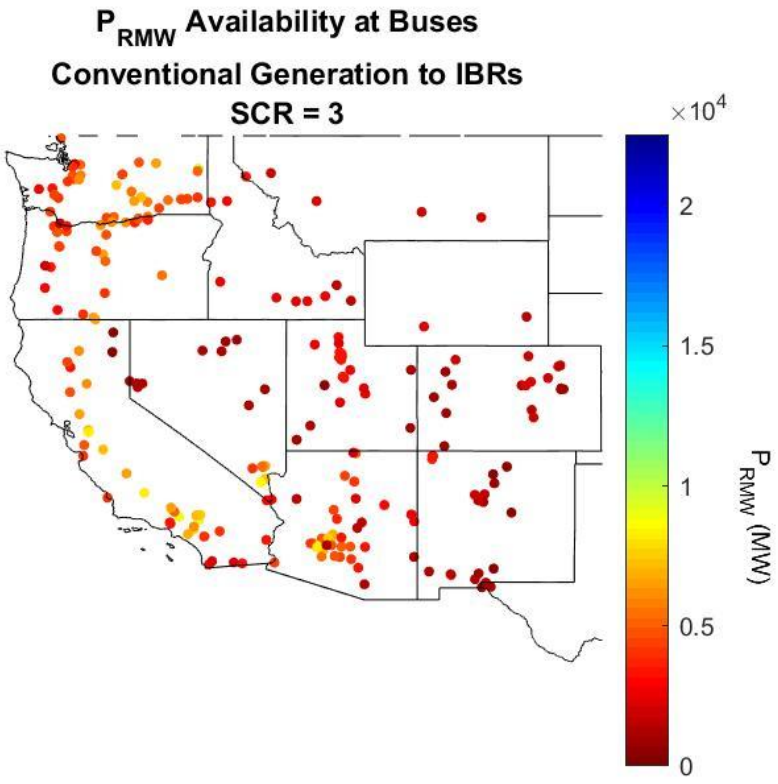

Fig. 50. IBR hosting capacity for WECC converted fully renewable.

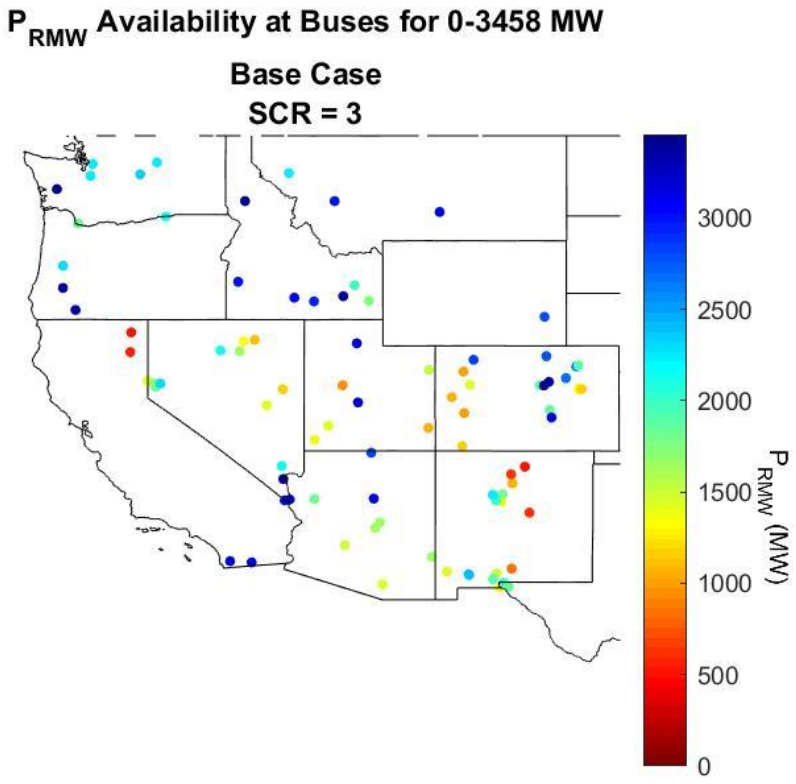

Fig. 51. IBR hosting capacity WECC base case – segment 1.

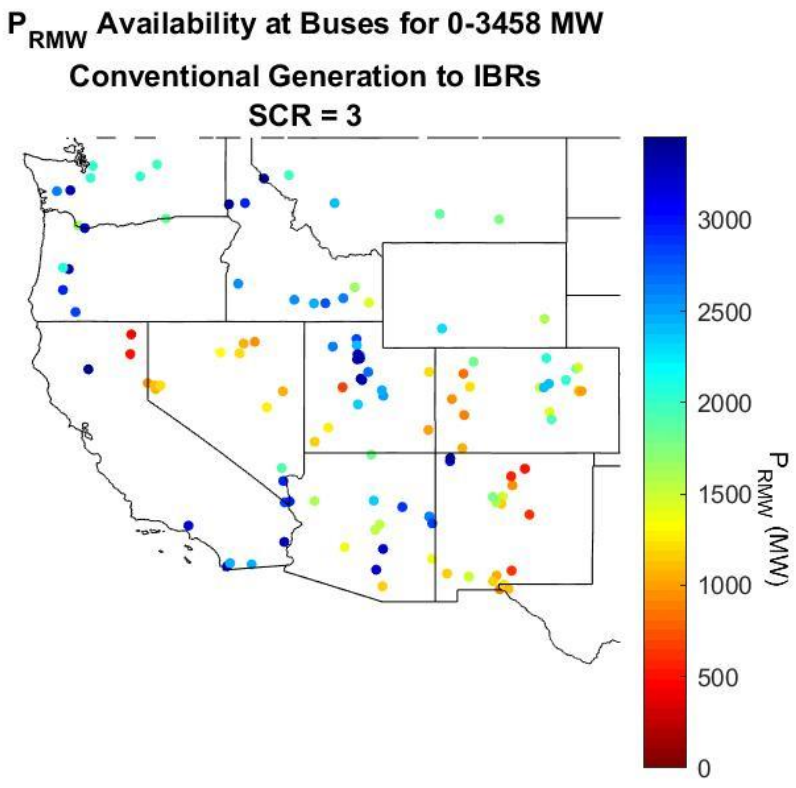

Fig. 52. IBR hosting capacity WECC fully renewable case – segment 1.

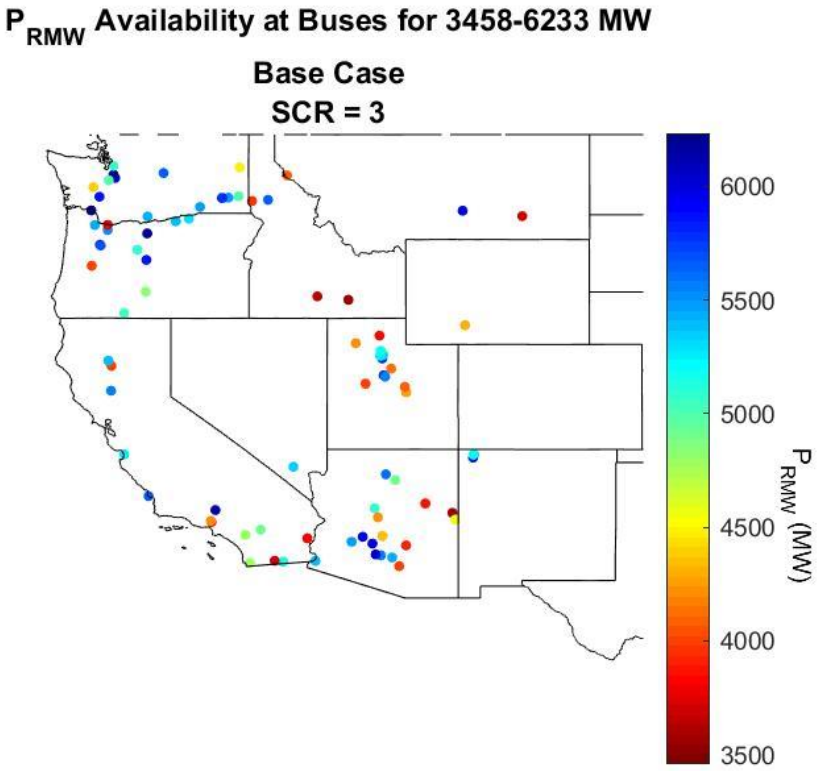

Fig. 53. IBR hosting capacity WECC base case – segment 2.

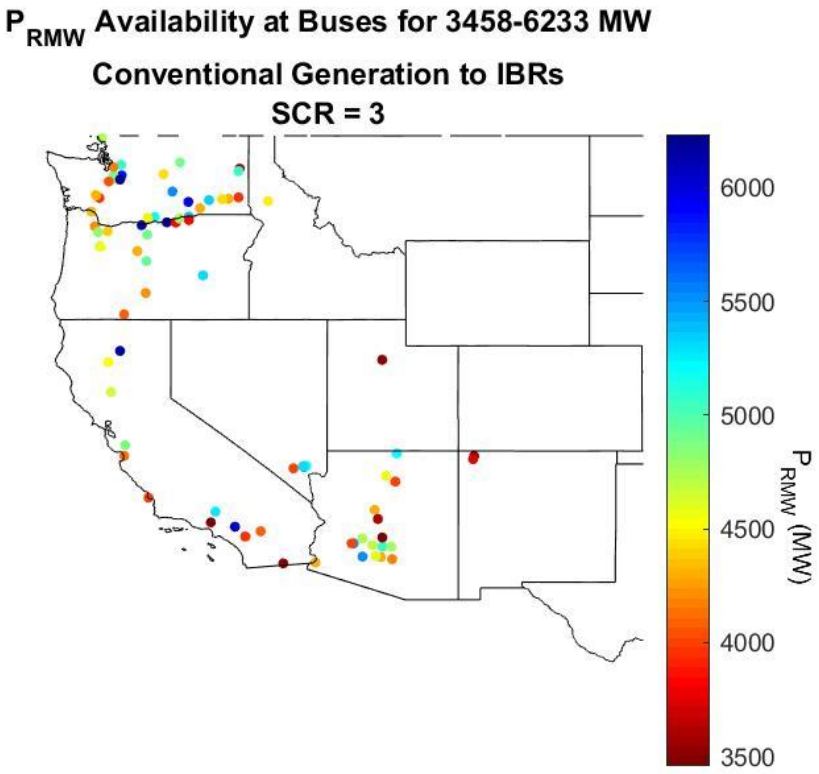

Fig. 54. IBR hosting capacity WECC fully renewable case – segment 2.

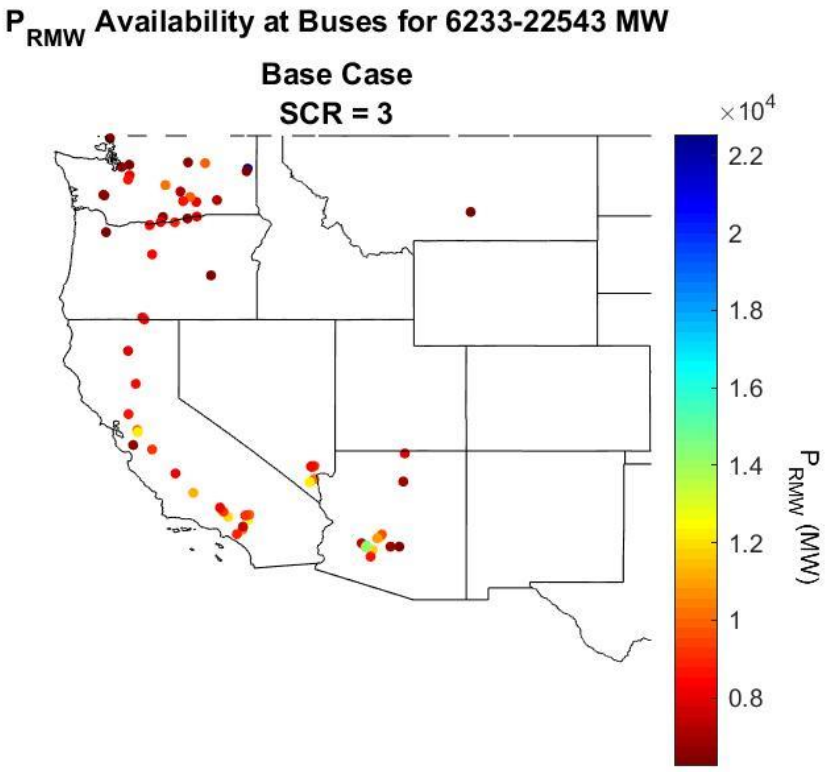

Fig. 55. IBR hosting capacity WECC base case – segment 3.

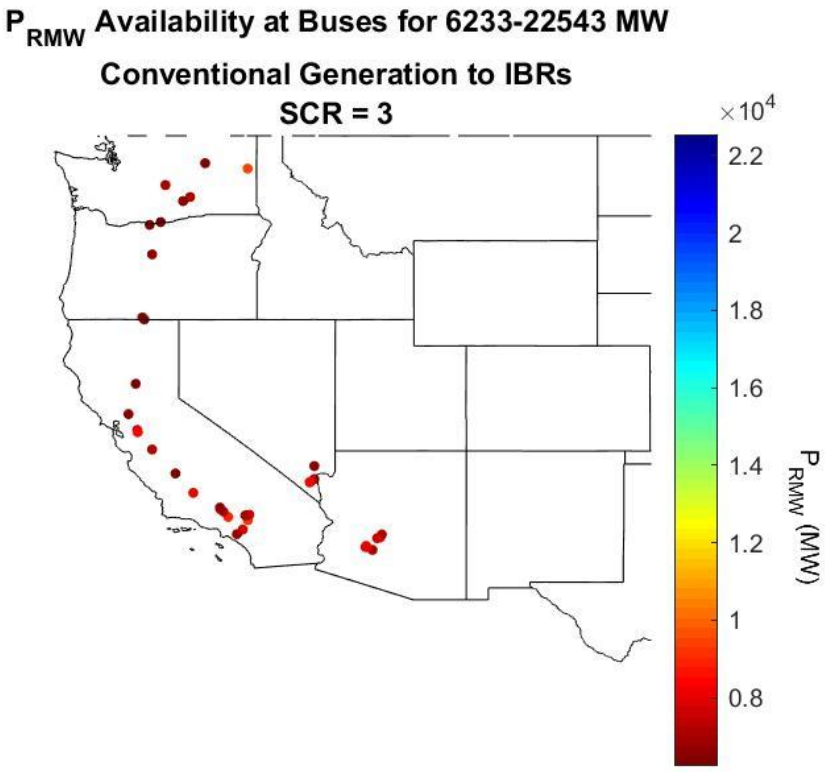

Fig. 56. IBR hosting capacity WECC fully renewable case – segment 3.

Further from the second test case it can be seen that SCMVA decreases more at each level of increased PV penetration. This work also shows the potential for additional IBR that could be added at each bus before the grid becomes weak. These results show how the grid strength changes with increased IBR, and the hosting capacity map identifies areas that are weaker which can be used to identify areas to add voltage assistance in the future.

1.6 Future Work

This topic has a lot of opportunity for future expansion such as calculating the SCMVA under contingency analysis, calculating variations of the SCR, or studying placement of where IBR would be installed instead of directly replacing the machines.

CHAPTER TWO
IMPACT OF HIGH PV PENETRATION ON TRANSIENT STABILITY — A CASE STUDY ON THE U.S. ERCOT SYSTEM

2.1 Introduction

The penetration of PV is increasing in many power systems due to concerns on environments and climate change. PV power plants have many unique physical features compared with conventional power plants. The increasing penetration of PV is changing many aspects on power system planning and operation.

Transient stability focuses on the capability of the system to keep synchronism under various disturbances in power systems [12] [13]. Typical theoretical study and demonstration on transient stability is usually based on a single machine and infinite bus system. Factors that influence transient stability include the generator loading condition, generator output during the fault, fault-clearing time, the infinite bus voltage magnitude (point of connection voltage magnitude), and etc. The dominant method for transient stability analysis for multi-machine power systems is time domain simulation based on numerical integration on differential equations and solving algebraic equations [14].

Some studies have already started to investigate the impact of PV on transient stability. Ref. [15] conducted a study on the WECC system and found that PV can have both detrimental and beneficial impact on the transient stability. The beneficial impact is generally associated with the fact that increased PV

penetration usually represents more distributed generation, thus losing one transmission component will be less likely to lead to severe consequences. The detrimental impact comes from high PV penetration usually resulting in larger voltage perturbation.

Ref. [16] studied the system transient stability by integrating PV generation to the New England test system. It found that the PV power plants could significantly change the voltage profile after disturbance and make the system more vulnerable to stability problems. Ref. [17] studied the impact of PV on the IEEE-39 bus system when PV plants operate at unity power factor (zero reactive power output). Its simulation results showed that the higher PV penetration will impair the transient stability of the study system. Also based on the IEEE-39 bus system, the study in Ref. [18] found that if PV plants can provide voltage control during disturbance, voltage recovery during faults can be improved, thus enhancing transient stability. It is also demonstrated that under-voltage disconnection of PV can be detrimental to system stability since it will result in more significant excursions after disturbances.

The study in [19] investigated the stability of the Ontario system with large-scale PV under various scenarios, namely distributed units, centralized farms with and without voltage control capabilities. The result showed that the centralized PV farms working in voltage control or unity power factor mode, which are modeled as PV or PQ generators, have no major impact on the system transient stability. On the other hand, the distribution PV units, which are

modelled as negative PQ loads, can significantly improve the voltage and transient stability. The underlying main reason of this improvement is that the increase of distributed PV corresponds to the reduction of load, thus improving transient stability metrics such as the critical clearing time. Ref. [20] displaced conventional generators by PV in a nine-bus model and found that the transient stability may be negatively affected by PV due to reduced inertia and higher generator reactance. This study also showed that the impact will be more serious if PV plants are simultaneously disconnected due to low voltage caused by disturbances. Ref. [21] utilized the IEEE 39-bus New England system to study the impact of PV on transient stability. Conducting small signal stability analysis and transient simulations, this study found that the factors pertaining to the detrimental or beneficial impact of PV on transient stability were the unit commitment and dispatch, and the protection/control strategy of PV during voltage swell or dip. Ref. [22] studied the impact of PV on a nine-bus system and found that PV generation deteriorates the stability of the system, while the P-V control mode of PV generation is better for transient stability compared with the P-Q control mode. Ref. [23] adopted the New England-New York test system and found that the integration of PV increases the angular separation of synchronous generators.

Although some studies have investigated some basic impact factors of PV generation to transient stability. The understanding of high PV generation on actual power systems is still unclear due to the complexity and non-linearity of

PV control's interaction with power system electro-mechanic dynamics. This paper studied the impact of up to 80% renewable penetration (with 65% PV) on the U.S. Electric Reliability Council of Texas (ERCOT) system model. Section 2.2 describes the high PV models of the ERCOT system. Section 2.3 presents the study results of high PV's impact on transient stability. The conclusion is given in Section 2.4.

2.2 Model Overview and Scenario Development

2.2.1 Model Overview

This study was based on a series of hypothetical models of ERCOT system under high PV situation. In a previous work supported by U.S. Department of Energy Solar Energy technologies Office [24][25][26][27][28][29]-[30], the high PV cases for the ERCOT system were developed in PSS®E for 5%, 25%, 45%, and 65% PV with 15% wind. The system consists of 6,102 buses and 690 machines.

2.2.2 Scenario Development

First, the effect of PV on transient stability was monitored on a small scale level. To study the impact of increasing PV penetration, conventional synchronous generators are gradually replaced by PV penetration. Three synchronous generators are displaced by PV power plants in steps, replacing one generator in each step. To monitor the effect of PV on transient stability, the W4 generator on bus 80411 was replaced with a PV generator. A dynamic simulation was run for 1 second, and then a fault was applied at bus 8958. The rotor angle was observed at bus 80411 to determine the critical clearing time

(CCT). This was done for the base case with no PV, and then repeated as each machine was transformed to PV. The PV machines were on bus 80411, generators W4, W2, and W3, respectively. A diagram with the location of the fault in relation to the PV machines is shown in Fig. 57.

Once the effect of adding just a few PV machines on transient stability is studied, the effect of adding many PV machines at the system level was then studied. First, the cases of 5%, 25%, 45%, and 65% PV with 15% wind each were studied. Then the study was made more granular to pinpoint at what percentage of renewables the transient stability was most effected.

2.3 Impact of PV Penetration on Transient Stability

2.3.1 Critical Clearing Time with Slight PV Increase

In order to determine if the CCT could be improved by increasing PV on the ERCOT system, machines were first changed to PV one at a time, up to three machines.

Fig. 58-Fig. 60 show the rotor angle when there was only one PV machine and the fault was cleared after 0.32 s, 0.33 s, and 0.34 s, respectively. When the fault is applied, the rotor angle is disturbed. If the rotor angle settles, then the case is stable. If the rotor angle diverges, then the case is unstable. It can be observed from Fig. 58-Fig. 60 that the addition of the PV machine slightly improves transient stability, since the CCT for the base case is 0.32 s, and the CCT for the case with the PV machine is 0.33 s. This can be seen by the “no PV” line diverging in Fig. 59 and then the “PV” line diverging in Fig. 60.

A second PV machine was then added to bus 80411 and the simulation

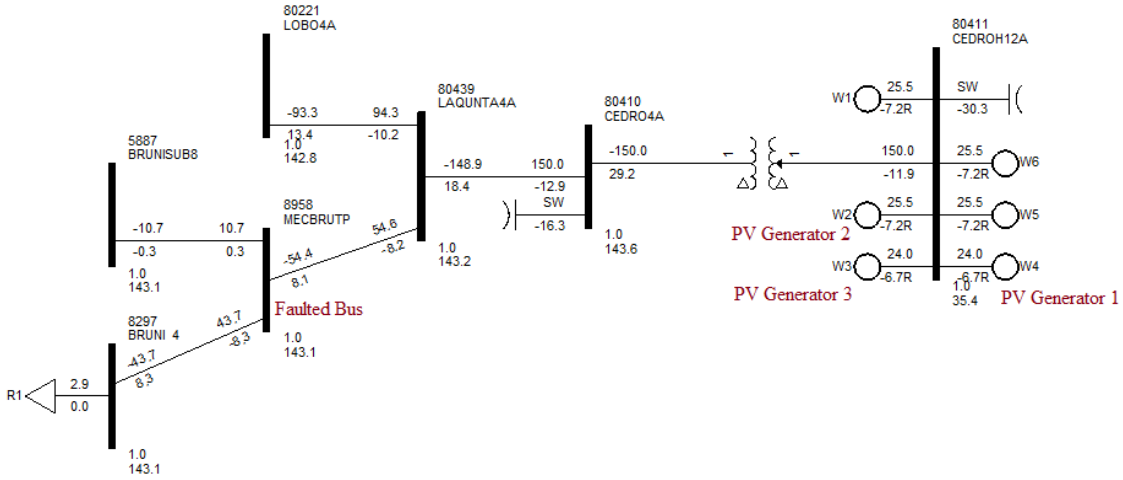

Fig. 57. PSS®E diagram of location of PV bus and faulted bus.

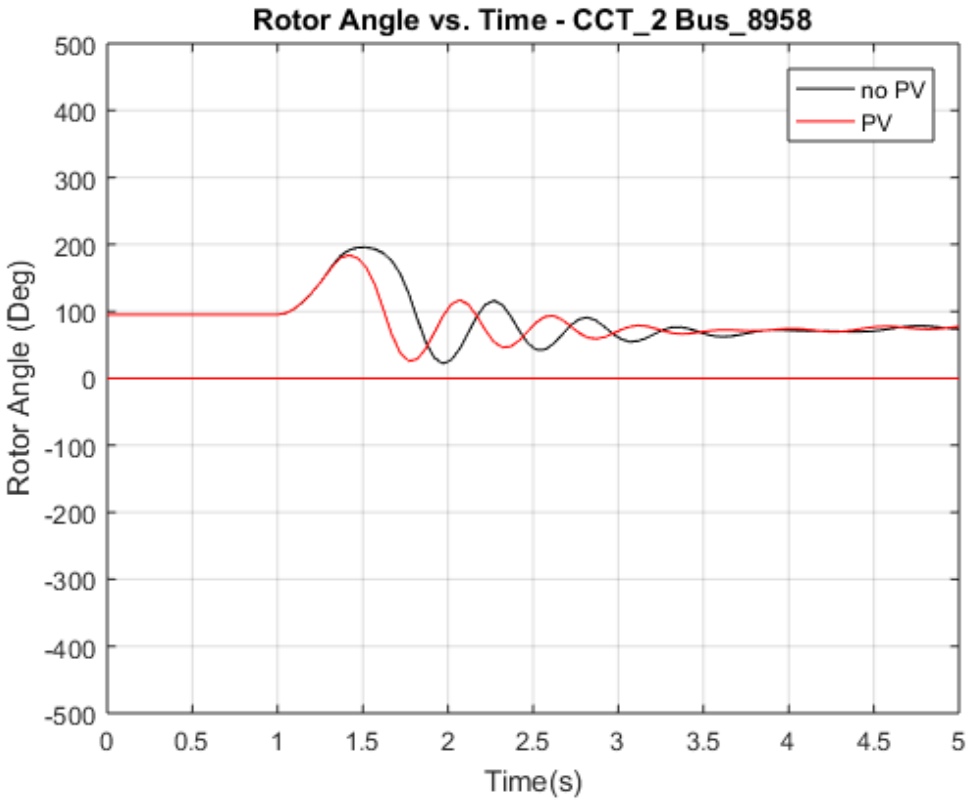

Fig. 58. Rotor angle when fault cleared after 0.32 s.

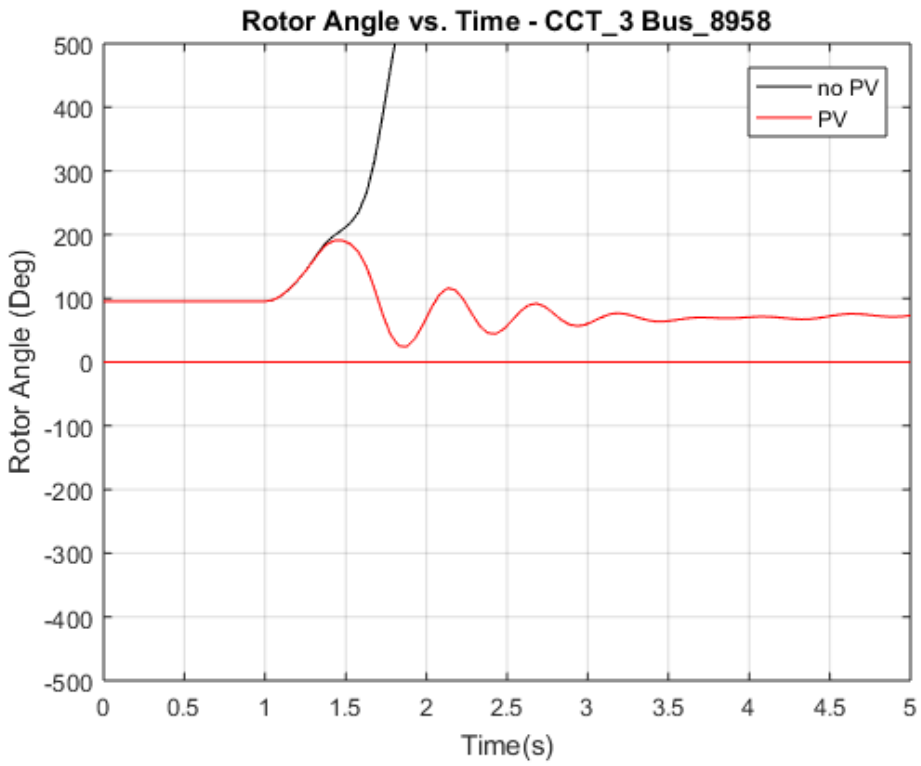

Fig. 59. Rotor angle when fault cleared after 0.33 s.

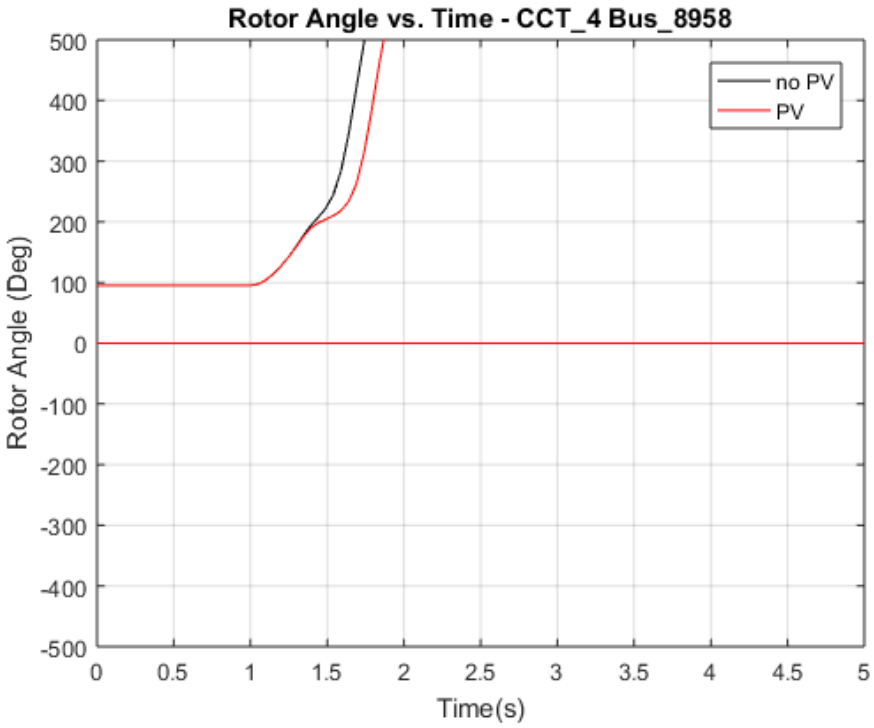

Fig. 60. Rotor angle when fault cleared after 0.34 s.

was run again. It was found that the CCT with two PV machines becomes 0.37 s, which is a further improvement from the CCT with one PV machine added.

To test further, a third generator was replaced with a PV machine and the simulation was run another time. The CCT with three generators replaced with PV machines was found to be 0.44 s.

Next the voltage was compared for the different cases at the CCT of the base case: 0.32 s. This is shown in Fig. 61. It can be seen that as PV is added, the voltage level decreases more during the fault, but the voltage recovers more quickly.

Although the voltage level during the fault decreases as PV increases due to limited reactive power current, which results in faster rotor speed acceleration and smaller CCT, the fast voltage regulation of PV inverters can recover voltage more quickly compared with conventional synchronous generators after faults, leading to CCT increase. From the results, it can be seen the fast voltage recovery has a larger impact when PV machines increase in a local area.

2.3.2 Critical Clearing Time with Varying Percentages of PV

Once the stability was tested with a few PV machines, it was then tested for four different percentages of renewables in the ERCOT system (5%, 25%, 45%, and 65% PV with 15% wind each). A fault was applied to a bus on the system and the rotor angles were plotted to determine the CCT. The rotor angles on buses that contained only synchronous generators for the 80% renewable case were plotted for all of the cases, so they could all be compared equally. The fault was first applied at bus 240, and then later the same test was run with the

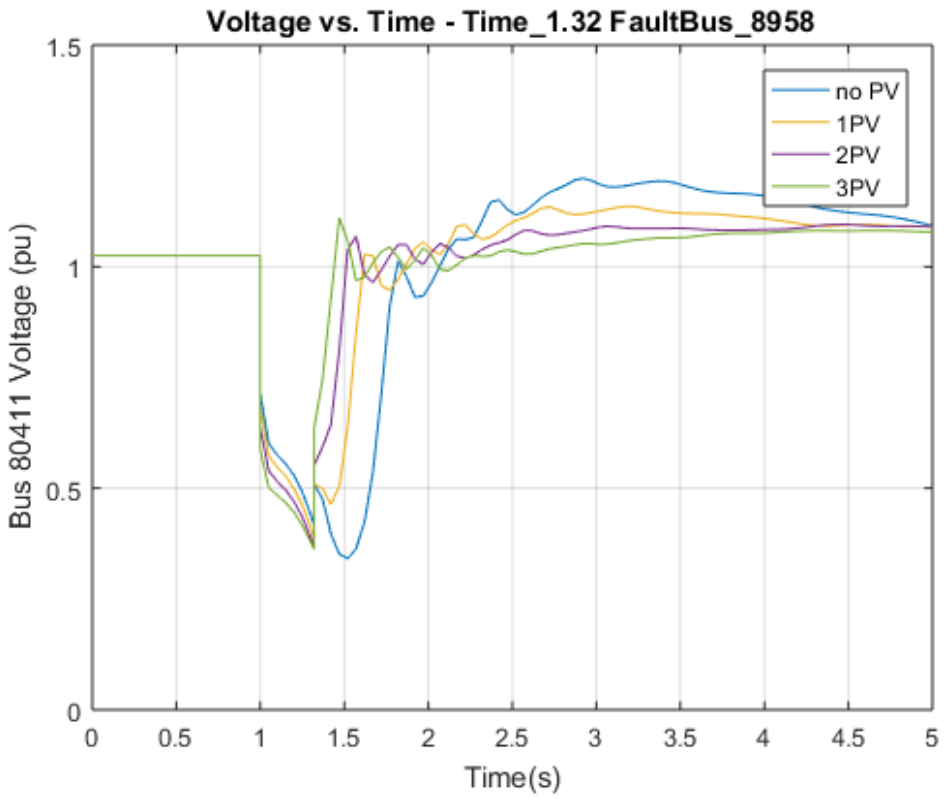

Fig. 61. Bus 80411 voltage for different amounts of PV Machines.

fault applied at bus 970 to confirm that the results would be similar with the fault on a different bus. To better view the results, the change in rotor angle was also plotted.

For the base case, with the fault on bus 240 the CCT was 0.25 s, and with the fault on bus 970 the CCT was 0.38 s. Fig. 62-Fig. 63 show the rotor angle for when the fault on bus 240 was cleared at 0.25 s after the fault and at 0.26 s, respectively. In Fig. 63 it is clear that the rotor angle diverges and therefore the system becomes unstable.

For the 20% renewable case (5% PV + 15% wind), with the fault on bus 240 the CCT was 0.25 s, and with the fault on bus 970 the CCT was 0.41 s. With the fault on bus 240, the CCT remained the same as the base case. With the fault on bus 970, the CCT increased slightly with the increase in PV.

For the 40% renewable case (25% PV + 15% wind), with the fault on bus 240 the CCT was 0.25 s, and with the fault on bus 970 the CCT was 0.39 s. With the fault on bus 240, the CCT remained the same. With the fault on bus 970, the CCT decreased slightly from the 20% renewable case with the increase in PV, although still an increased CCT from the base case.

For the 60% renewable case (45% PV + 15% wind), with the fault on bus 240 the CCT was 0.25 s, and with the fault on bus 970 the CCT was 0.31 s. With the fault on bus 240, the CCT remained the same. With the fault on bus 970, the CCT decreased by a tenth of a second from the 40% renewable case. This decrease also meant a CCT below that of the base case.

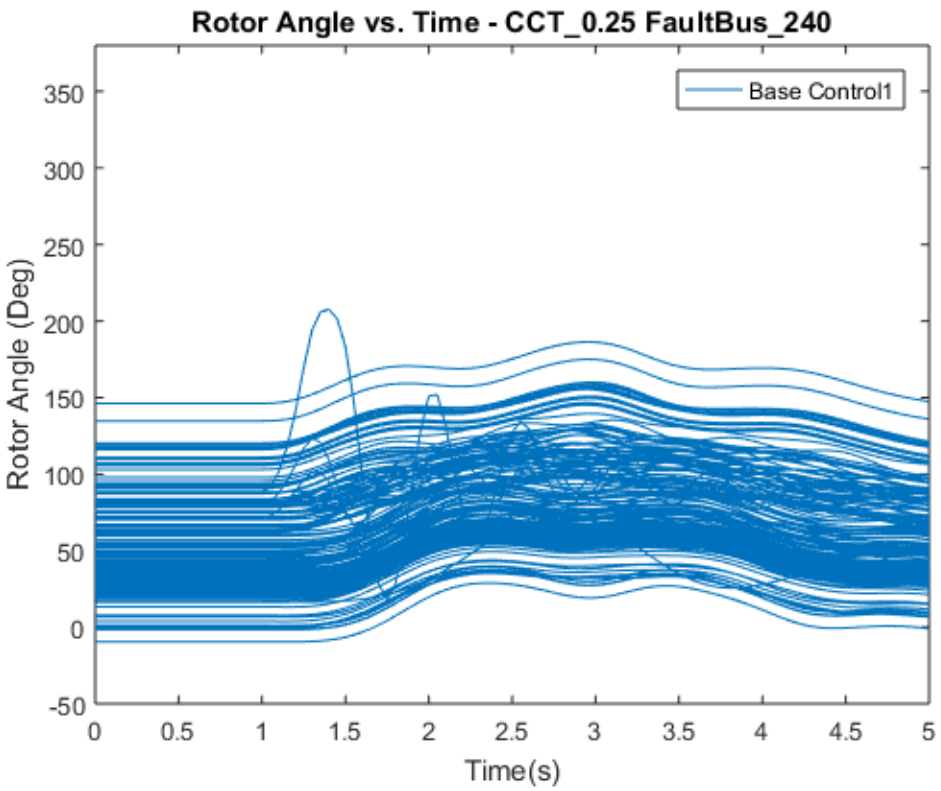

Fig. 62. Rotor angles when fault on bus 240 cleared at 0.25 s.

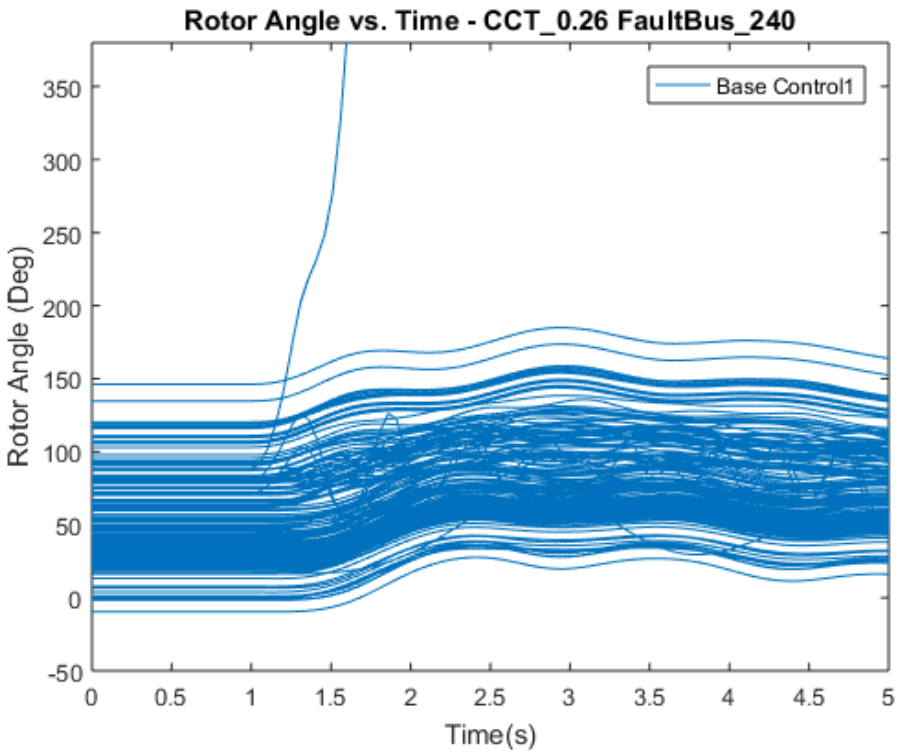

Fig. 63. Rotor angles when fault on bus 240 cleared at 0.26 s.

For the 80% renewable case (65% PV + 15% wind), with the fault on bus 240 the CCT was 0.01 s, and with the fault on bus 970 the CCT was 0.115 s. For both cases, the CCT decreased significantly.

The CCT results were then graphed, and those results are shown in Fig. 64-Fig. 65. From these results it was determined that more buses should be faulted to test if similar results would be achieved.

The CCT was then tested for faulting each bus above 200 kV. The results were similar to faulting buses 240 and 970, and a couple more examples are given in Fig. 66-Fig. 67, showing buses 1685 and 3109 faulted, respectively. From these it can be observed that while the transient stability is sometimes slightly improved by added PV, by the time the system has reached 80% renewables the transient stability is adversely effected.

2.3.3 Visualization of Critical Clearing Time for the ERCOT System

To better understand the impact of PV generation on overall transient stability of the ERCOT system, the CCT of multiple high voltage buses were simulated. A color map of the ERCOT system was then created testing the CCT for faulting each bus 200 kV and above. The maps were created for each renewable case: 0%, 20%, 40%, 60%, and 80%. Fig. 68-Fig. 72 contain the maps for each renewable case. The colors represent the CCT when the bus in that part of the ERCOT system is faulted. The CCT value for each faulted bus is mapped to its color using the color bar to the right of each map.

As can be seen from Fig. 68-Fig. 72, the effect on the CCT of adding PV

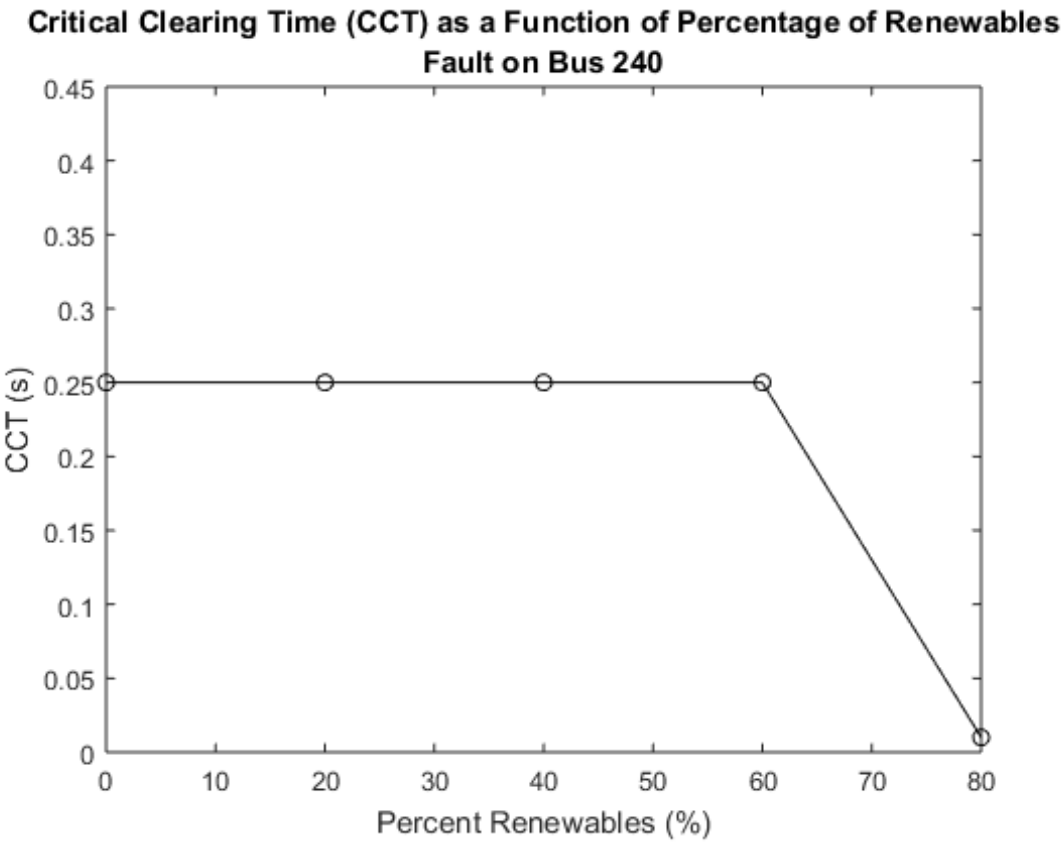

Fig. 64. CCTs for fault on bus 240.

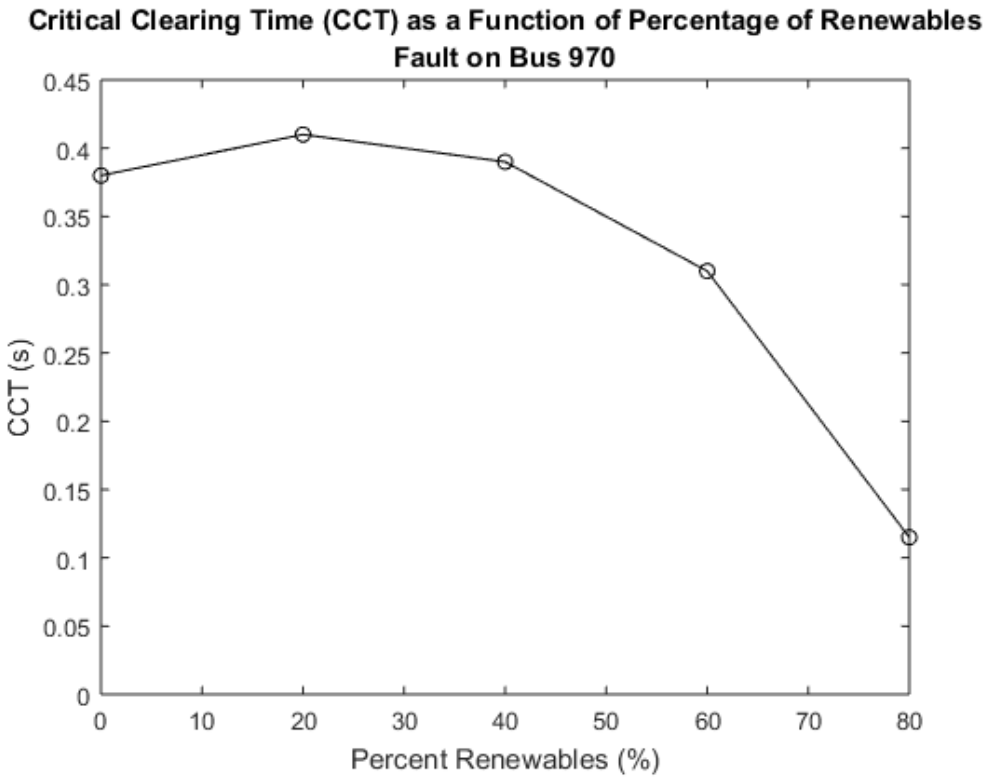

Fig. 65. CCTs for fault on bus 970.

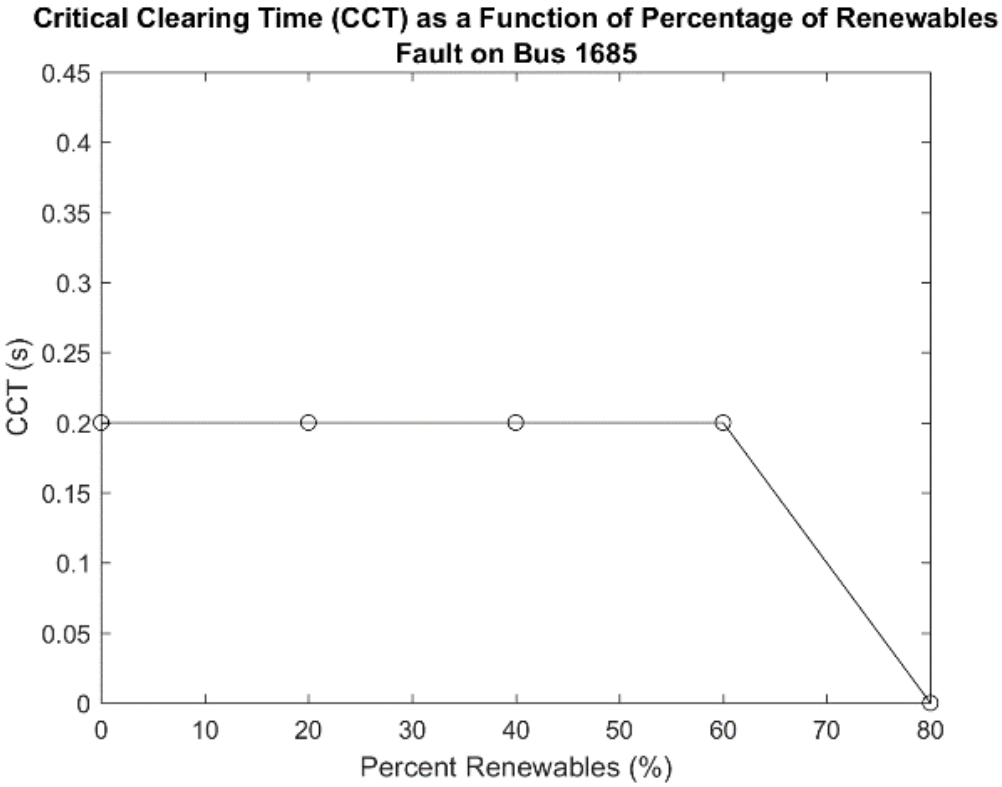

Fig. 66. CCTs for fault on bus 1685.

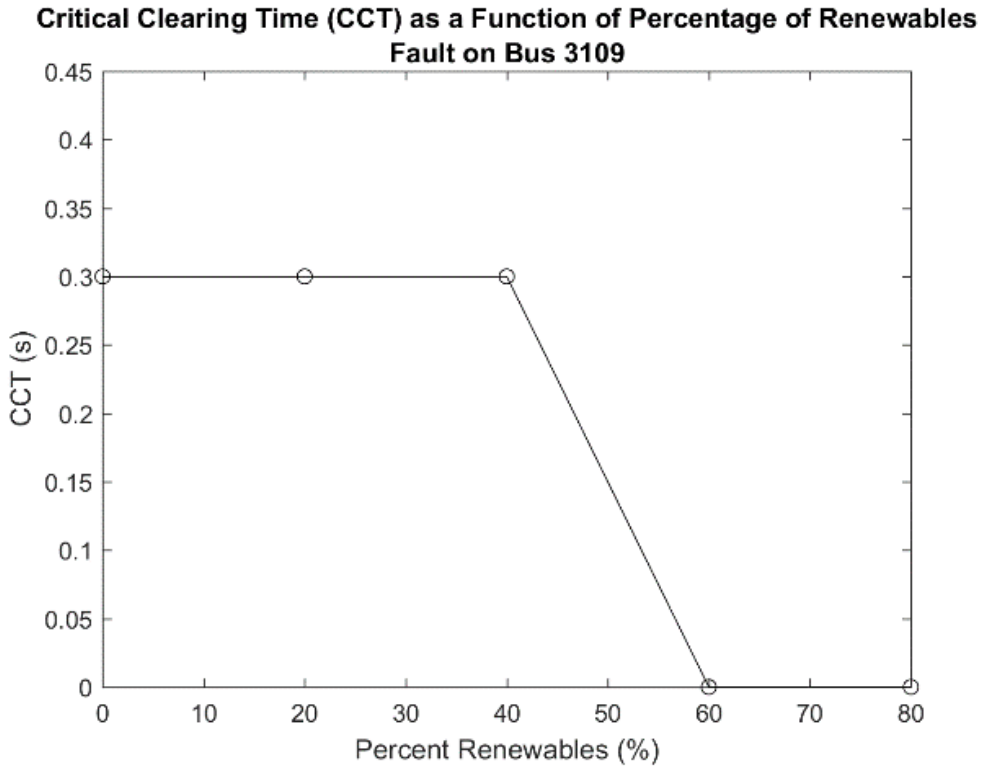

Fig. 67. CCTs for fault on bus 3109.

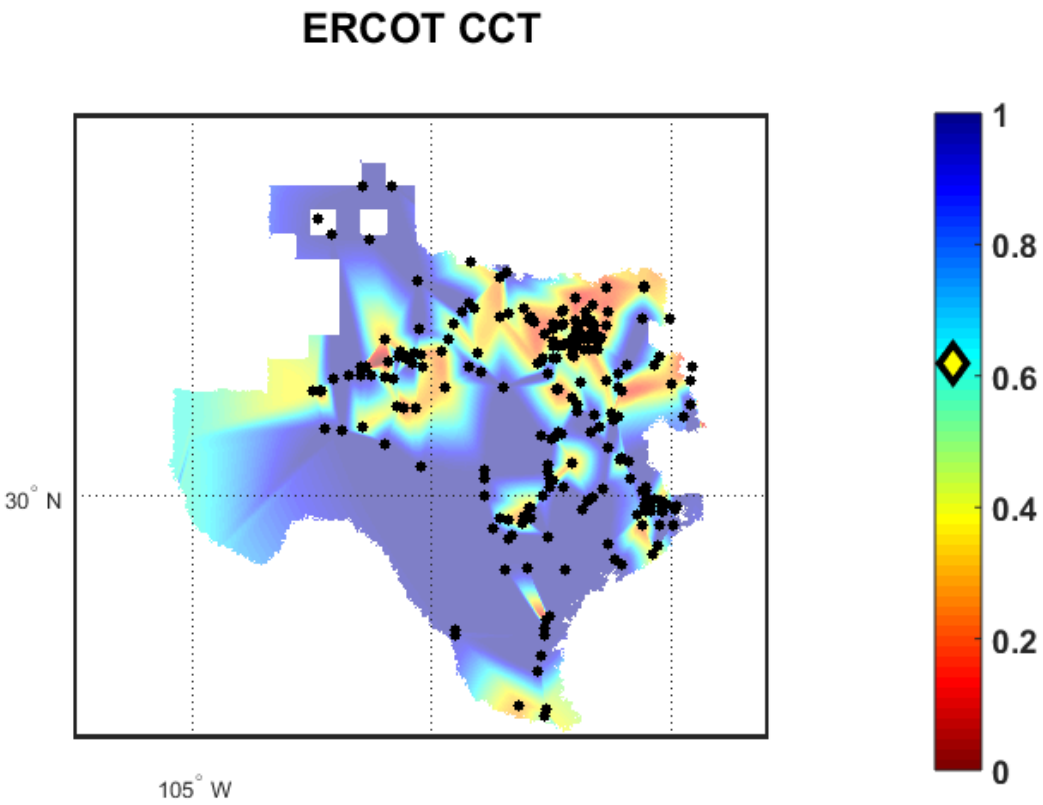

Fig. 68. Base case CCT map.

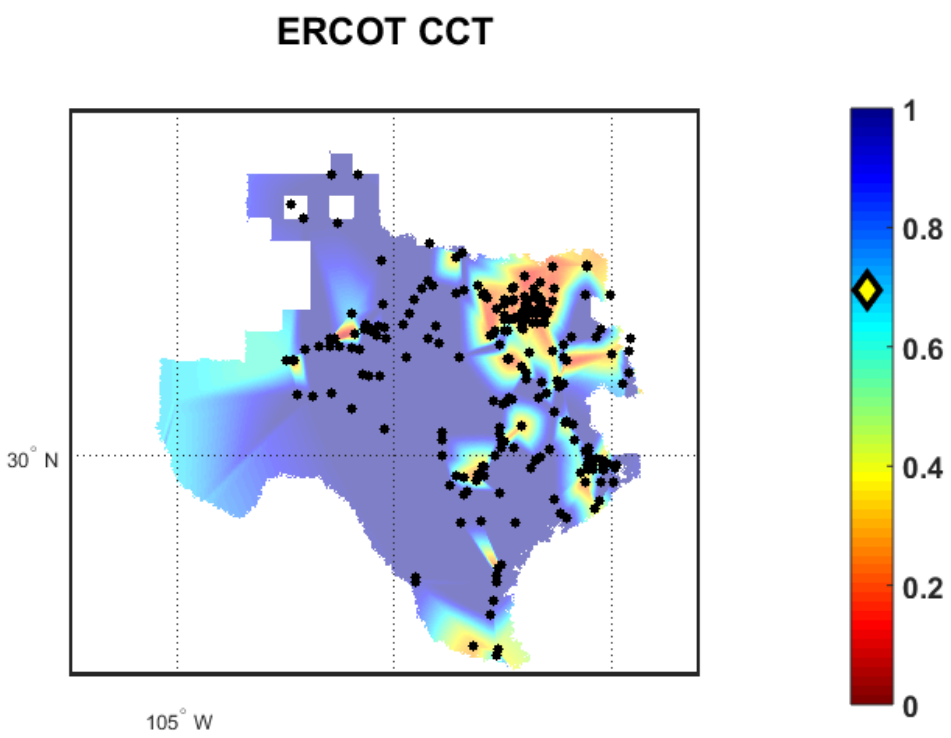

Fig. 69. 20% renewables CCT map.

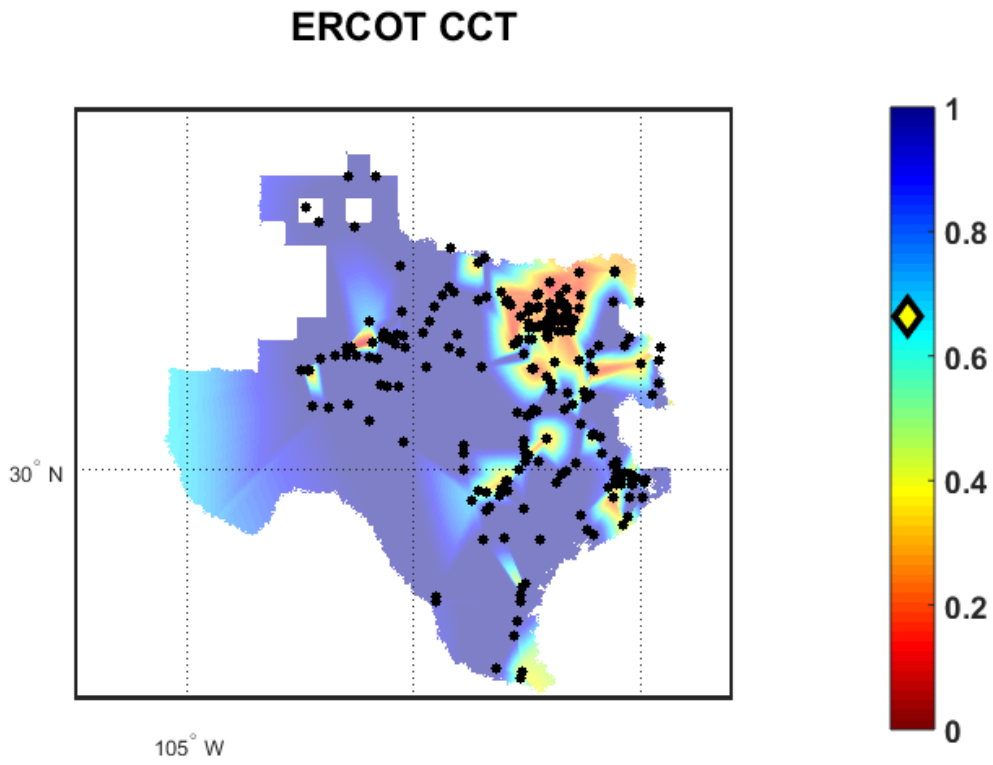

Fig. 70. 40% renewables CCT map.

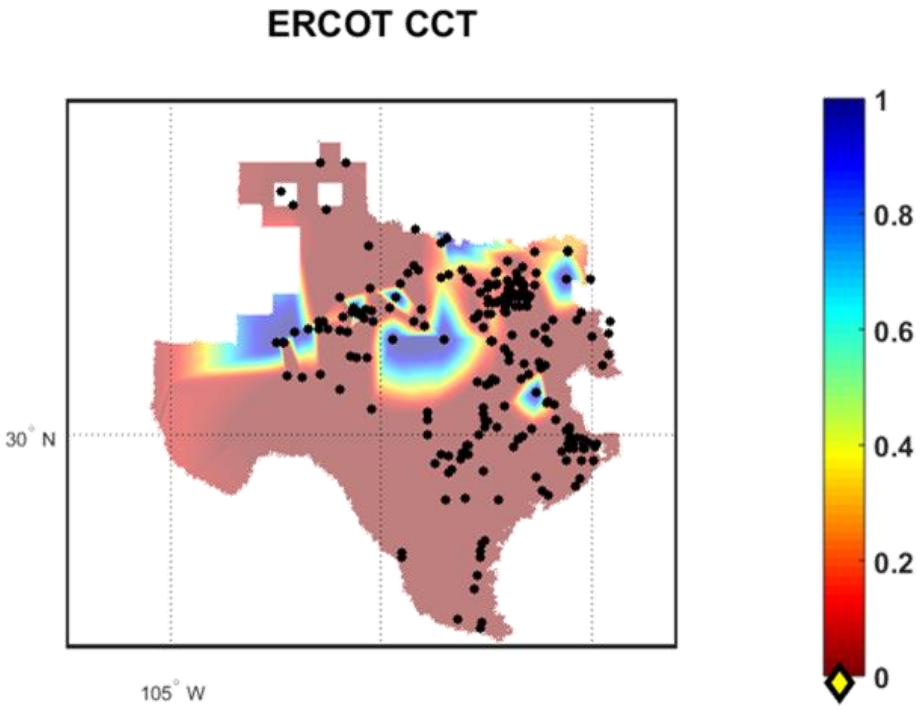

Fig. 71. 60% renewables CCT map.

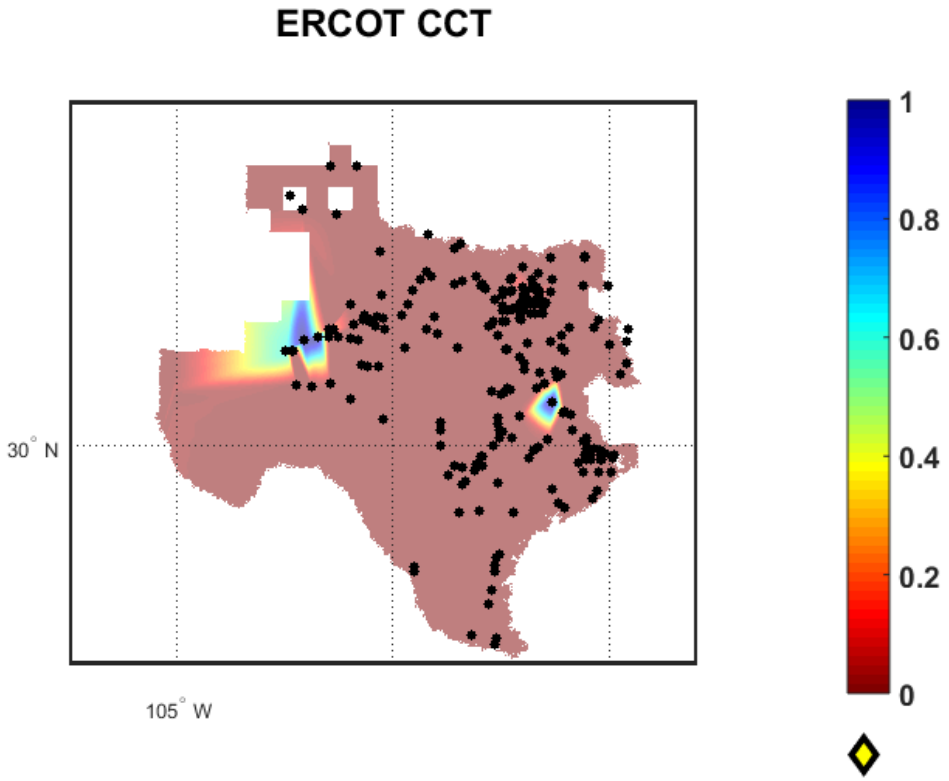

Fig. 72. 80% renewables CCT map.

increases sharply between 40% and 60%. The difference between the 40%-60% renewable cases were then investigated to determine what caused the CCT to decrease so significantly for most areas. The cases were broken down further to 45%, 50%, and 55% renewables. The 50% and 55% renewables cases are shown in Fig. 73-Fig. 74 and appear similar to the 40% and 60% cases, respectively.

There was a difference of 13 generators between the 50% and 55% renewables cases. These generators were then changed to PV one at a time to determine the effect on the CCT. It was found that when the renewable percentage reached 54.2% that the CCT was effected significantly, as shown in Fig. 75-Fig. 76. It was further found, however, that if different generators were displaced by PV, it was possible to reach a renewable percentage of 56.3% before the CCT was effected significantly.

This result shows that the impact of PV on ERCOT system frequency stability is non-linear. The incorporation of high PV penetration at the system level will fundamentally change the transient stability of a large-scale system and make the system very vulnerable to transient stability issues after a certain PV penetration point.

2.4 Conclusion

This study was performed to test the impact of PV on transient stability of the ERCOT system. Study results show when adding just a few PV machines for the ERCOT system, adding the PV machines slightly improves stability of the system. For system-level high renewables penetration in the ERCOT system,

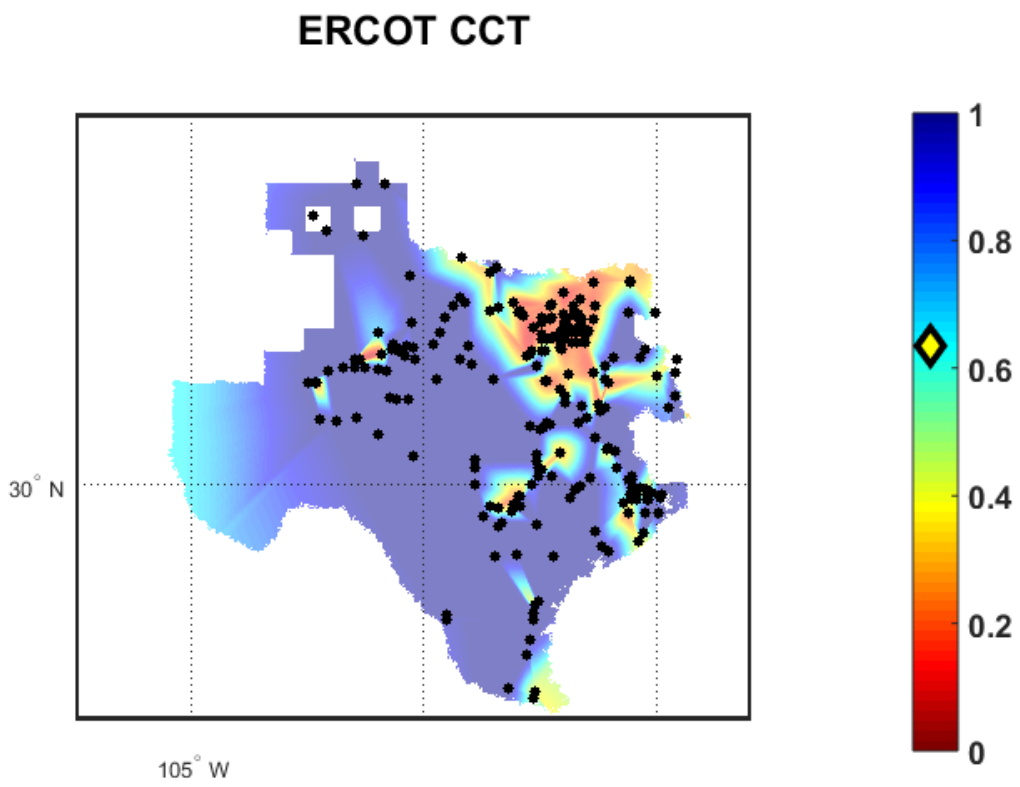

Fig. 73. 50% renewables CCT map.

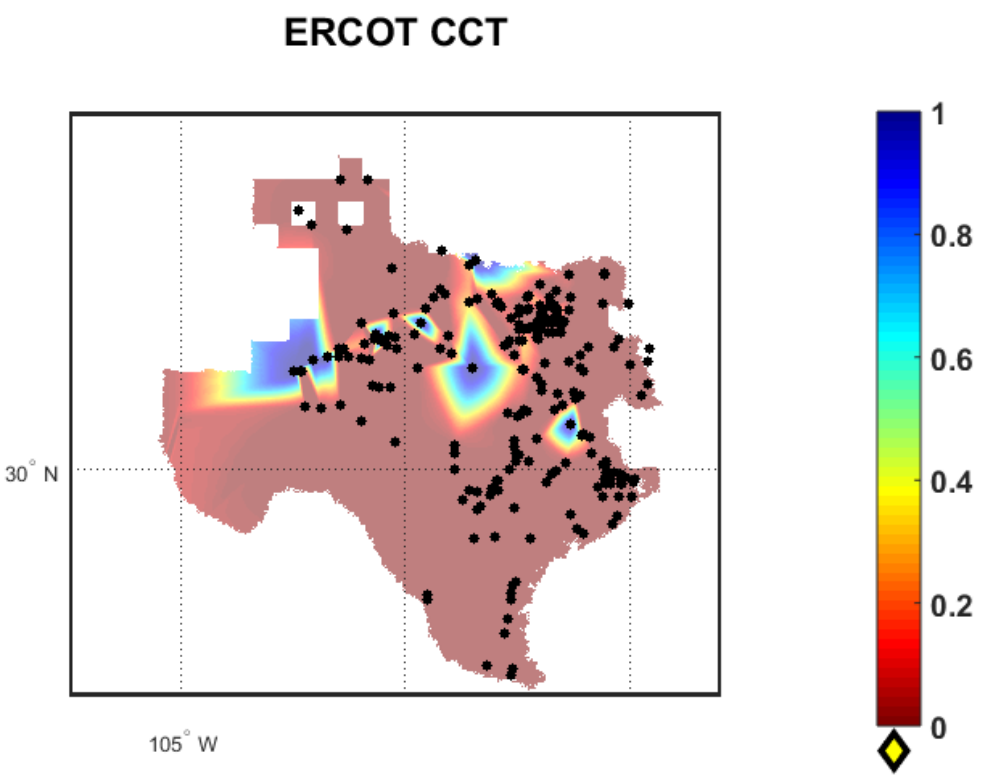

Fig. 74. 55% renewables CCT map.

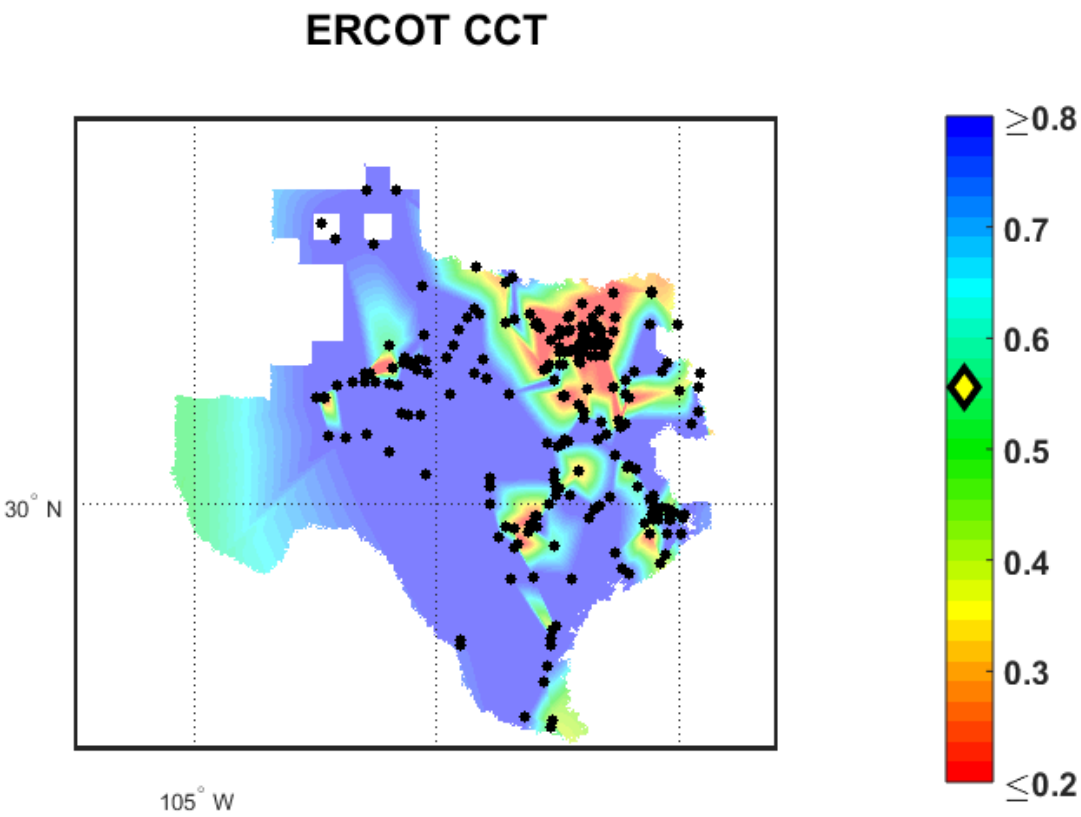

Fig. 75. 53.8% renewable CCT map.

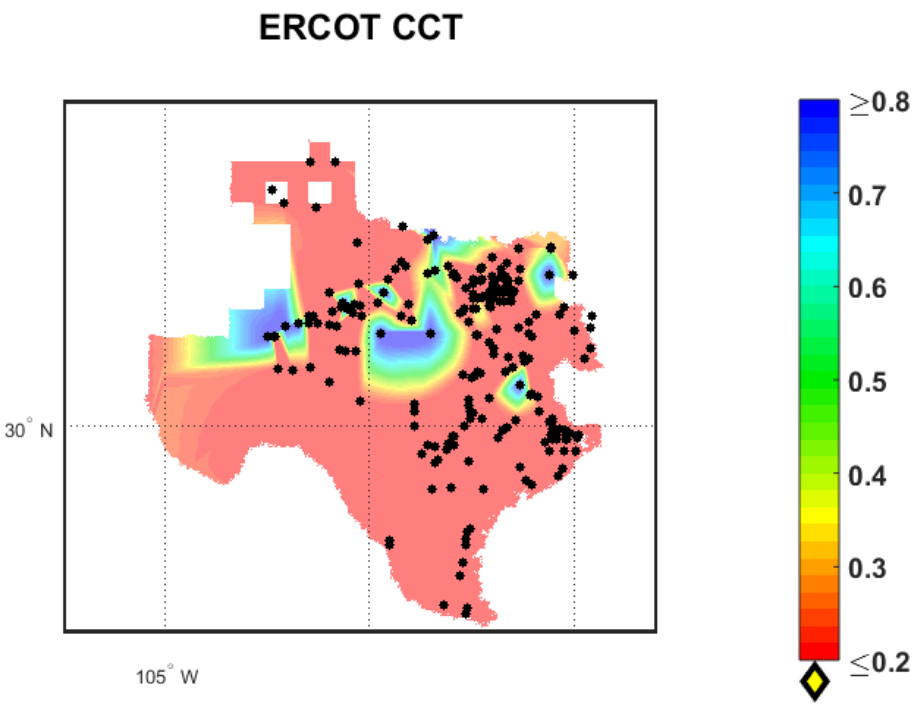

Fig. 76. 54.2% renewable CCT map.

adding considerable amounts of renewables, the stability may slightly increase or be approximately the same up to approximately 54%, after which the stability drops considerably.

These findings are similar to other studies done testing transient stability with increased IBR on other systems [15], [31]- [36]. IBR can be capable of stronger and faster support [31]. PV is also more helpful when disturbances occur some distance from the PV machines [15].

2.5 Future Work

Further work could be done on this subject by exploring options to increase the transient stability. This could include synchronous condensers and extracted wind kinetic energy [37].

CHAPTER THREE
VOLTAGE ANGLE DIFFERENCE LIMITS AS AN INDICATOR OF EARLY EVENT AWARENESS

3.1 Introduction

It is important for utilities to have a wide area view of the power system so that they can be aware of what is occurring on their system as well as the systems around them [38]. The 2003 black out is a good example of why Wide-Area Measurement Systems (WAMS) are needed [39]. After the 2003 black out it was determined that there was not enough awareness and communication of what was happening on the system, and that better real-time tools were necessary [40]. This helped pave the way for increased placement and application of phasor measurement units (PMUs) as valuable monitoring and prediction tools [41] [42].

This project investigates setting and monitoring dynamic voltage phase angle difference limits between two PMU monitored locations, to monitor stress on an interface. Phase angle difference potentially gives a good indication of the stress on a monitored area, and if the system becomes too stressed then the grid could become unstable [43]- [44]. Phase angle difference has also been proven to have a relation to power transfer of an interface, and can be used to monitor the stress on the system due to power transfer [45]- [46]. Monitoring phase angle difference can be useful as an additional indicator of system stress, in case system stress is not clear from just monitoring active power flow [47].

Currently phase angle limits are typically set using a static limit from off-line studies. However, in real-time operations, the limits can change based on actual system conditions [48]. Some researchers have already started testing methods to use dynamic phase angle difference limits [48]- [49]. One purpose of setting dynamic limits is to use PMUs to determine the real-time effect of power transferred into the system through tie lines from neighboring utilities. The tie lines may not be directly monitored in real-time using PMUs because they are typically owned by two different utilities, so a method must be developed to monitor the effect they cause, i.e., monitoring the interface without using the phase angle pair difference on the PMUs located at both ends of tie lines. Active power and voltage phase angle are correlated [47], therefore monitoring voltage phase angle difference can help determine the effect of the power transfer on the tie lines by identifying a voltage phase angle pair within the monitored region that somehow correlates with the monitored interface flow.

For this study, the normal operating conditions for an interface consisting of a number of tie lines and two correlated angle pairs were studied. This allows a baseline to be obtained and helps anticipate future conditions [50]. Anticipating future conditions for the angle pairs will help to determine what the phase angle limits should be. Studying the normal operating conditions also helps to determine how the tie line flow effects the angle difference for each pair.

After the baselining study, two active power interfaces were tested with multiple voltage angle pairs to check if a high correlation could be found between

the interfaces and voltage angle pairs were PMUs are located. Then using the highest correlated active power interface and voltage phase angle pair, a method was tested for setting voltage phase angle limits that would alert when the phase angle difference for the pair is outside of normal operation.

3.2 Determination of Active Power Interface and Voltage Angle Pairs and Baselining of Data

The active power flow on a transmission line is correlated to the voltage phase angle difference between the sending end and the receiving end [46]. For this study, it was intended to find an angle pair that correlated with the desired interface flow consisting of a number of tie lines, because then a change in the voltage phase angle difference would indicate a similar change in the interface flow. This section outlines the angle pairs found and how useful they are for describing the effect of the interface flow. This interface is consisting of twelve (12) tie lines, including two (2) 500 kV, four (4) 230 kV, and six (6) 115 kV lines between Southern Company system and some neighboring utilities.

Fig. 77 shows the distribution for the active power for the interface in the year of 2014. Fig. 78 and Fig. 79 show the corresponding angle pairs that were found to have the best correlation to the active power flow of the interface. As marked, the x axis for the graphs are either degrees, for the angle pairs, or active power (MW), for the interface flow. The angle pair distributions show the distribution for the voltage phase angle difference between two locations. The y axis for the graphs show the number of occurrences for any given value. The bars in the graph are read by taking the x value on the left edge of the bar and

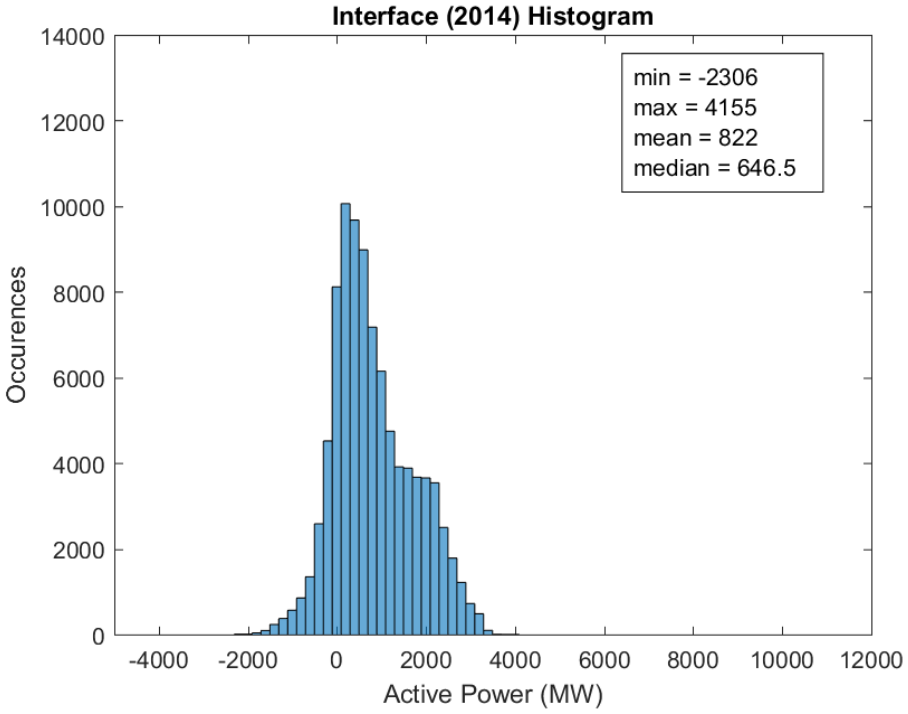

Fig. 77. Interface Distribution 2014.

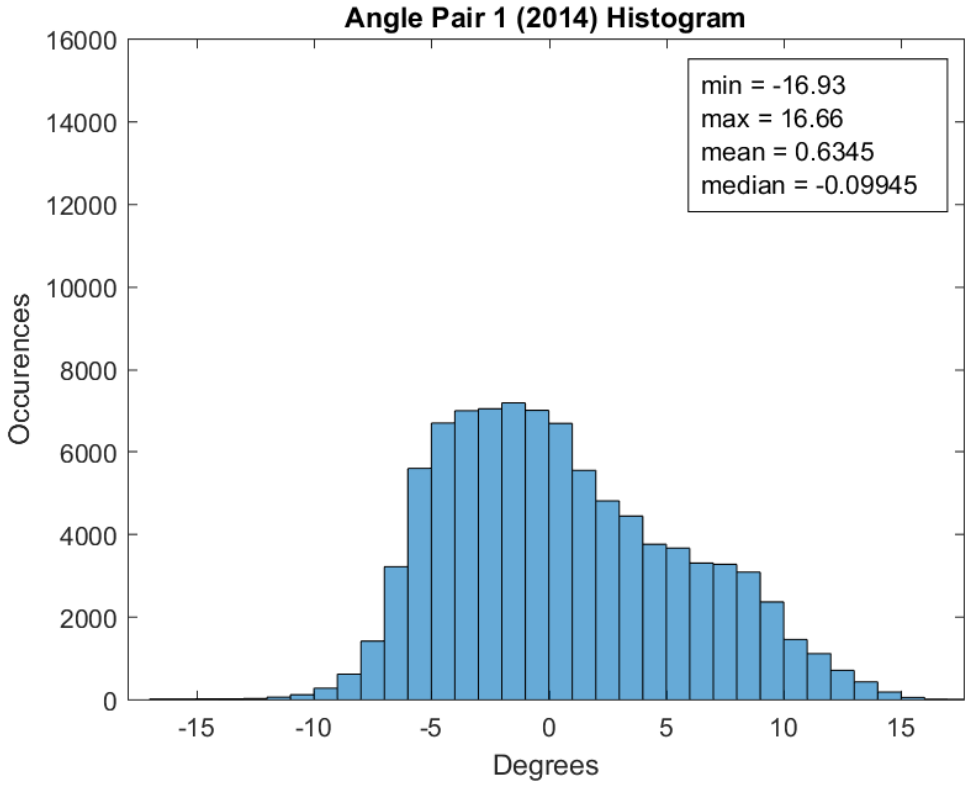

Fig. 78. Angle Pair 1 Distribution 2014.

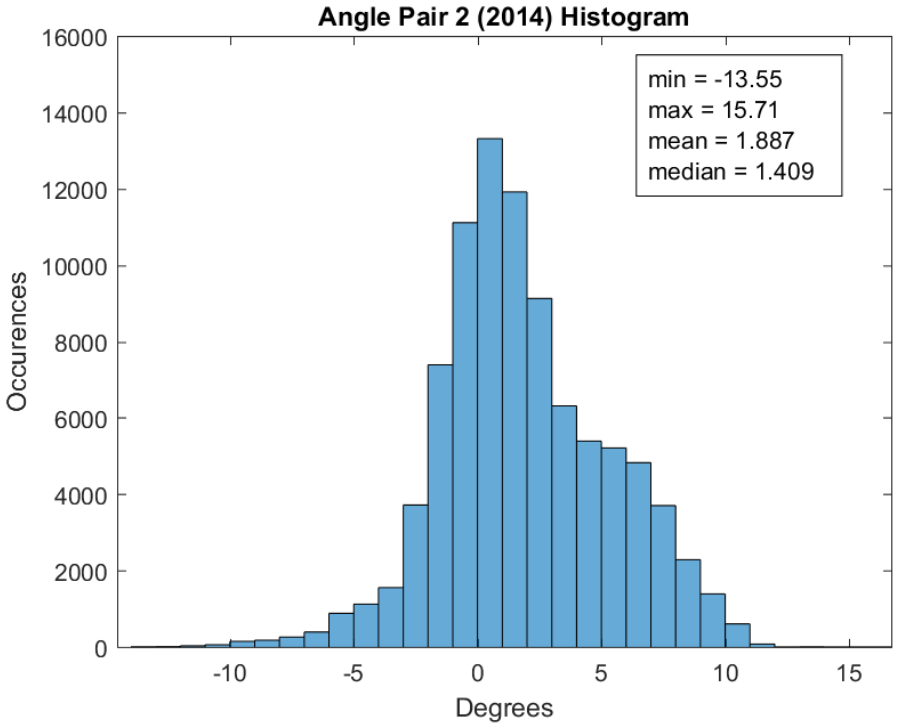

Fig. 79. Angle Pair 2 Distribution 2014.

the y value at the top of the bar. For the angle pairs, the bar width is 1°. For the interface flow, the bar width is 200 MW.

Although the interface graph has a different scale to the angle pair graphs, if the angle pairs are correlated to the interface power flow then they will have a similar shape. As can be seen from Fig. 78, the first angle pair (Angle Pair 1) looks similar to the interface distribution in shape, but not as similar as the second angle pair (Angle Pair 2) shown in Fig. 79. Using the Pearson Correlation Coefficient in MATLAB, it was determined that Angle Pair 2 has a 97% correlation to the interface flow and Angle Pair 1 has an 83% correlation to the interface. However, while Angle Pair 2 is more correlated to the interface, that angle pair uses a PMU which is not real time accessible (i.e., PMU owned by another utility) within the monitored region, so while it is helpful for this baselining study it is not practical for use in real time application.

3.2.1 Active Power and Angle Distributions by Year

The active power and angle distributions were evaluated over a three-year period. Fig. 77 shows the interface distribution for the first year, the year of 2014. As labeled on the graph, the average active power flow was 822 MW. A negative power flow indicates a reversed flow direction. Fig. 80 shows the second year. The average active power for the interface was 1101 MW. Fig. 81 shows the third year for the interface distribution. The average active power was 911.7 MW. For each of the three years, the minimum and maximum values are hard to identify on the graph because they occur infrequently. The minimum and maximum year

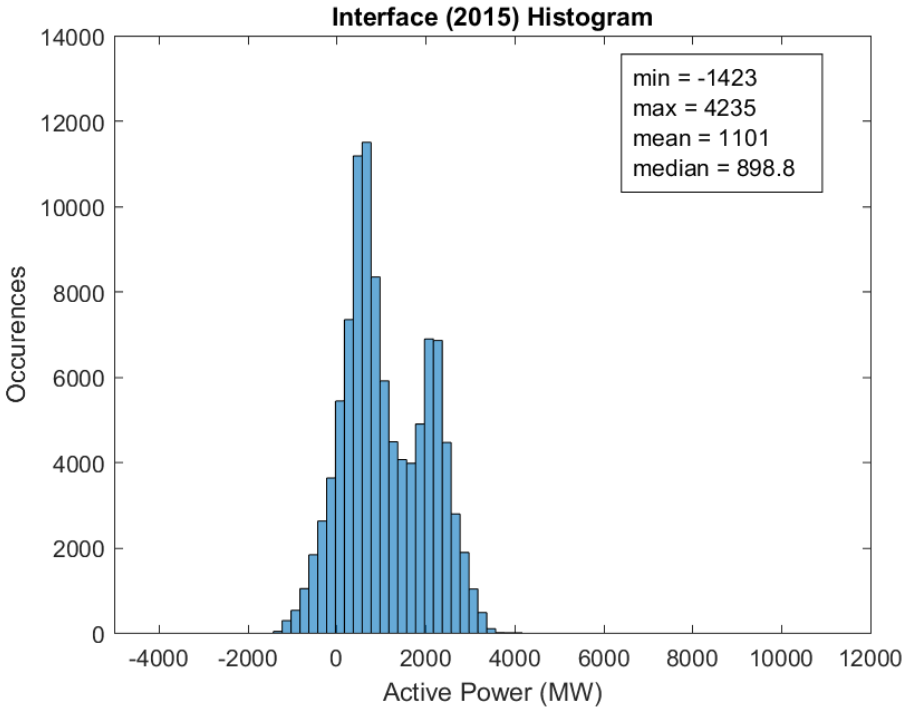

Fig. 80. Interface distribution 2015.

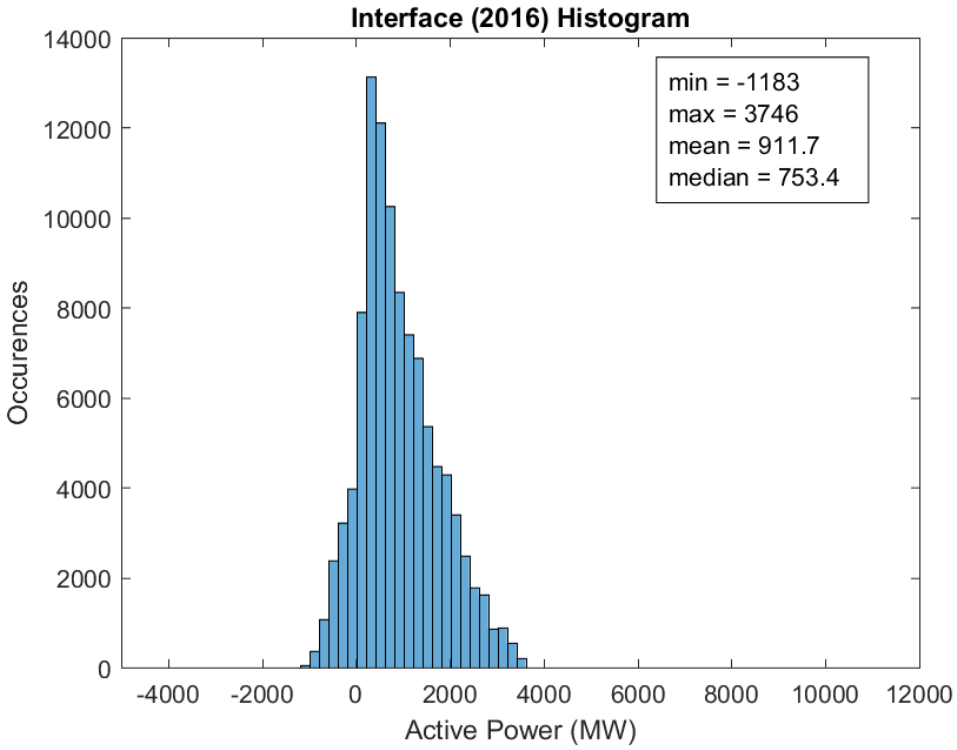

Fig. 81. Interface distribution 2016.

for the interface distribution. The average active power was 911.7 MW. For each of the three years, the minimum and maximum values are hard to identify on the graph because they occur infrequently. The minimum and maximum values give the limits for the known operating region, but the normal operating value is expected to be close to the most frequently occurring values, which will be either approximately the average value or, in the case of two operating peaks, it might be on either side of the average value.

If the infrequent points are ignored, then all three years seem to be in approximately the same distribution range. This means that there can be some difference by year, but overall the range should be approximately the same. The first and third year the distributions are similar in shape with one operating point, but the second year they have two operating points. It was not determined why this difference occurred.

3.2.2 Distribution by Season

The active power and angle distributions were also evaluated for each season: winter (December–February), spring (March–May), summer (June–August), and fall (September–November). The interface's 2014 fall distribution is shown in Fig. 82. The average active power was 904.5 MW. The interface's 2014 spring is shown in Fig. 83. The average active power was 496.9 MW. The interface flow for 2014 summer is shown in Fig. 84. The average active power flow was 1704 MW. The interface flow for 2014 winter is shown in Fig. 85. The average active power was 196.1 MW. Although not shown, the distributions for the years 2015 and 2016 are similar, although in 2016 there is less variation

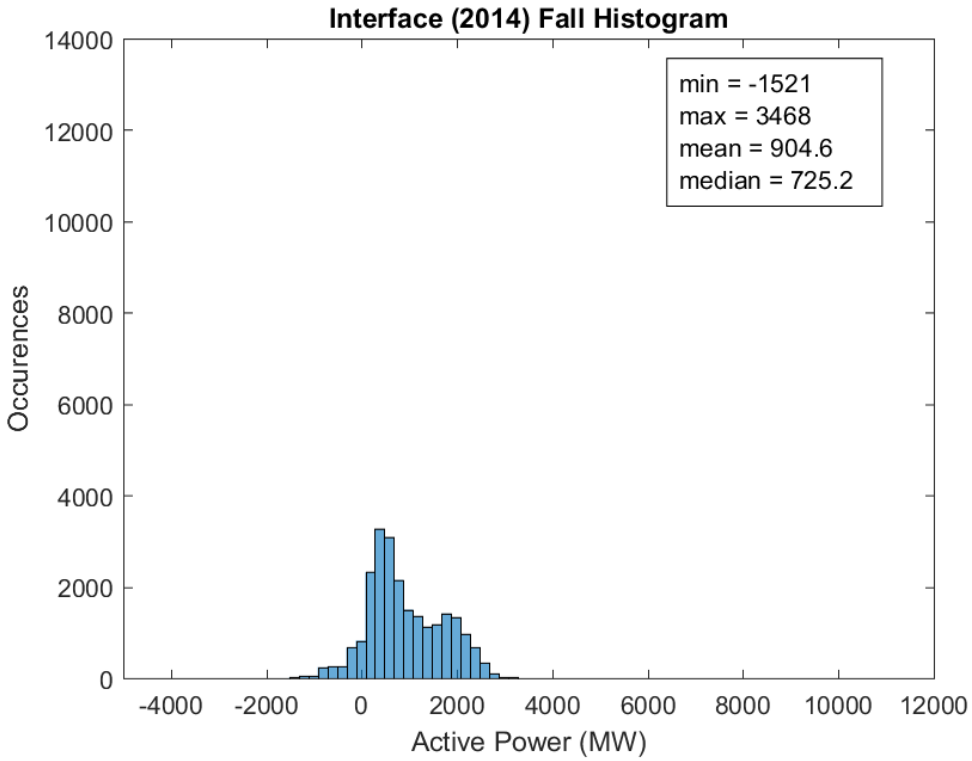

Fig. 82. Interface distribution fall 2014.

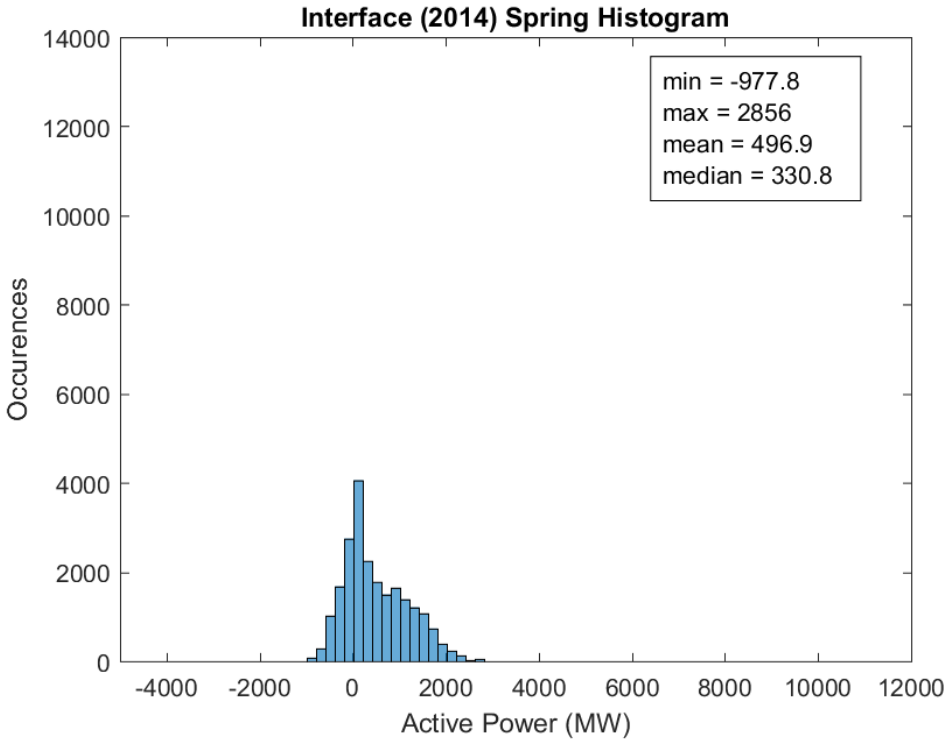

Fig. 83. Interface distribution spring 2014.

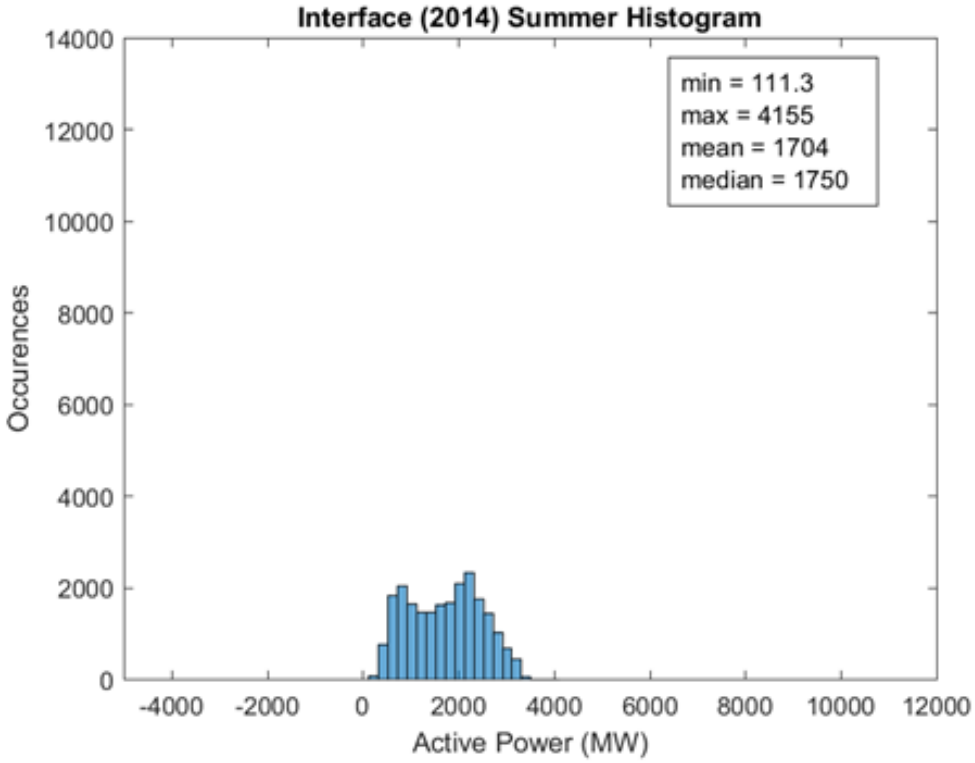

Fig. 84. Interface distribution summer 2014.

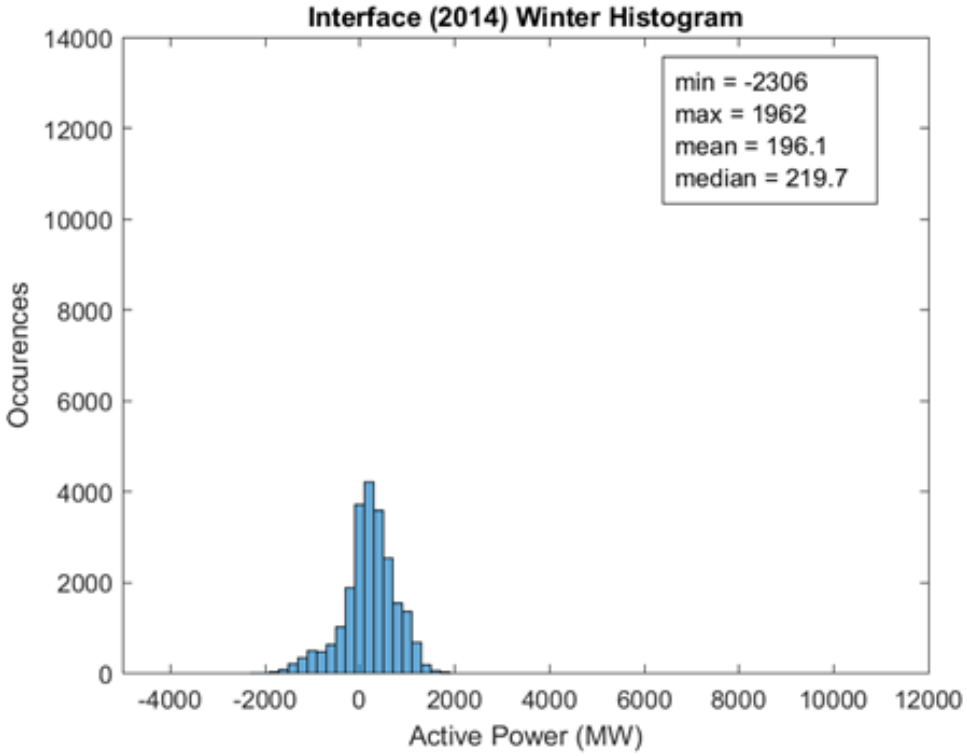

Fig. 85. Interface distribution winter 2014.

between the fall and spring seasons. Comparing the differences between numbers, and also visibly by how the graphs appear, it is clear that the distributions vary by season. The distributions for spring and fall are mostly positive active power values but include some negative active power values. The distribution for winter is split more evenly between positive and negative values. The distribution for summer is made up of entirely positive values, except for 2016 where it appears to be mostly positive.

The active power value that occurs most frequently, or the normal operating point for the active power, stays between 0 and 400 MW except for the summer season. The fall, spring, and winter seasons each have one normal operating point, while the summer season has two normal operating points. The summer season will be further explored later in this paper.

3.2.3 Distribution by Day of the Week

Next the active power flow and angle distributions were evaluated for each day of the week. Sunday is shown in Fig. 86. The average active power was 869.6 MW. Monday is shown in Fig. 87. The average active power was 871.3 MW. Tuesday is shown in Fig. 88 and the average active power was 771.8 MW. Wednesday is shown in Fig. 89. The average active power was 780.2 MW. Thursday is shown in Fig. 90 with an average active power of 797.3 MW. Friday is shown in Fig. 91. The average active power was 870.7 MW. Saturday is shown in Fig. 92. The average active power was 793.4 MW. The distributions for each day of the week change slightly, but all hold approximately the same normal operating point. The average active power of the distribution for each day of the

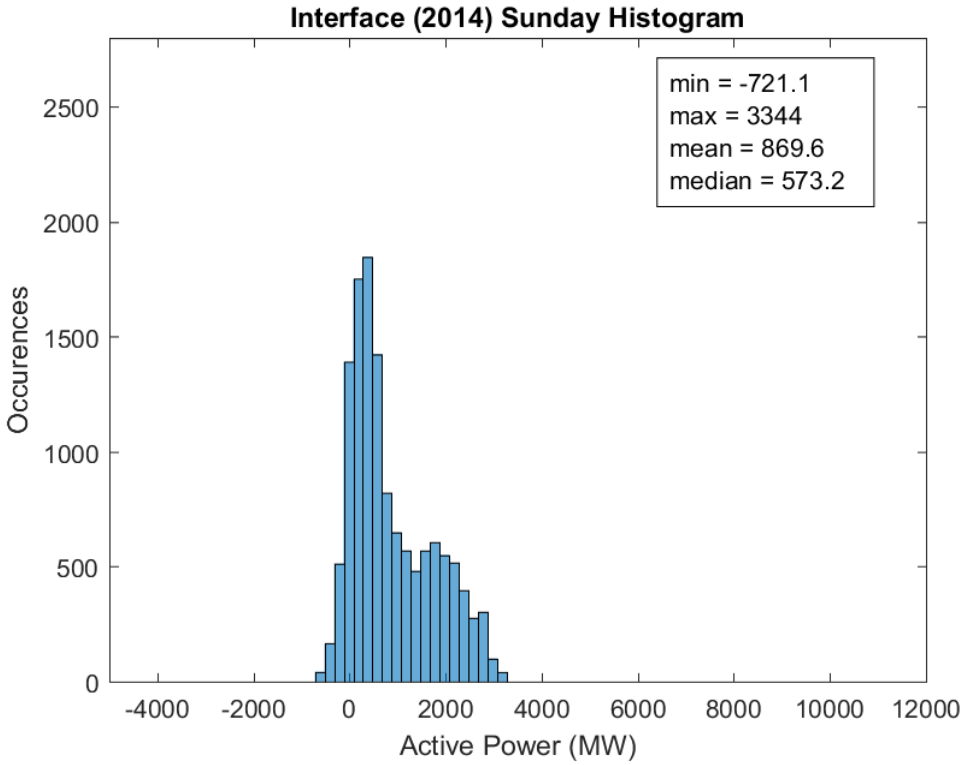

Fig. 86. Interface distribution Sunday 2014.

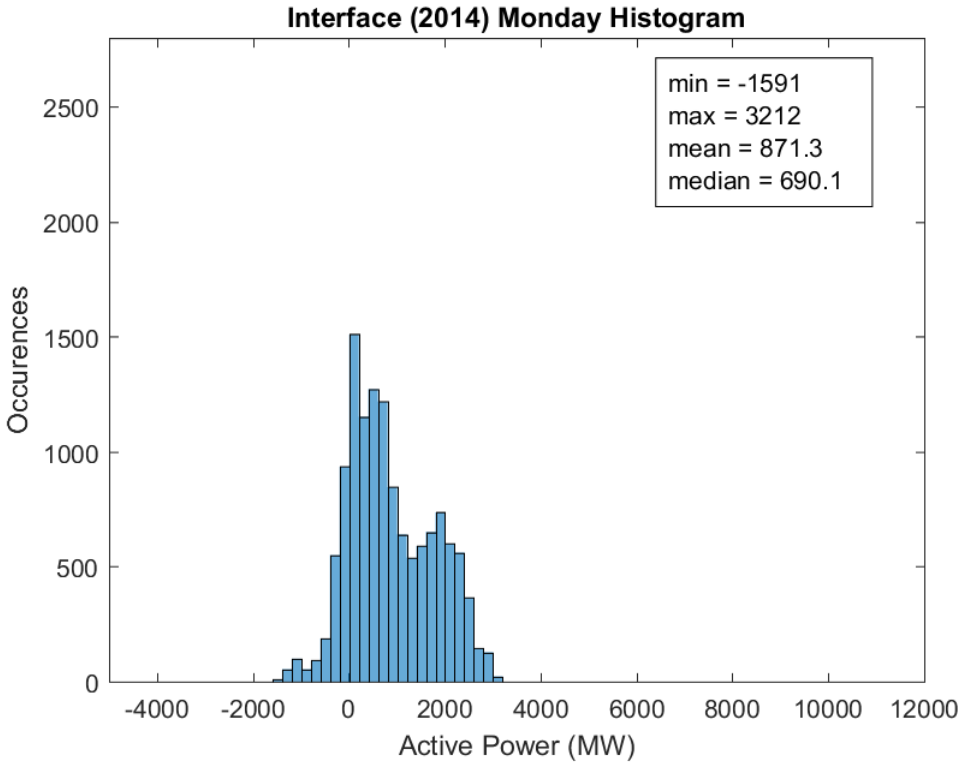

Fig. 87. Interface distribution Monday 2014.

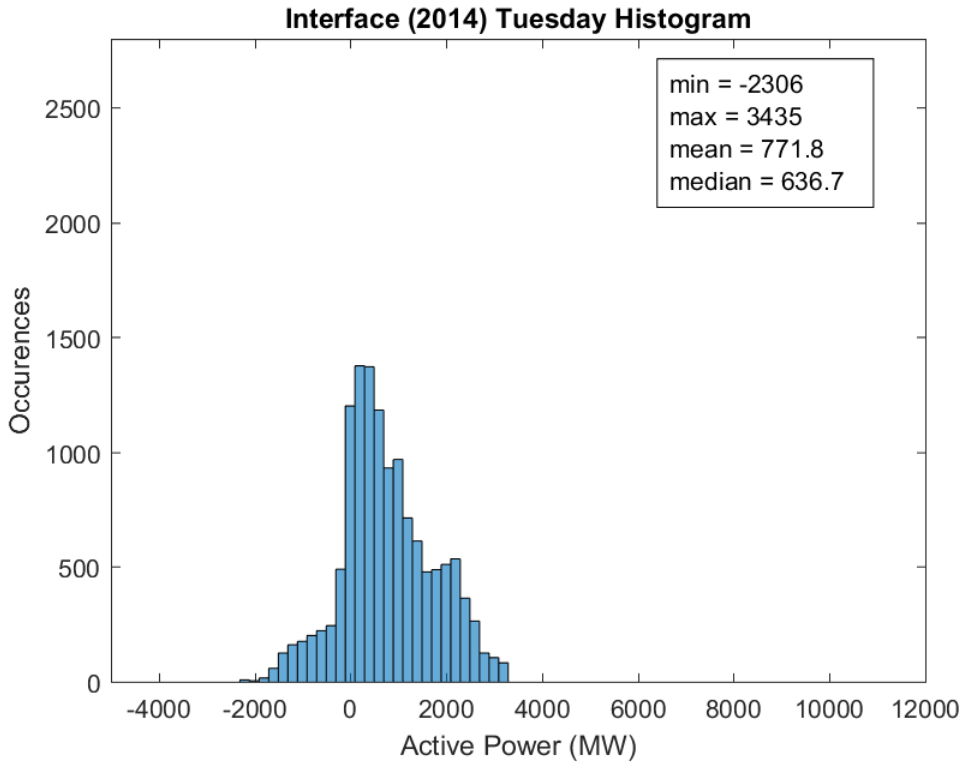

Fig. 88. Interface distribution Tuesday 2014.

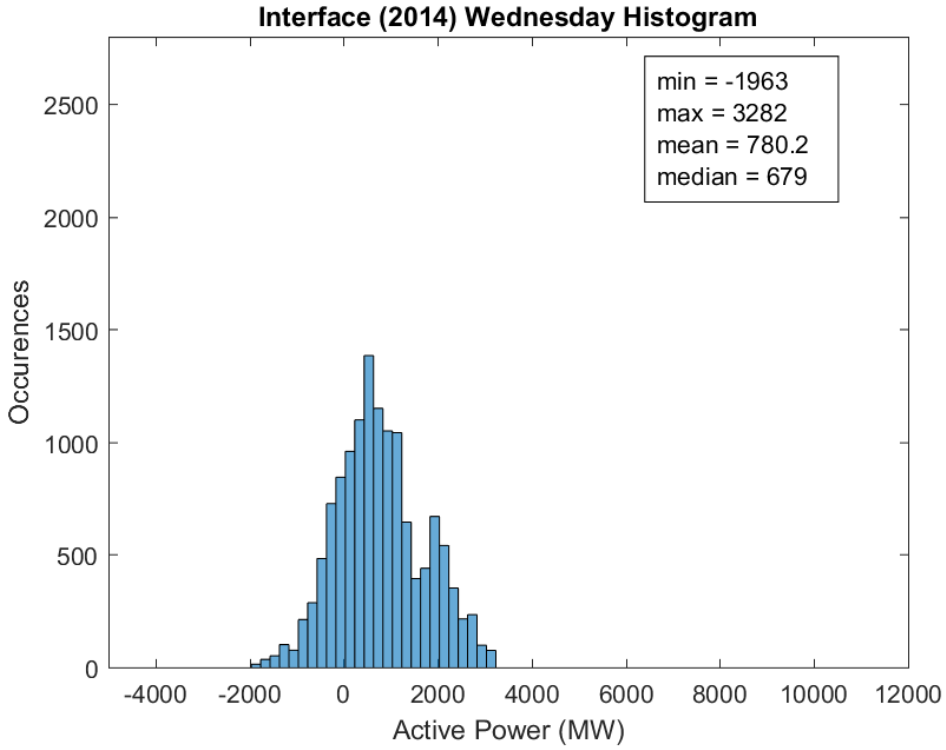

Fig. 89. Interface distribution Wednesday 2014.

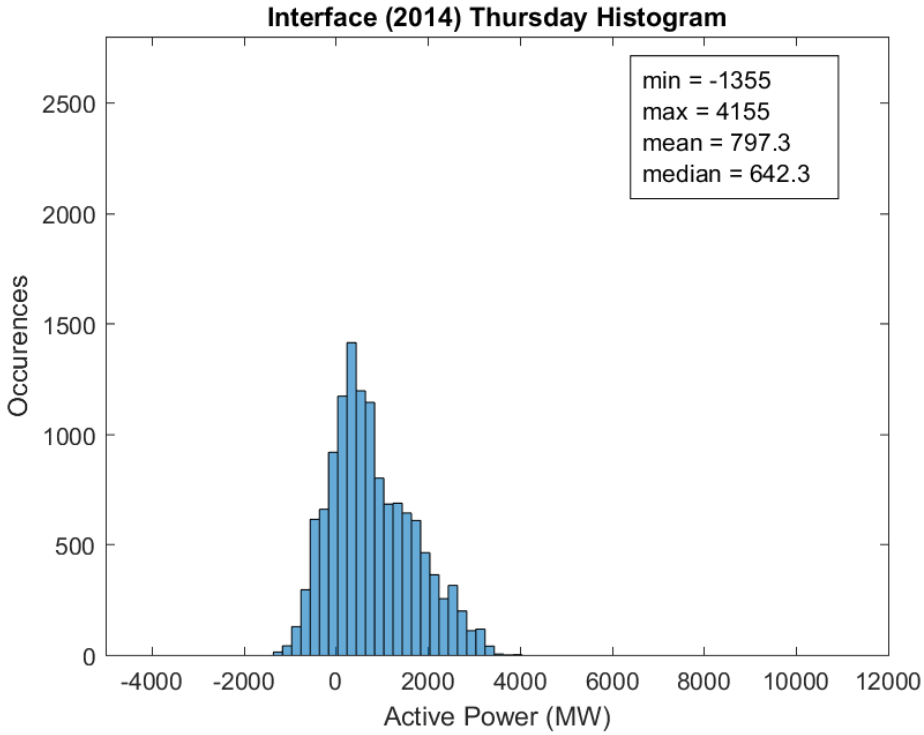

Fig. 90. Interface distribution Thursday 2014.

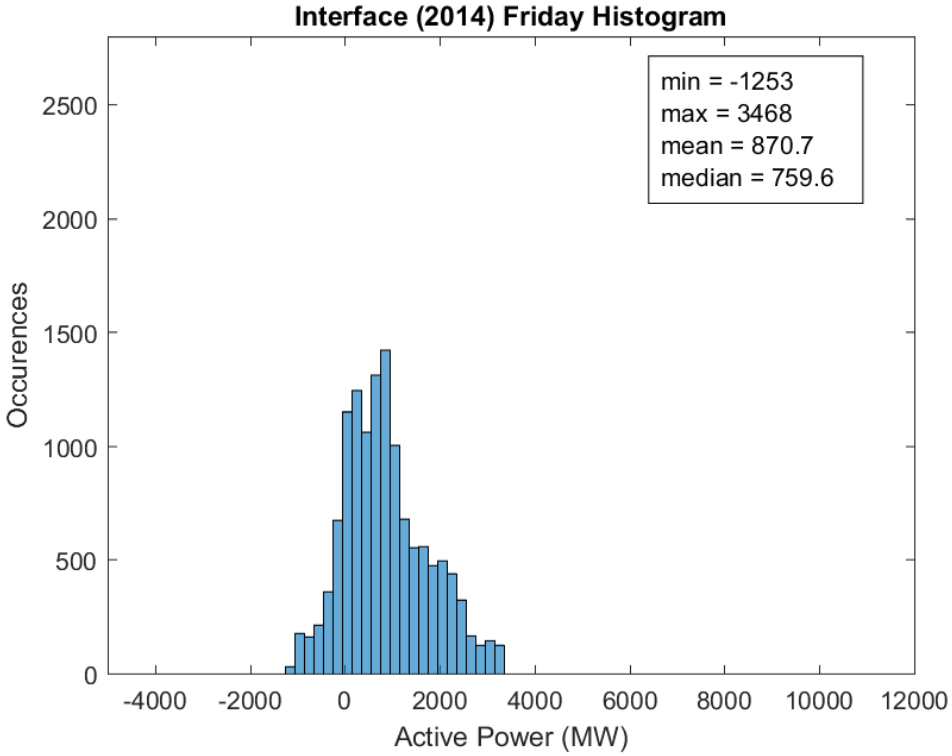

Fig. 91. Interface distribution Friday 2014.

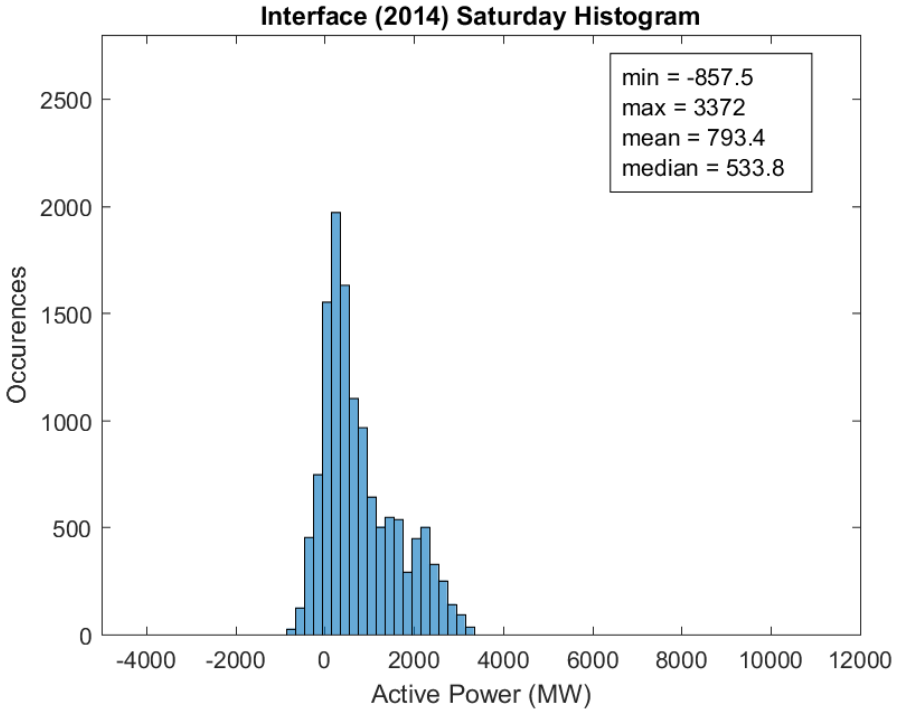

Fig. 92. Interface distribution Saturday 2014.

week is within 100 MW of every other day, which is true within each of the three years studied. There does not seem to be a significant difference between days of the week when evaluated for a whole year in 2014, 2015, or 2016.

3.2.4 Distribution by Season and Day of the Week

After the seasons and days of the week were evaluated separately, they were then evaluated together, looking at days of the week for each season. Fig. 93 shows the Sunday distribution for fall of 2014. The average active power was 913.4 MW. Fig. 94 shows the Monday distribution for fall 2014. The average active power was 1013 MW. Fig. 95 shows the Saturday distribution for fall 2014. The average active power was 716.2 MW.

From the figures that were created for all three years, it is clear that although when graphing the day of the week for a whole year there was not much change, graphing the day of the week for each season shows a greater difference. Graphing the days of the week for each year produced no difference between the days of the week for each year greater than 100 MW. When graphing the days of the week by season for each year, summer of 2014 was the only season in the three years studied that the interface difference in active power by day of the week was less than 100 MW. The other seasons varied in greatest difference between days of the week from 107 to 353 MW difference.

For all the seasons there is frequently a normal operating point between 0 and 1000 MW for the interface flow, excepting Wednesday in the spring of 2014 (for which the operating point is close to 0 MW but slightly negative) and Monday in the summer of 2014. Particularly in summer, but also during some days in the

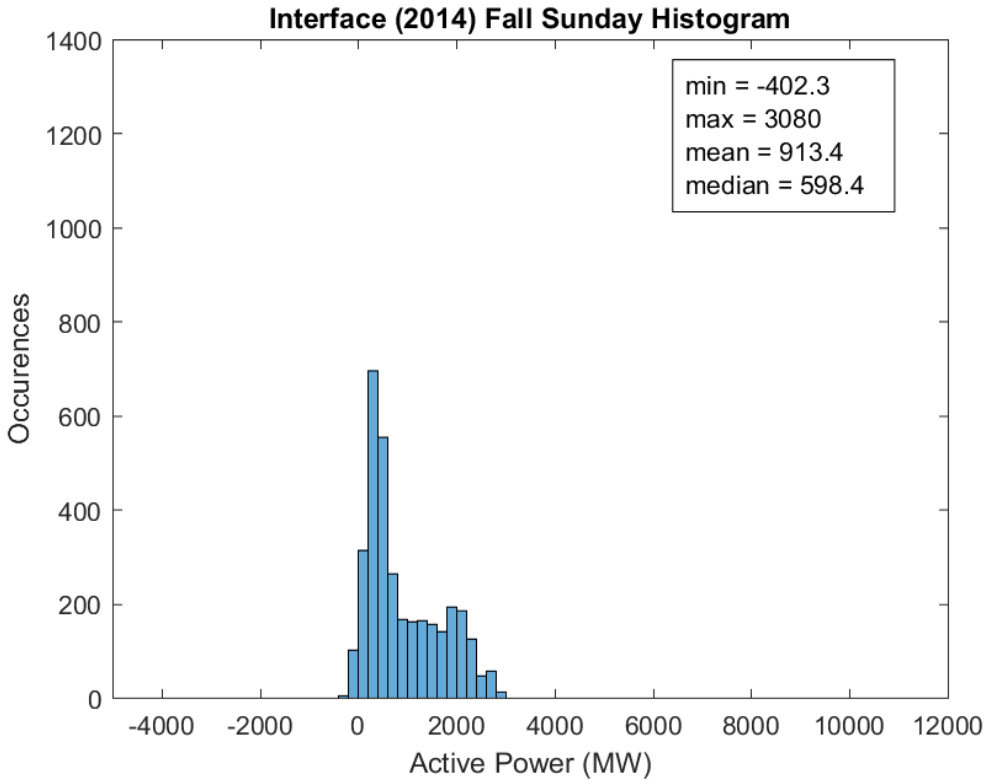

Fig. 93. Interface distribution fall Sunday 2014.

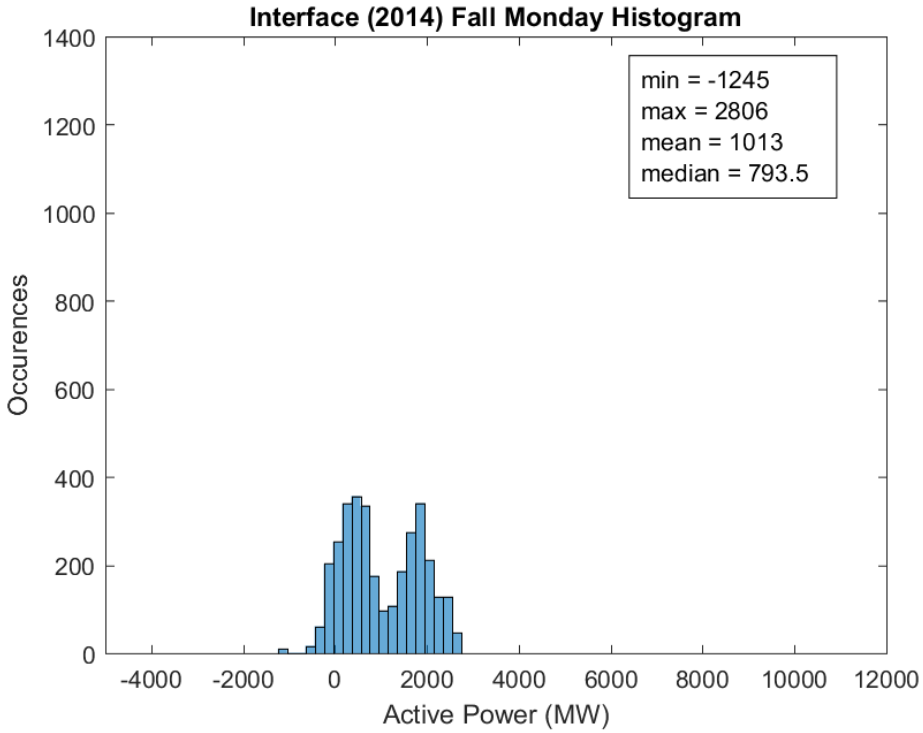

Fig. 94. Interface distribution fall Monday 2014.

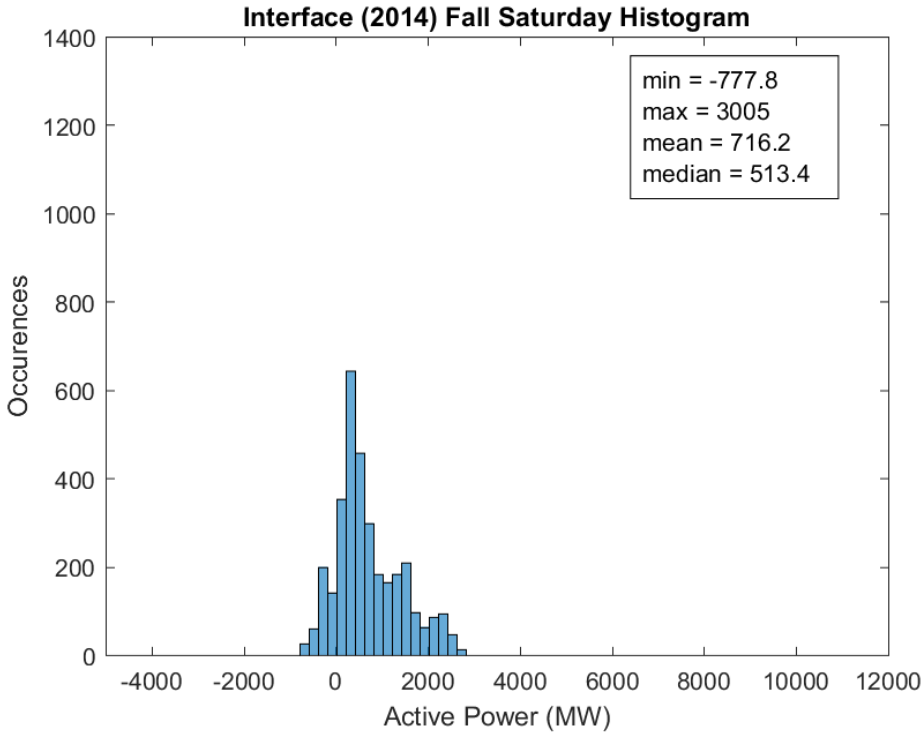

Fig. 95. Interface distribution fall Saturday 2014.

fall and spring, there is a second operating point. This second operating point seems to always occur at 2000 MW ± 1000 MW. Since the two peaks were very pronounced during Saturdays in summer, this was further investigated by breaking Saturdays in summer into morning and evening time, splitting the day in half using 12:00 am and 12:00 pm, to see if the two operating points were based on different times of the day.

Fig. 96 shows the Saturday distribution for summer of 2014. The average active power was 1720 MW, but it is clear that the average falls between two normal operating points. Fig. 97 shows the morning distribution for Saturdays in summer while Fig. 98 shows the evening distribution. It is clear from these figures that the operating point between 0 and 1000 MW occurs in the morning and the operating point at 2000 MW ± 1000 MW occurs in the evening.

3.2.5 Baselining Conclusion

The characteristics of the active power flow of a particular interface and angle distribution of a selected PMU pair were studied. It was determined that the distribution between years has slight variance, but not significant. The distribution varies when examining between different seasons. The distribution does not vary much by day when looking at the whole year, however it does vary looking at the different days within each season. It was also shown that if there are two peaks in the angle distribution, the time of day can have great significance.

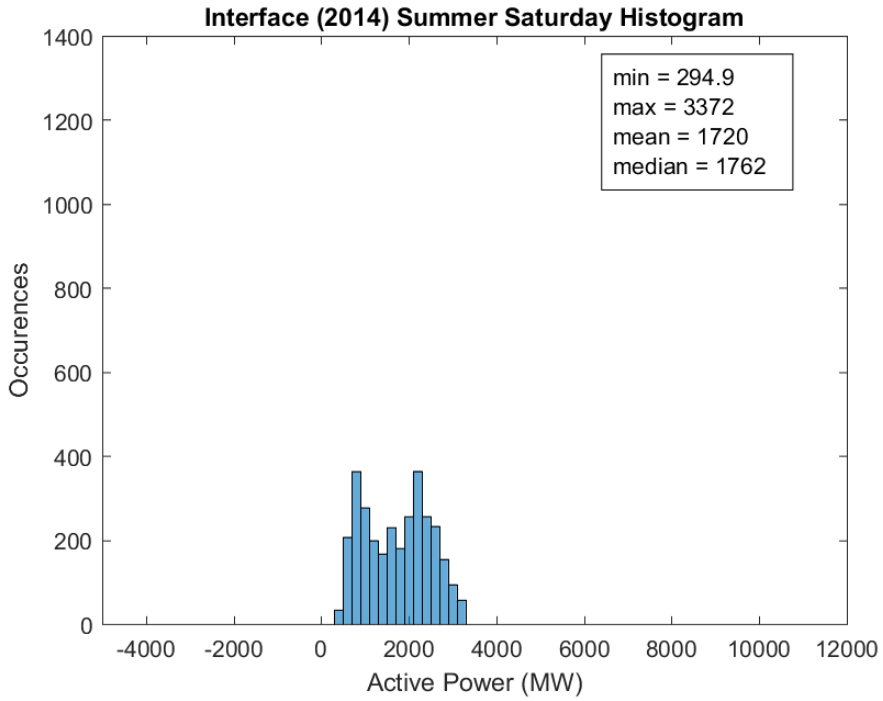

Fig. 96. Interface distribution summer Saturday 2014.

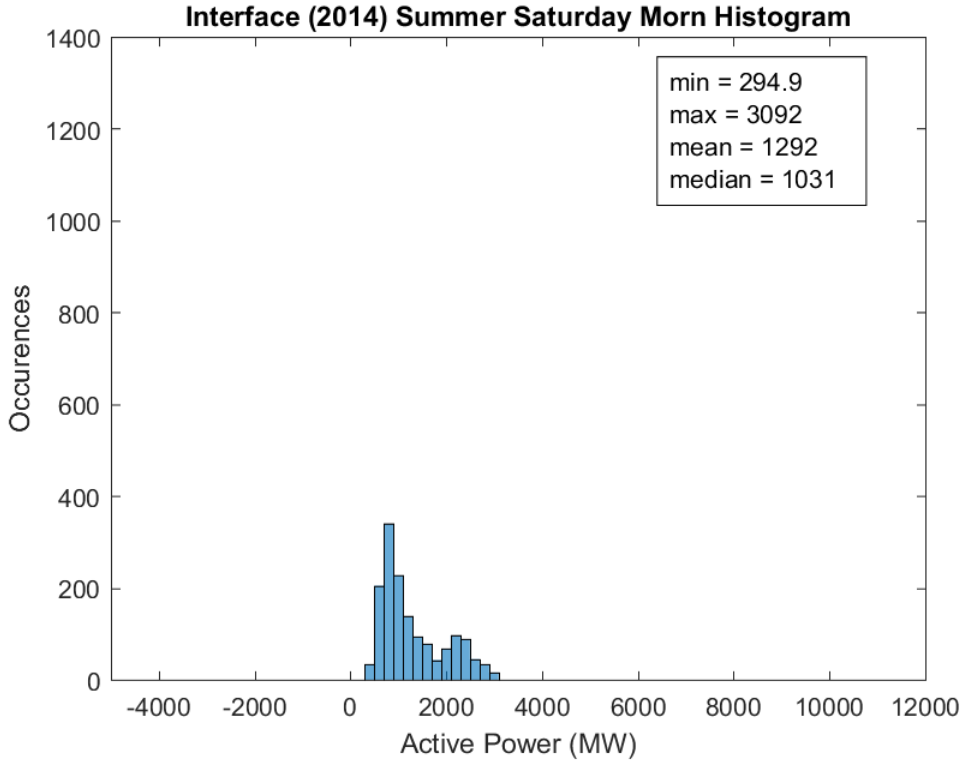

Fig. 97. Interface distribution summer Saturday morning 2014.

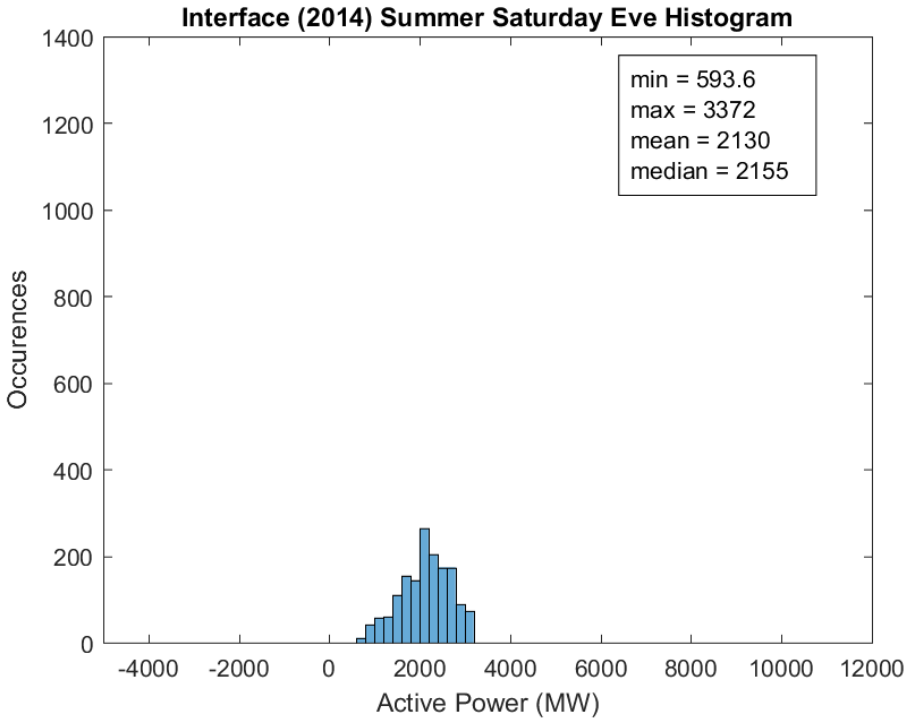

Fig. 98. Interface distribution summer Saturday evening 2014.

3.3 Correlation of Active Power Interface and Voltage Angle Pairs

After performing the baseline study, two different active power interfaces were chosen, each with a set voltage phase angle pairs that were thought to have potentially high correlation with the power interface, and the correlation between the power and angle pairs were tested. The first power interface was tested against 12 angle pairs and the correlation plots are shown in Fig. 99-Fig. 110.

One of the locations used in the angle pairs was outside of the Southern Company system. It was used to help verify that the active power interface could have high correlation with a voltage angle pair, but could not be used in real-time monitoring of an angle pair. Thus, while the angle pairs in Fig. 100, Fig. 104, and Fig. 110 had the highest correlation, they were not considered for further study because there was not a PMU on both ends. The angle pair shown in Fig. 99 was therefore found to have the highest correlation at 83.6%.

The second active power interface and its potentially related voltage angle pairs were then tested to determine if a higher correlation could be found. The highest correlation that was found was 43.9% as shown in Fig. 111. Since no suitably correlated voltage angle pair could be found for the second interface, and the correlation was much less than the highest found for the first interface, the first interface and highest correlated voltage angle pair were used for further study.

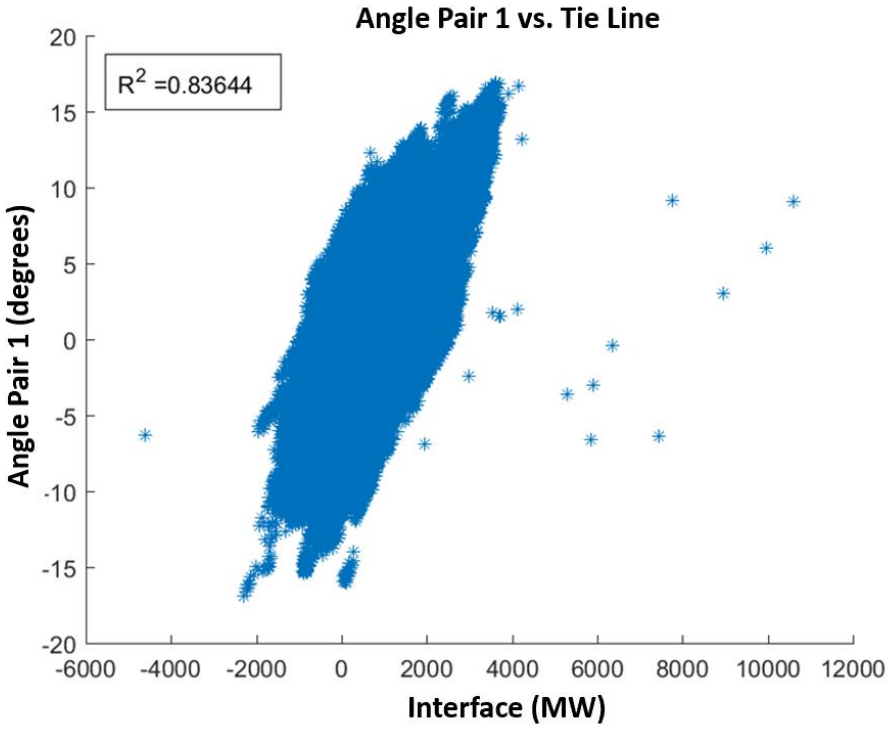

Fig. 99. Interface 1 vs. Angle Pair 1 correlation.

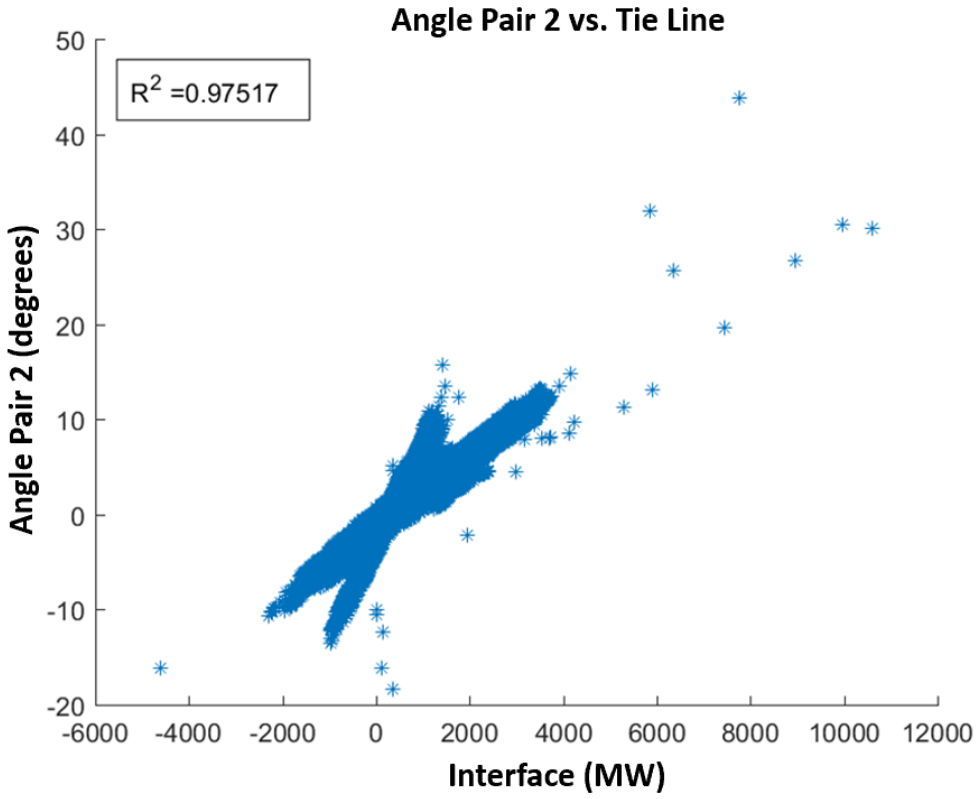

Fig. 100. Interface 1 vs. Angle Pair 2 correlation.

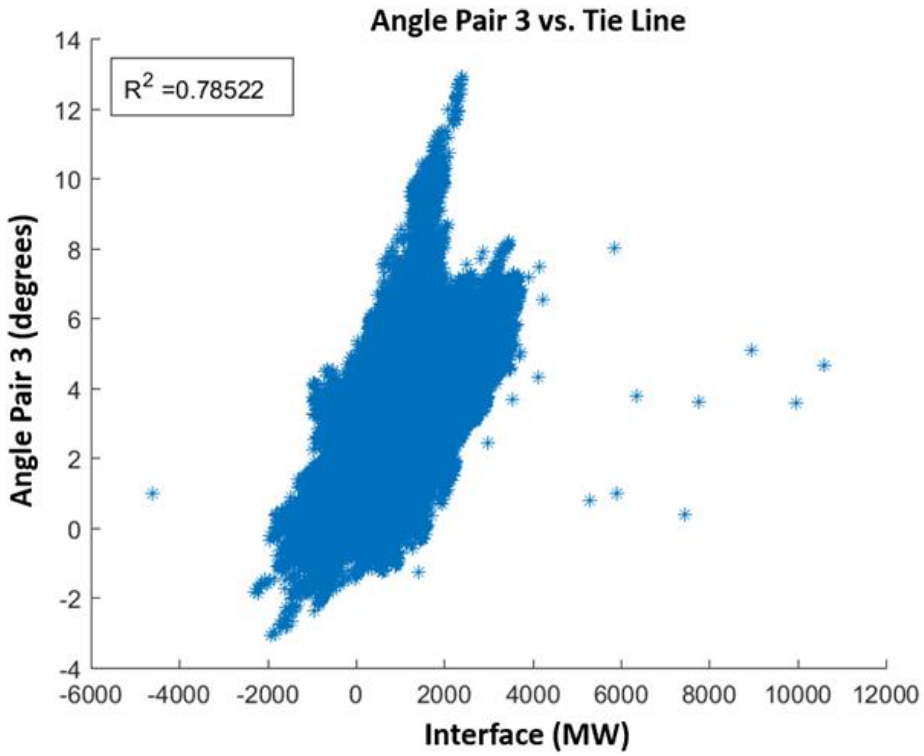

Fig. 101. Interface 1 vs. Angle Pair 3 correlation.

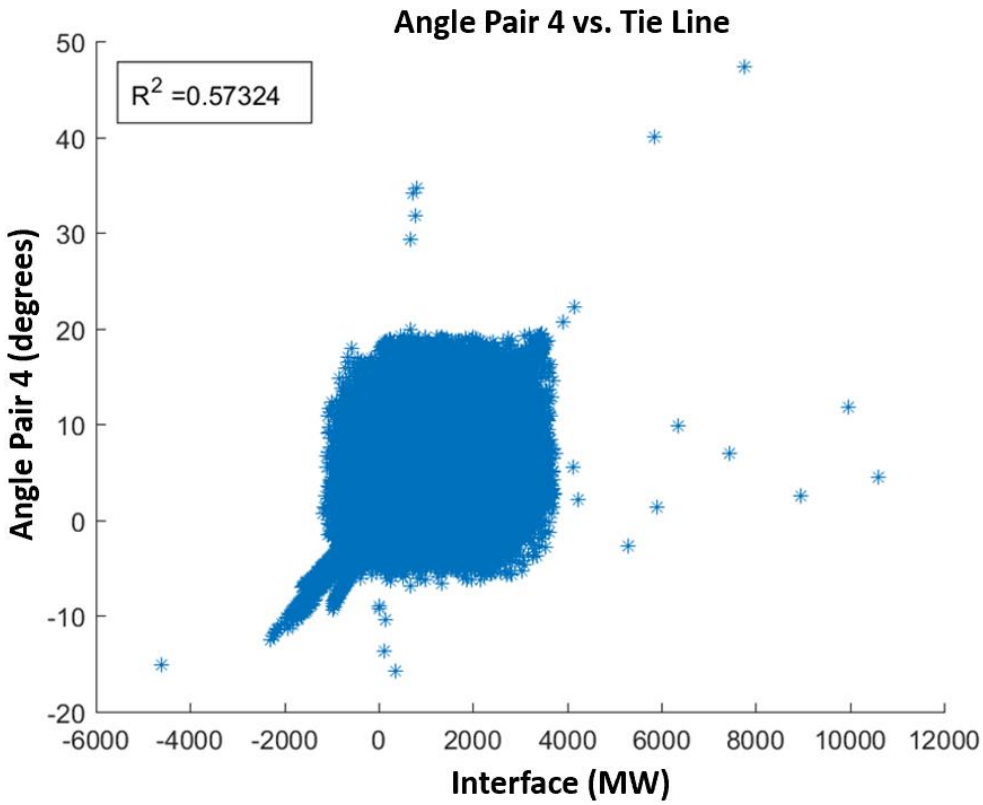

Fig. 102. Interface 1 vs. Angle Pair 4 correlation.

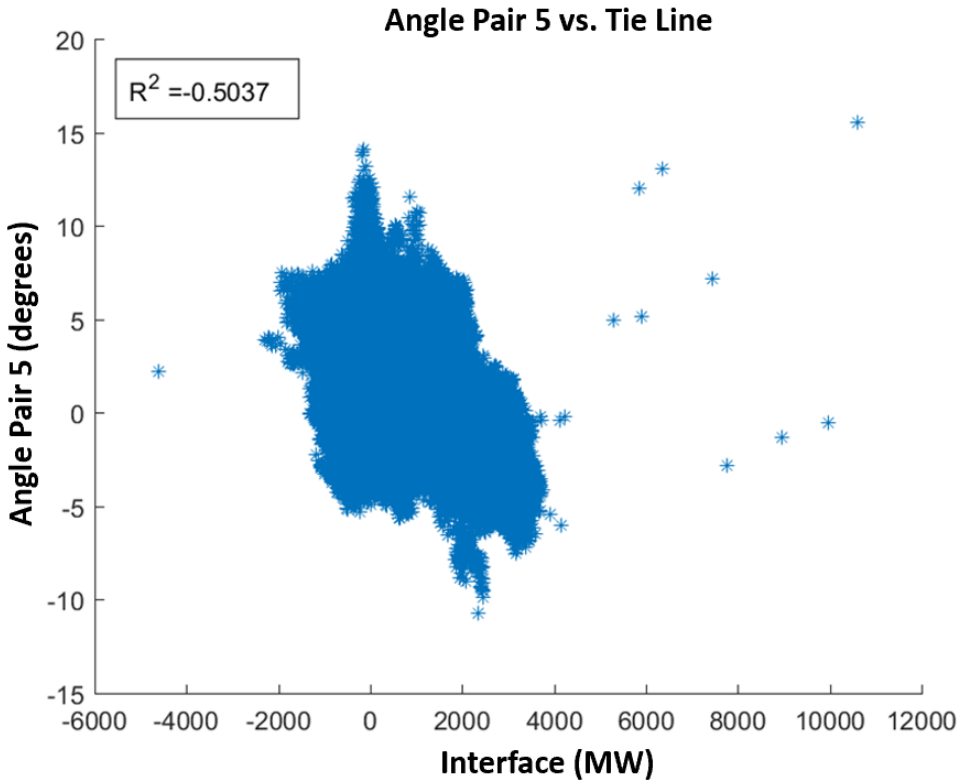

Fig. 103. Interface 1 vs. Angle Pair 5 correlation.

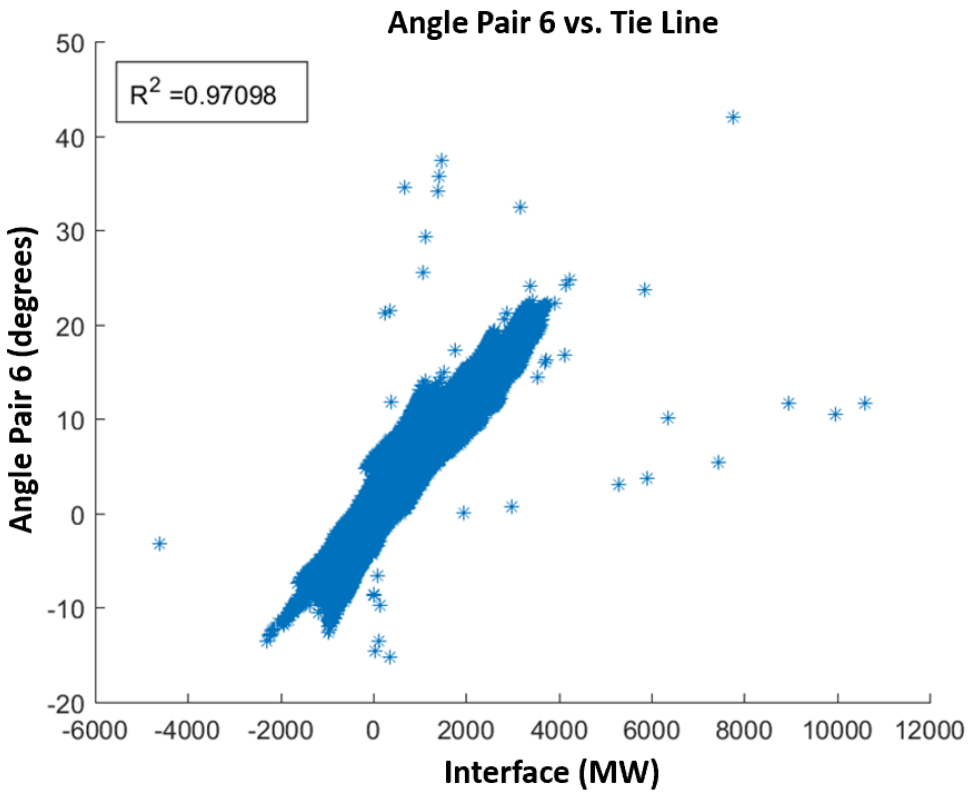

Fig. 104. Interface 1 vs. Angle Pair 6 correlation.

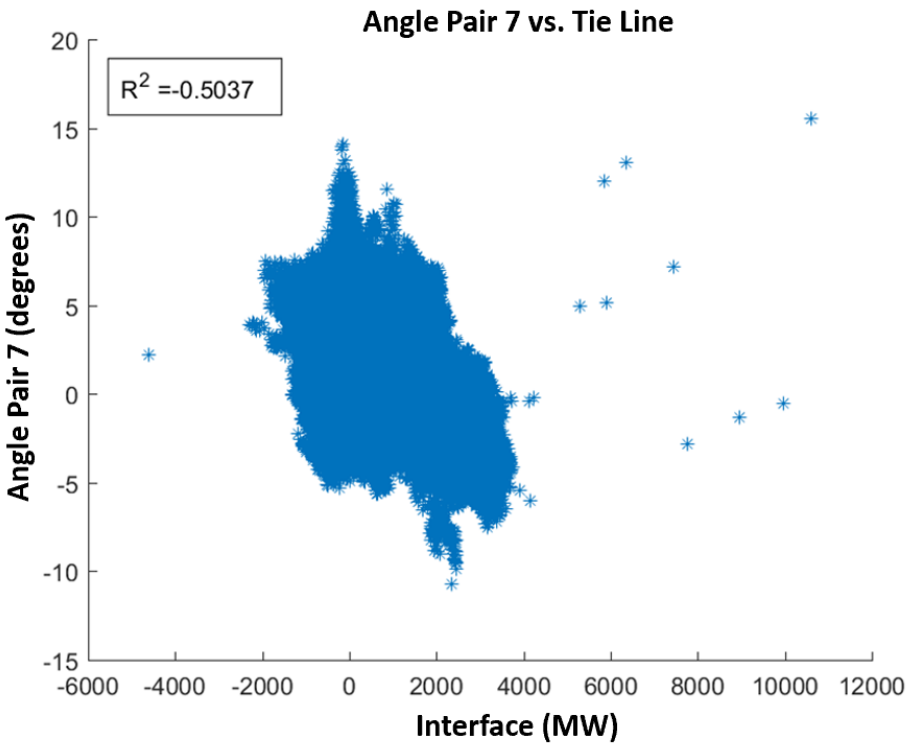

Fig. 105. Interface 1 vs. Angle Pair 7 correlation.

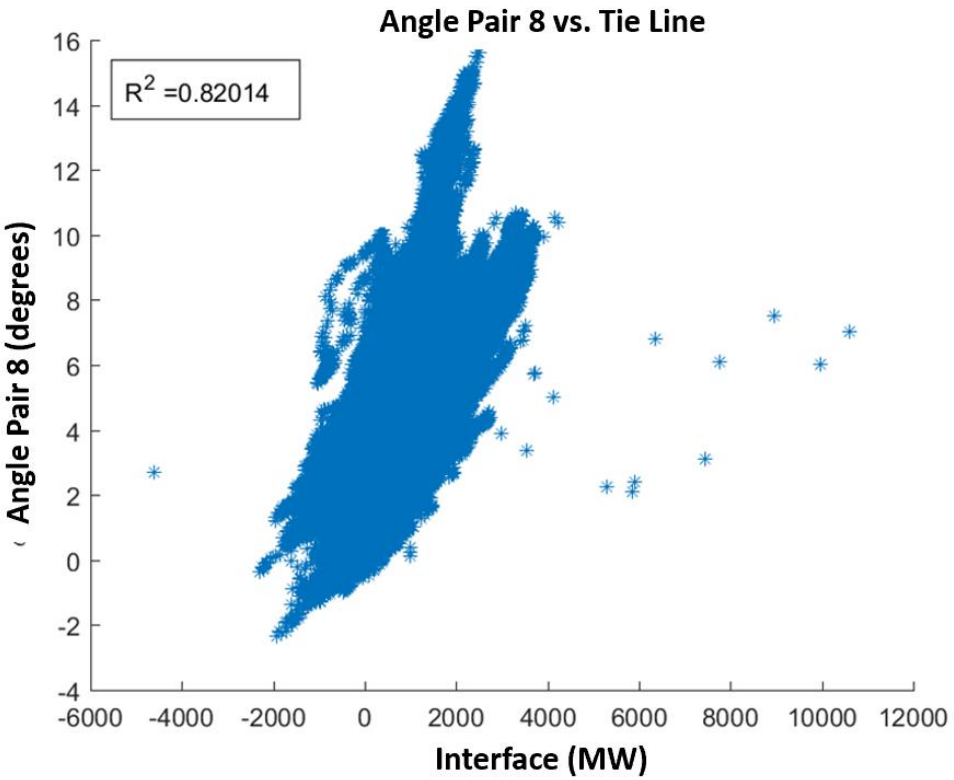

Fig. 106. Interface 1 vs. Angle Pair 8 correlation.

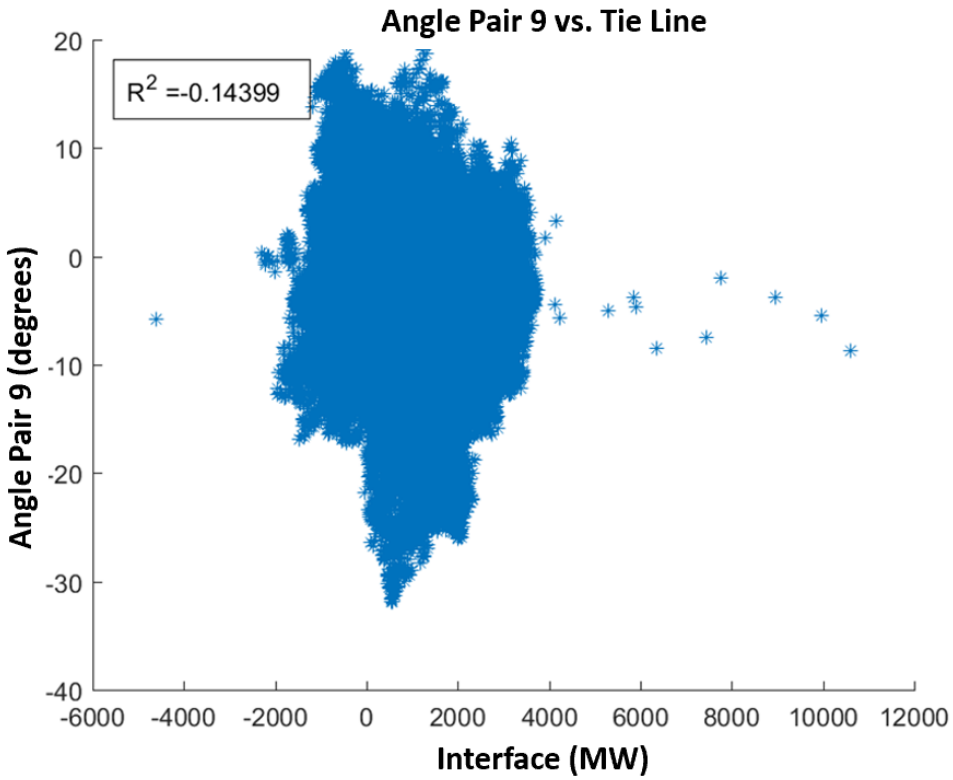

Fig. 107. Interface 1 vs. Angle Pair 9 correlation.

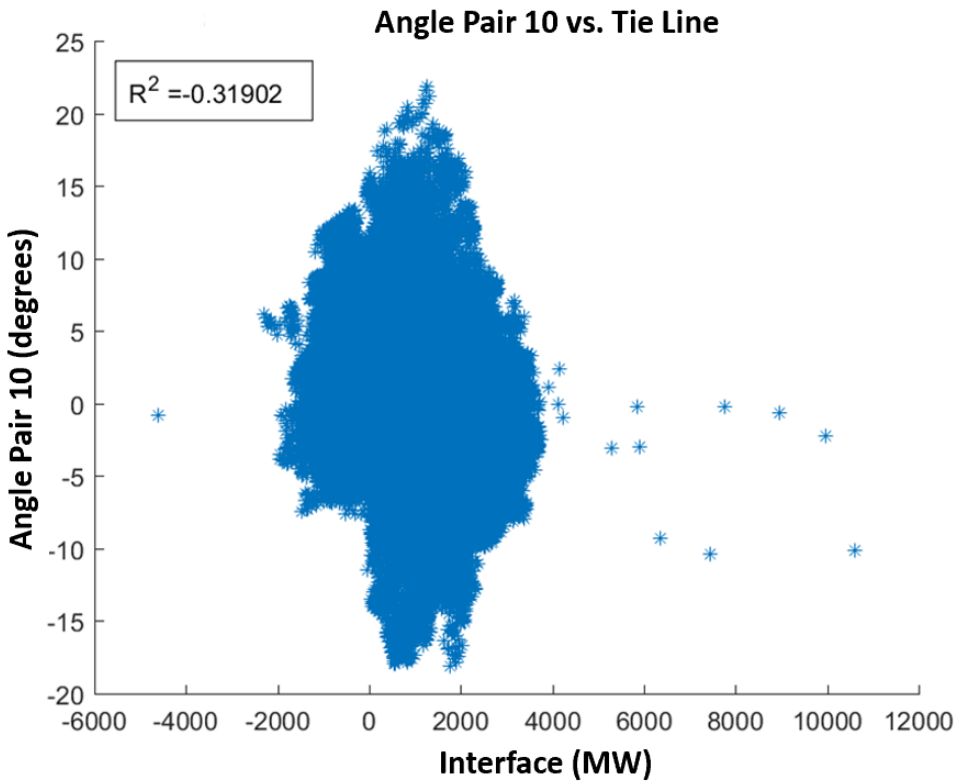

Fig. 108. Interface 1 vs. Angle Pair 10 correlation.

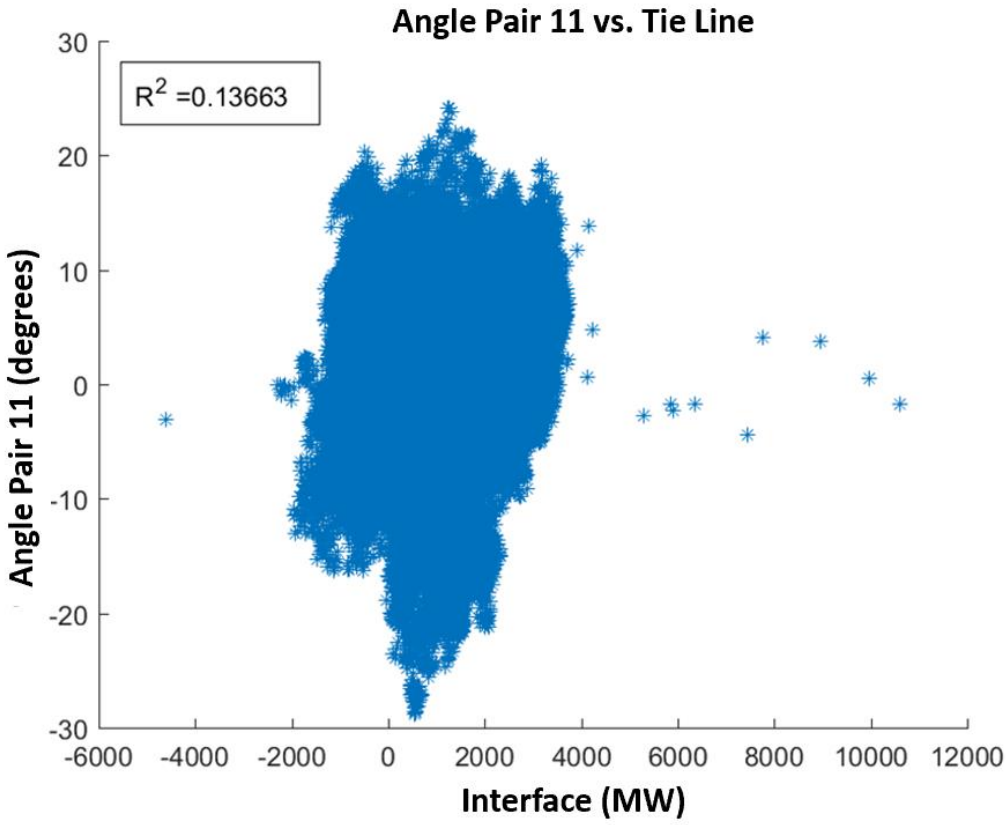

Fig. 109. Interface 1 vs. Angle Pair 11 correlation.

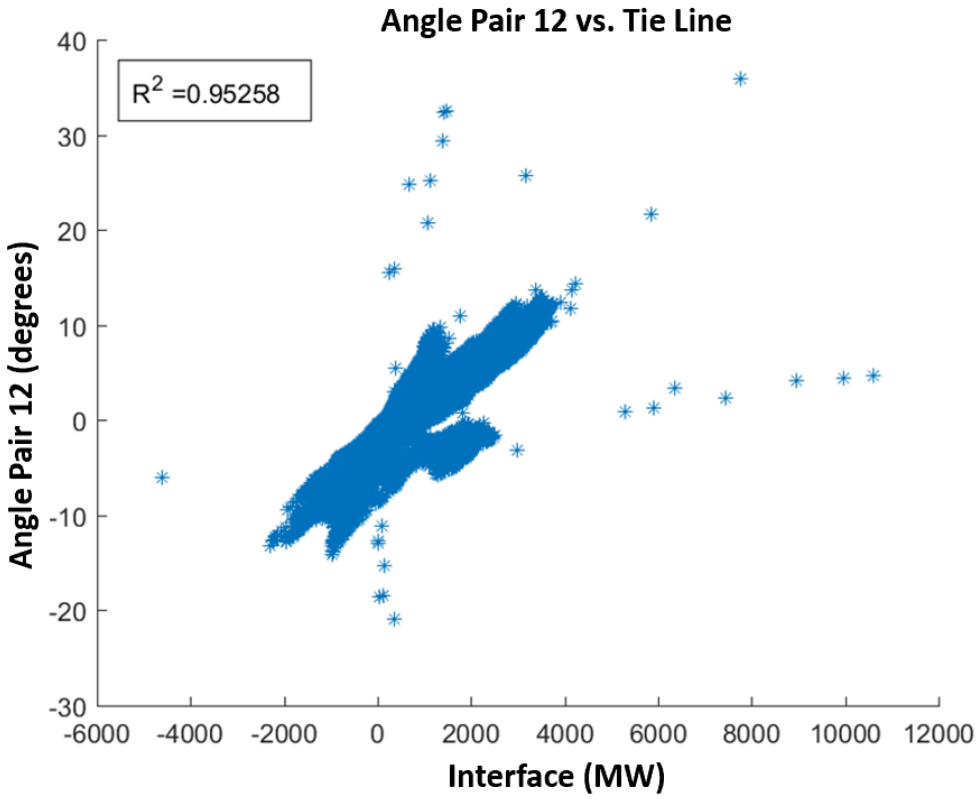

Fig. 110. Interface 1 vs. Angle Pair 12 correlation.

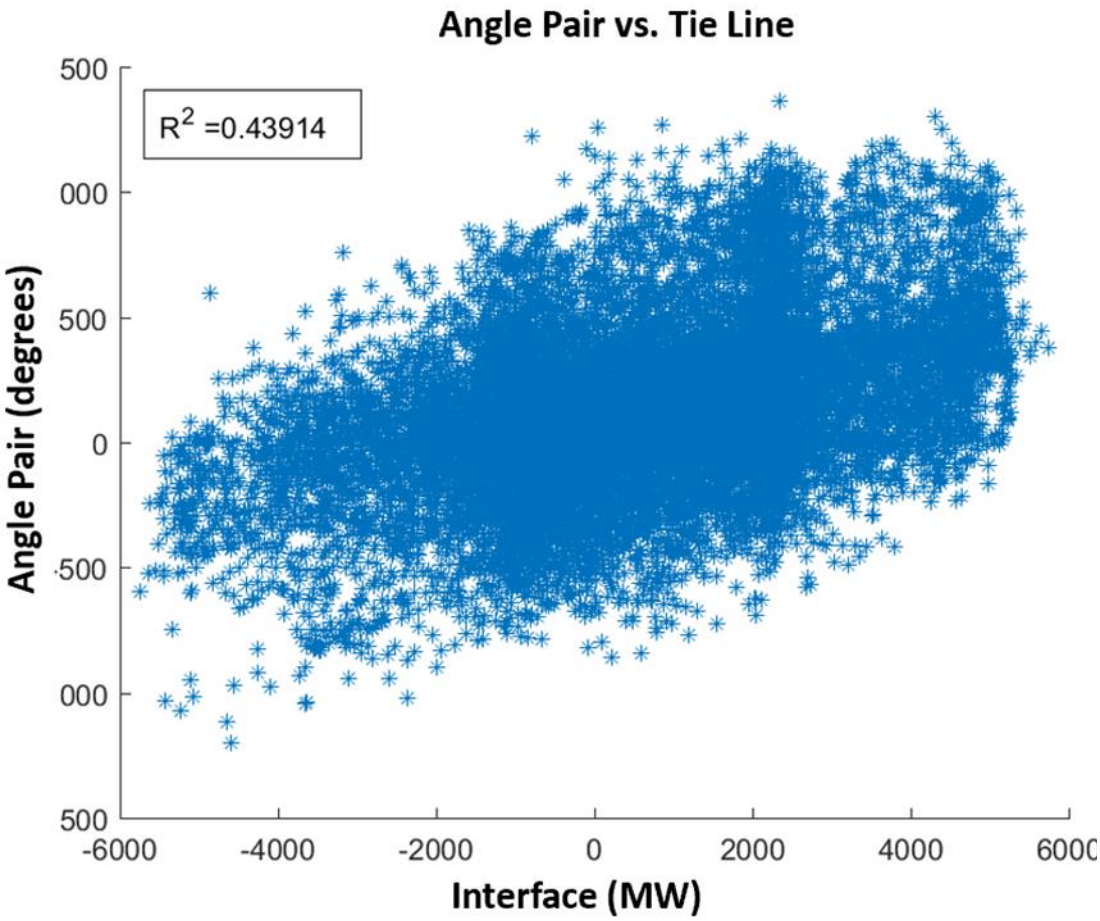

Fig. 111. Interface 2 vs. Angle Pair correlation.

3.4 Attempt to Set Voltage Angle Limits within Normal Operation

Since the baselining work had been done to determine the power and angle difference during normal operation and a power interface and voltage angle pair had been determined, multiple methods were tested to monitor when the voltage angle pair, and thus the power interface, was outside normal operation. The normal angle pair difference for certain time, active power values, active power values during certain times, and load schedule values was considered as possibilities for setting angle difference limits. An example of setting limits for angle difference for active power values is shown in Fig. 112. The limits are set by sectioning the power, in Fig. 112 every 1000 MW, and determining the range in angle difference during normal operation, and then the limits would be used to monitor for when the angle difference deviates from that in real-time.

As can be seen from Fig. 112, the limits had too wide of a range to be practical since for some of the power ranges the voltage difference included most of the range at any power level. This was found for all of the methods tested, so active power, time, and load schedule were not found to be suitable for angle difference limits to test for normal or abnormal operation. Since the data would be less spread with a higher correlated angle pair, there is potential that this could be different with an angle pair more highly correlated to the power interface.

3.5 Conclusion

This study looked at baselining data for active power flow and voltage

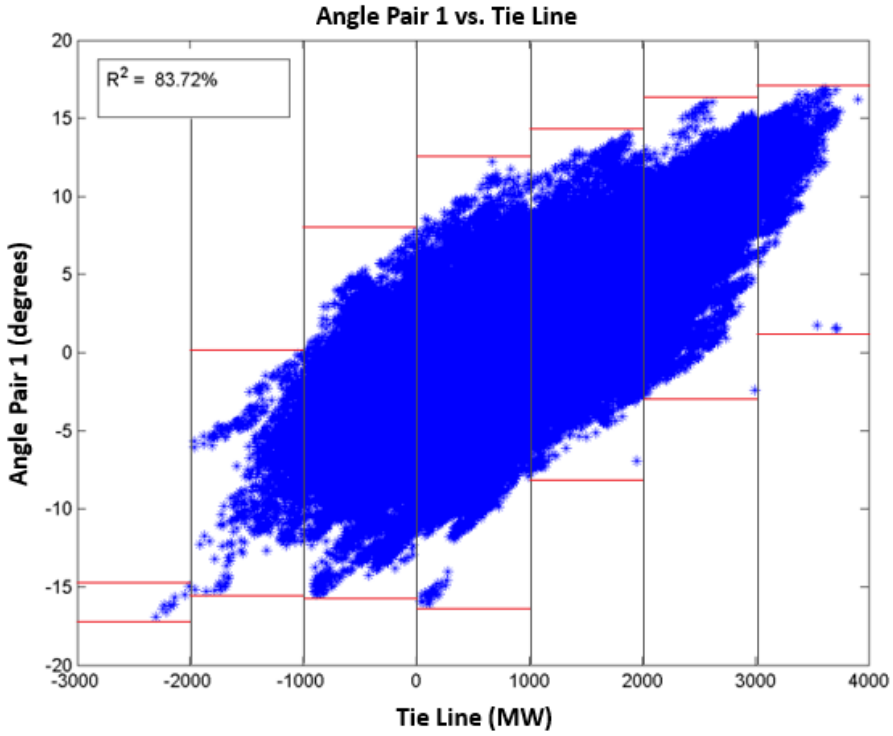

Fig. 112. Angle Pair 1 vs Power Interface with Red Lines Drawn to Demonstrate Angle Difference Limits.

phase angle difference to determine normal operation and use that to try to determine abnormal operation which could indicate system stress. The baselining was performed, and a correlation study to find correlated power interface and voltage angle pairs was done. The methods attempted to detect abnormal operation were not successful and it was determined that the correlation between the power interface and the angle pair used was not enough for the methods used.

3.6 Future Work

Although a method to determine abnormal operation, in particular in relation to the interface power flow, was not found using the angle difference, there is potential that the change in angle difference from one time to the next could be used as an indicator of a change in topology. In the future this could be explored to determine if a large change in angle difference could indicate an abnormal state

REFERENCES

[1] North American Electric Reliability Corporation, "Essential Reliability Services Task Force Measures Framework Report," NERC, 2015.

[2] Australian Energy Market Operator, "System strength in the NEM explained," AEMO Information & Support Hub, 2020.

[3] O. Gomis-Bellmunt, J. Song, M. Cheah-Mane and E. Prieto-Araujo, "Steady-state impedance mapping in grids with power electronics: What is grid strength in modern power systems?," *International Journal of Electrical Power & Energy Systems,* vol. 136, 2022.

[4] D. Bowman, D. Ramasubramanian, R. McCann, E. Farantatos, A. Gaikwad and J. Caspary, "SPP Grid Strength Study with High Inverter-Based Resource Penetration," *2019 North American Power Symposium (NAPS),* pp. 1-6, 2019.

[5] R. W. Kenyon, M. Bossart, M. Markovic, K. Doubleday, R. Matsuda-Dunn, S. Mitova, S. A. Julien, E. T. Hale and B.-M. Hodge, "Stability and control of power systems with high penetrations of inverter-based resources: An accessible review of current knowledge and open questions," *Solar Energy,* vol. 210, pp. 149-168, 2020.

[6] North American Electric Reliability Corporation, "Short-Circuit Modeling and System Strength White Paper," NERC, 2018.

[7] North American Electric Reliability Corporation, "Integrating Inverter-Based Resources into Low Short Circuit Strength Systems Reliability Guideline," NERC, 2017.

[8] Y. Zhang, S.-H. F. Huang, J. Schmall, J. Conto, J. Billo and E. Rehman, "Evaluating system strength for large-scale wind plant integration," in *2014 IEEE PES General Meeting* | *Conference & Exposition*, National Harbor, MD, 2014.

[9] M. Maharjan, A. Ekic, M. Beedle, J. Tan and D. Wu, "Evaluating grid strength under uncertain renewable generation," *International Journal of Electrical Power & Energy Systems,* vol. 146, 2023.

[10] U.S. Energy Information Administration, "Form EIA-860 detailed data with previous form data (EIA-860A/860B)," eia, 9 Sept. 2021. [Online]. Available: https://www.eia.gov/electricity/data/eia860/. [Accessed 23 Feb. 2022].

[11] Siemens Industry, Inc, "Chapter 11 Fault Analysis," in *Program Application Guide Volume 1*, Schenectady, NY, Siemens Industry, Inc, 2022.

[12] P. Kundur, Power System Stability and Control, McGraw Hill, 1994.

[13] S. Sharma, S. Pushpak, V. Chinde and I. Dobson, "Sensitivity of Transient Stability Critical Clearing Time," *IEEE Transactions on Power Systems,* vol. 33, no. 6, pp. 6476-6486, 2018.

[14] K. Prabha, "Power System Stability and Control," Palo Alto, Electrical Power Research Institute (EPRI)-McGraw-Hill, 1994, p. 202.

[15] S. Eftekharnejad, V. Vittal, G. T. Heydt, B. Keel and J. Loehr, "Impact of increased penetration of photovoltaic generation on power systems," *IEEE transaction on power systems,* vol. 28, pp. 893-901, 2013.

[16] T. Alquthami, H. Ravindra, M. Faruque, M. Steurer and T. Baldwin, "Study of photovoltaic integration impact on system stability using custom model of PV arrays integrated with PSS/E," *North American Power Symposium (NAPS),* pp. 1-8, 2010.

[17] Y. T. Tan, "Impact on the power system with a large penetration of photovoltaic generation," *North American Power Symposium (NAPS),* pp. 1-8, 2010.

[18] S. Achilles, S. Schramm and J. Bebic, "Transmission system performance analysis for high-penetration photovoltaics: National Renewable Energy Laboratory," 2008.

[19] B. Tamimi, C. Canizares and K. Bhattacharya, "System stability impact of large-scale and distributed solar photovoltaic generation: the case of Ontario, Canada," *IEEE transactions on sustainable energy,* vol. 4, pp. 680-688, 2013.

[20] M. Yagami, N. Kimura, M. Tsuchimoto and J. Tamura, "Power system transient stability analysis in the case of high-penetration photovoltaics," *PowerTech (POWERTECH),* vol. 2013 IEEE Grenoble, pp. 1-6, 2013.

[21] P. G. Bueno, J. C. Hernandez and F. J. Ruiz-Rodriguez, "Stability assessment for transmission systems with large utility-scale photovoltaic units," *IET Renewable Power Generation,* vol. 10, pp. 584-597, 2016.

[22] N. K. Roy, "Stability assessment of power systems integrated with large-scale solar PV units," *Advances in Solar Photovoltaic Power Plants,* pp. 215-230, 2016.

[23] R. Shah, N. Mithulananthan and R. Bansal, "Oscillatory stability analysis with high penetrations of large-scale photovoltaic generation," *Energy Conversion and Managment,* vol. 65, pp. 420-429, 2013.

[24] S. You, Y. Liu, J. Tan, M. T. Gonzalez, X. Zhang, Y. Zhang and Y. Liu, "Comparative assessment of tactics to improve primary frequency response without curtailing solar output in high photovoltaic interconnection grids," *IEEE Transactions on Sustainable Energy,* vol. 10, pp. 718-728, 2018.

[25] Y. Liu, S. You, J. Tan, Y. Zhang and Y. Liu, "Frequency response assessment and enhancement of the US power grids toward extra-high photovoltaic generation penetrations-an industry perspective," *IEEE Transactions on Power Systems,* vol. 33, pp. 3438-3449, 2018.

[26] S. You, G. Kou, Y. Liu, X. Zhang, Y. Cui, M. J. Till, W. Yao and Y. Liu, "Impact of high PV penetration on the inter-area oscillations in the US eastern interconnection," *IEEE Access,* vol. 5, pp. 4361-4369, 2017.

[27] S. You, Y. Liu, G. Kou, X. Zhang, W. Yao, Y. Su, S. W. Hadley and Y. Liu, "Non-invasive identification of inertia distribution change in high renewable systems using distribution level PMU," *IEEE Transactions on Power Systems,* vol. 33, pp. 1110-1112, 2017.

[28] S. You, Y. Liu, X. Zhang, M. T. Gonzalez and Y. Liu, "US Eastern Interconnection (EI) Electromechanical Wave Propagation and the Impact of High PV Penetration on Its Speed," *2018 IEEE/PES Transmission and Distribution Conference and Exposition (T&D),* pp. 1-5, 2018.

[29] S. You, Y. Liu, Y. Liu, A. Till, H. Li, Y. Su, J. Zhao, J. Tan, Y. Zhang and M. Gong, "Energy Storage for Frequency Control in High Photovoltaic Power Grids," *EUROCON 2019,* pp. 1-6.

[30] S. You, Y. Liu, X. Zhang, Y. Su, L. Wu, Y. Liu and S. W. Hadley, "Impact of high PV penetration on US eastern interconnection frequency response," *2017 IEEE Power & Energy Society General Meeting,* pp. 1-5, 2017.

[31] G. Kou, "Dynamic Modeling and Renewable Integration Studies on the U.S. Power Grids," University of Tennessee, 2016.

[32] H. R. Shabani and M. Kalantar, "Real-time transient stability detection in the power system with high penetration of DFIG-based wind farms using transient energy function," *International Journal of Electrical Power & Energy Systems,* vol. 133, 2021.

[33] S. R. Mohamed, P. A. Jeyanthy and D. Devaraj, "Investigation on the impact of high-penetration of PV generation on transient stability," in *2017 IEEE International Conference on Intelligent Techniques in Control, Optimization and Signal Processing (INCOS)*, Srivilliputtur, India, 2017.

[34] E. Munkhchuluun, L. Meegahapola and A. Vahidnia, "Impact on rotor angle stability with high solar-PV generation in power networks," in *2017 IEEE PES Innovative Smart Grid Technologies Conference Europe (ISGT-Europe)*, Turin, Italy, 2017.

[35] M. A. Chowdhury, W. X. Shen, N. Hosseinzadeh and H. R. Pota, "A review on transient stability of DFIG integrated power system," *International Journal of Sustainable Engineering,* vol. 8, no. 6, pp. 405-416, 2015.

[36] N. Srisaen and A. Sangswang, "Effects of PV Grid-Connected System Location on a Distribution System," *Proc. IEEE Asia Pacific Conf. Circuits and Systems,* pp. 852-855, 2006.

[37] P. Denholm, T. Mai, R. W. Kenyon, B. Kroposki and M. O'Maley, "Inertia and the Power Grid: A Guide Without the Spin," NREL, Golden, CO: National Renewable Energy Laboratory, 2020.

[38] W. Ling, "Power System Frequency Measurment Based Data Analytics and Situational Awareness," The University of Tennessee, Knoxville, Knoxville, 2018.

[39] J. Y. Cai, Z. Huang, J. Hauer and K. Martin, "Current Status and Experience of WAMS Implementation in North America," *IEEE/PES Transmission & Distribution Conference & Exposition: Asia and Pacific,* pp. pp. 1-7, 2005.

[40] U.S.-Canada Power System Outage Task Force, "Final Report on the August 14, 2003 Blackout in the United States and Canada: Causes and Recommendations," 2004.

[41] B. Vandiver, A. Apostolov and F. Steinhauser, "Testing of Phasor Measurement Units," in *63rd Annual Conference for Protective Relay Engineers*, College Station, 2010.

[42] N. E. A. T. T. (EATT), "Data Mining Techniques and Tools for Synchrophasor Data," NASPI, 2019.

[43] NASPI Control Room Solutions Task Team, "Using Synchrophasor Data for Phase Angle Monitoring," NASPI, 2016.

[44] A. Kaci, I. Kamwa, S. A. Dessaint and S. Guillon, "Synchrophasor data baselining and mining for online monitoring of dynamic security limits," *IEEE Trans. Power Syst.,* vol. 29, no. 6, pp. 2681-2695, 2014.

[45] Y. Wu, L. Badesa, M. T. Musavi and P. Lerley, "Monitoring power system transient stability using synchrophasor data," in *2015 IEEE Power & Energy Society General Meeting*, Denver, CO, 2015.

[46] A. Kaci, I. Kamwa, L. A. Dessaint and S. Guillon, "Phase angles as predictors of network dynamic security limits and further implications," in *2014 IEEE PES General Meeting | Conference & Exposition*, National Harbor, MD, 2014.

[47] NERC Synchronized Measurement Subcommittee, "Phase Angle Monitoring: Industry Experience Following the 2011 Pacific Southwest Outage Recommendation 27," NERC, 2016.

[48] M. Vaiman, "Phase Angle Alarming in ROSE for Steady-State Stability Analysis," in *JSIS Meeting*, 2015.

[49] T. Belalcazar, J. Duran and L. Ramirez, "Angle Characterization Using PMUs for Control Centers," in *NASPI*, 2016.

[50] D. Kosterev and M. Patel, "Baselining Analysis," June 2010.

VITA

Abigail Till was born in Knoxville, Tennessee. She got her B.S. in Electrical Engineering at Tennessee Technological University in 2016. From there she started working towards her Ph. D. degree at the University of Tennessee, Knoxville, as well as a concurrently awarded M.S. degree, in Electrical Engineering - Power Systems.